Received: 28 September 2020 | Revised: 18 March 2021 | Accepted: 24 March 2021

DOI: 10.1111/joa.13442

Journal of Anatomy

ANATOMICAL SOCIETY WILEY

ORIGINAL PAPER

3D skull modelling and description of a new baurusuchid (Crocodyliformes, Mesoeucrocodylia) from the Late Cretaceous (Bauru Basin) of Brazil

Gustavo Darlim[1] | Felipe C. Montefeltro[2] | Max C. Langer[1]

[1]Laboratório de Paleontologia de Ribeirão Preto, FFCLRP, Universidade de São Paulo, Ribeirão Preto, Brazil

[2]Laboratório de Paleontologia e Evolução de Ilha Solteira, UNESP, Ilha Solteira, Brazil

Correspondence
Gustavo Darlim, Laboratório de Paleontologia de Ribeirão Preto, FFCLRP, Universidade de São Paulo, Ribeirão Preto-SP, Brazil.
Email: gustavo.darlim@gmail.com

Funding information
Coordenação de Aperfeiçoamento de Pessoal de Nível Superior, Grant/Award Number: Finance Code 001; Fundação de Amparo à Pesquisa do Estado de São Paulo, Grant/Award Number: 2019/06311-4

Abstract

Baurusuchidae is one of the most diverse groups of South American notosuchians, unambiguously recorded in Late Cretaceous deposits of Brazil and Argentina. The group is characterized by a reduced tooth formula, a lateromedially compressed rostrum, and a verticalized quadrate, representing one of the top predators of their faunas. Historically, skull morphology is the most employed tool to investigate the relationships of baurusuchids, as most of the species have been primarily based on cranial remains. The present study describes a new baurusuchid species from the Bauru Basin of Brazil, based on the first tridimensional digital reconstruction of individualized skull bones for Notosuchia, and discusses its phylogenetic position within the group. The new species differs from all the other known baurusuchids by a depression on the posterior portion of the nasal bearing a crest, an infraorbital crest of the jugal that extends until the anterior margin of the lacrimal, the dorsal surface of the frontal lacking a longitudinal crest or depression, and the lateral convexity of the squamosal prongs participating in the occipital wall. The new taxon is consistently positioned as sister to the remaining baurusuchines, with *Aplestosuchus sordidus* and *Stratiotosuchus maxhechti*, as successive sister-taxa to a monophyletic *Baurusuchus* (*Ba. albertoi*, *Ba. Salgadoensis*, and *Ba. pachecoi*). Our updated phylogenetic analysis helps to differentiate the two major Baurusuchidae lineages, Baurusuchinae and Pissarrachampsinae. Yet, the new species shares morphological features with both groups, suggesting the occurrence of "Zones of Variability" in the radiation of Baurusuchidae.

KEYWORDS
baurusuchidae, CT scan, evolution, mesoeucrocodylia, skull

1 | INTRODUCTION

Baurusuchidae is a group of terrestrial crocodyliforms that were top predators during the Cretaceous of what is South America today (Godoy et al., 2014; Montefeltro et al., 2020; Riff & Kellner, 2011). The fossil record of the group is mostly limited to the Adamantina/Vale do Rio do Peixe Formation, in Brazil, and the Bajo de La Carpa Formation, in Argentina. The group was originally proposed (Price, 1945) based on *Baurusuchus pachecoi* and defined by the unique combination of morphological features of that species (e.g., reduced tooth formula, laterally compressed rostrum, ziphodont dentition, verticalized quadrate, and large ectopterygoids participating in the borders of the internal narial openings). Later discoveries revealed Baurusuchidae as the most diverse group of Crocodyliformes in the Adamantina/Vale do Rio do Peixe Formation (Godoy et al., 2014), including seven additional species: *Stratiotosuchus maxhechti* Campos et al., 2001, *Ba. salgadoensis* Carvalho et al., 2005, *Ba. alberoi* Nascimento & Zaher,

2010, *Campinasuchus dinizi* Carvalho et al., 2011, *Pissarrachampsa sera* Montefeltro et al., 2011, *Gondwanasuchus scabrosus* Marinho et al., 2013, and *Aplestosuchus sordidus* Godoy et al., 2014. Two Argentinean species are assigned to Baurusuchidae, *Cynodontosuchus rothi* Woodward, 1896, and *Wargosuchus australis* Martinelli & Pais, 2008, as well as a possible third form, *Pehuenchesuschus enderi* (Turner & Calvo, 2005). In addition, the Pakistani *Pabwehshi pakistanensis* Wilson et al., 2001 might also represent a baurusuchid. These occurrences highlight the exuberance of the group in the Late Cretaceous of Gondwana.

In 2012, an expedition led by the Laboratório de Paleontologia, FFCLRP-USP, to the municipality of Jales, São Paulo State, Brazil, resulted in the discovery of a new specimen (LPRP/USP 0697) of Baurusuchidae from the Adamantina/Vale do Rio do Peixe Formation. The material, composed of an almost complete skeleton, can be easily referred to the group due to its reduced maxillary tooth formula, verticalized quadrate, and mediolaterally compressed rostrum. The Fazenda Furnas site, where the specimen was found, has previously yielded other baurusuchid specimens, including a nearly complete articulated tail (Avilla et al., 2004) and a series of vertebrae articulated with a partial pelvic girdle (Araújo Júnior & Silva Marinho, 2013). Furthermore, eggs possibly associated to Baurusuchidae were also found in the same outcrop (Oliveira et al., 2011).

Few studies have employed CT scanning of baurusuchid bones to generate 3D (tree-dimensional) models. Vasconcellos (2009) digitally reconstructed both cranial and postcranial elements of *Ba. salgadoensis* to analyze morphofunctional aspects, but such study did not include extensive osteological descriptions. More recently, Fonseca et al., (2020) published the anatomy of the encodracanial cavities of *Ca. dinizi*. Additionally, the specimen described herein was used as a digital model in the work of Montefeltro et al., (2020), which employed tridimensional images of LPRP 0697 for Finite Element Analyses (FEA) in order to characterize cranial functional morphology. Here, we present the first tridimensional description of individual skull bones for a baurusuchid, and notosuchians in general, using CT scan image stacks and digital reconstructions. A new species is proposed, followed by a discussion of early Baurusuchidae evolution.

1.1 | Geological settings

During the opening of the Atlantic Ocean, the continental break-up produced a huge depression in what southeastern Brazil is today, allowing the accumulation of the Bauru Basin sediments, which now covers large areas of Paraná, São Paulo, Mato Grosso, Mato Grosso do Sul, Goiás, and Minas Gerais states (Fernandes & Coimbra, 1996). The lithostratigraphic framework of the basin is composed of two groups: the Caiuá Group includes the Rio Paraná, Goio Erê, and Santo Anastácio formations; the Bauru Group, includes the Adamantina/Vale do Rio do Peixe, Uberaba, Araçatuba, and Marilia formations (Batezelli & Ladeira, 2016; Fernandes & Ribeiro, 2015; Menegazzo et al., 2016; Paula e Silva et al., 2003). The Adamantina/Vale do Rio do Peixe Formation may be given a general late Santonian-Campanian age, according to the records of ostracods, sauropods, and many other vertebrates, including crocodyliforms (Menegazzo et al., 2016). This is in agreement with the first radioisotopic age estimated using high-precision U-Pb geochronology for the Adamantina/Vale do Rio do Peixe Formation (Castro et al., 2018), which indicates a post-Coniacian to Maastrichthian age.

The Adamantina/Vale do Rio do Peixe Formation was first defined by Soares et al., (1980) and is exposed in Goiás, Mato Grosso do Sul, Minas Gerais, and São Paulo states of Brazil. This unity is known by its extensive fossil record, including algae, mollusks, crustaceans, anurans, turtles, lizards, snakes, non-avian dinosaurs, mammals, birds, and an exuberant diversity of crocodyliforms (Arruda et al., 2004; Carvalho & Bertini, 1999; Carvalho et al., 2005; Castro et al., 2018; Dias-Brito et al., 2001). Deposits of the Adamantina/Vale do Rio do Peixe Formation are usually composed of fine-grained sandstones and subordinate mudstones, with granulometric patterns that suggest a fluvial sedimentation in meandering canals in a semi-arid climate (Paula e Silva et al., 2005). A progressive increase in aridity, due to the persistence of a hot climate, and topographic heights surrounding the basin, resulted in the establishment of alluvial plains, braided rivers, and ponds (Dias-Brito et al., 2001; Fernandes, 1998; Fernandes & Coimbra, 1996). Araújo Júnior and Silva Marinho (2013) provided a lithofaciological analysis of the strata where LPRP 0697 was collected (Figure 1), indicating that it represents a succession of floodplain deposits.

2 | METHODS

2.1 | CT scanning

Image stacks of LPRP 0697 were acquired using the CT scanner *Toshiba Aquilion Prime*, with voltage of 120 kV, and current of 150 μA. A total of 1917 slices with thickness of 0.5 mm were generated and voxel size of 0.546002 × 0.546002 × 0.3 mm. Raw CT scan data (DICOM stack format) are available on the following link to MorphoSource Ark: http://n2t.net/ark:/87602/m4/348679. The fossil was segmented and the tridimensional surfaces were generated using the software *Avizo 7.0*.

2.2 | Phylogenetic analysis

The new taxon represented by LPRP 0697 was included in the data matrix of Godoy et al., (2014), which is an updated version of that of Montefeltro et al., (2011). That matrix is the most up-to-date phylogenetic dataset built exclusively to investigate baurusuchid relationships. It is composed of 74 characters and 13 taxa; that is, ten baurusuchids and the outgroup composed of *Armadillosuchus arrudai*, *Mariliasuchus amarali*, and *Notosuchus terrestris* (operational outgroup). We expanded the data matrix of Godoy et al., (2014) using the software Mesquite

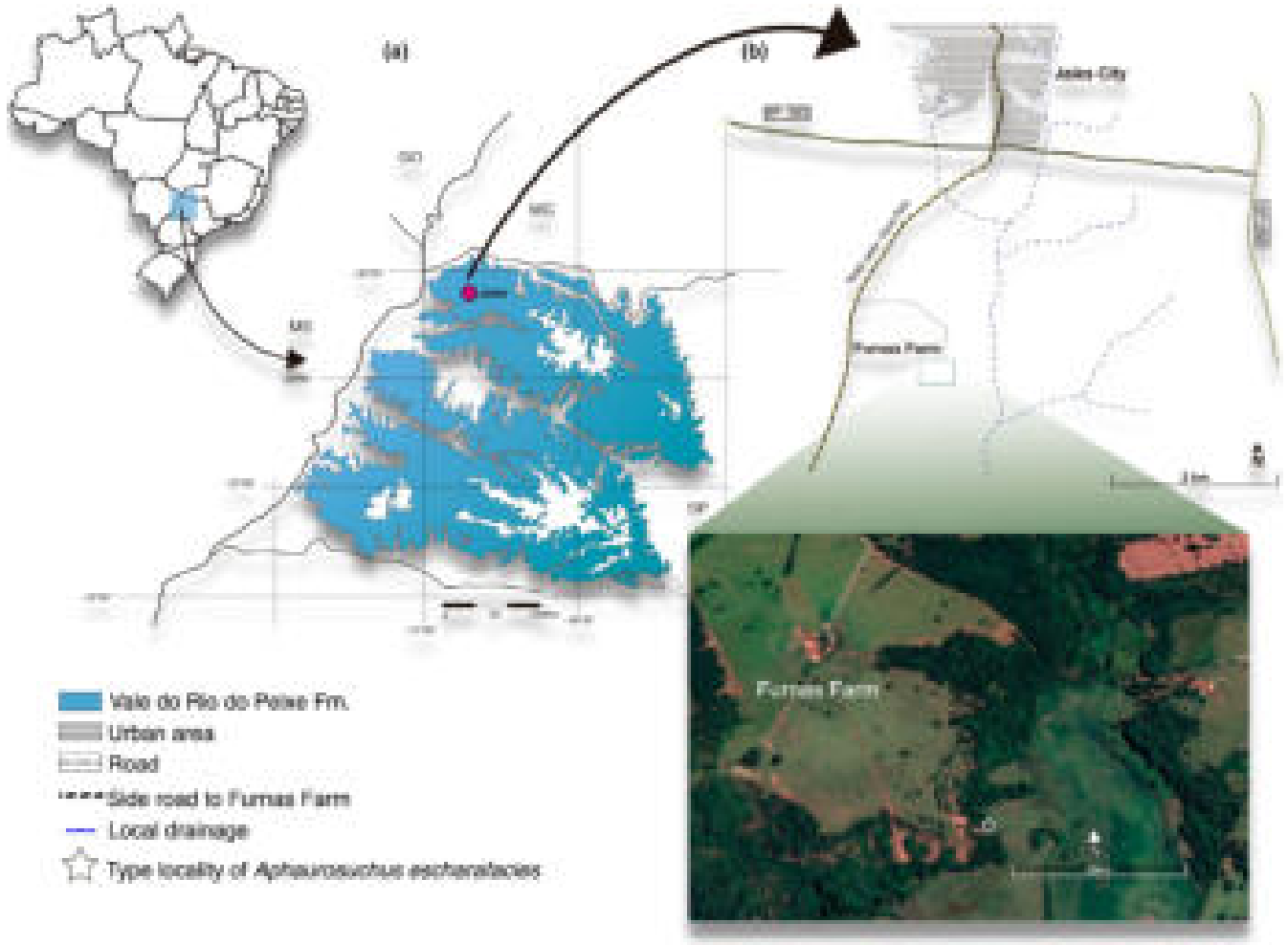

FIGURE 1 Location where *Aphaurosuchus escharafacies* was collected. (a) Map showing the distribution of Vale do Rio do Peixe Formation, within São Paulo State (modified from Fernandes, 2004). (b) Drawing scheme of Jales city and a satellite image of the type locality of *Aphaurosuchus escharafacies* at Furnas Farm

v.3.6 (Maddison, 2008), adding six characters (75–80; data S2) and the new taxon. The tree search strategy followed the parameters of the previous works (Godoy et al., 2014; Montefeltro et al., 2011), using equally weighted parsimony in *TNT v.1.1* (Goloboff et al., 2008) based on the implicit enumeration search algorithm. Bootstrap resampling was run with *TNT* to infer node support and only values higher than 50% were indicated on the trees. Bremmer support (Bremer, 1994) values were calculated using *TNT* script. Characters 5, 11, 12, 22, 27, 32, and 41 were treated as additive, following Godoy et al., (2014). Also, we rescored some characters for *Ba. pachecoi* (20 and 24) and *G. scabrosus* (6, 8, 10, 15, 28, 30, 43, and 73), based on our first-hand analyses of the holotypes (DGM 299-R and UFRJ DG 408-R, respectively). The complete list of rescoring and the newly added characters are presented in the supplementary material.

2.3 | Nomenclatural acts

The electronic version of this article in Portable Document Format (PDF) will represent a published work according to the International Commission on Zoological Nomenclature (ICZN), and hence the new names contained in the electronic version are effectively published under that Code from the electronic edition alone. This published work and the nomenclatural acts it contains have been registered in ZooBank, the online registration system for the ICZN. The ZooBank LSIDs (Life Science Identifiers) can be resolved and the associated information viewed through any standard web browser by appending the LSID to the prefix http://zoobank.org/. The LSID for this publication is: [urn:lsid:zoobank.org:act:2F532D44-C2DE-4870-8F6C-41DD1DBA3D6B].

2.4 | Institutional abbreviations

CPPLIP- Centro de Pesquisas Paleontológicas, L.I. Price, Universidade Federal do Triângulo Mineiro, Uberaba; DGM-Museu de Ciências da Terra do Departamento Nacional de Produção Mineral, Rio de Janeiro; LPRP- Laboratório de Paleontologia de Ribeirão Preto, Universidade de São Paulo; MPMA- Museu de Paleontologia de Monte Alto, Monte Alto; UFRJ

DG- Departamento de Geologia da Universidade Federal do Rio de Janeiro.

3 | RESULTS

3.1 | Systematic Paleontology

Baurusuchia Walker, 1968 [this work; Table 1].
Baurusuchidae Price, 1945 [this work; Table 1].
Baurusuchinae Montefeltro, Larsson & Langer, 2011 [this work; Table 1].
Aphaurosuchus escharafacies gen. et sp. nov.

3.2 | Holotype

LPRP 0697, an almost complete skeleton, preserved in six main blocks (Figure 2). The first is composed of the skull, associated with atlas, axis, and six other cervical vertebrae (III-VIII) and ribs. That block also includes the first to fourth trunk vertebrae (I-IV), a sagittal row of paired parasagittal osteoderms, two almost complete scapulae and the articulated coracoids, the right of which is heavily damaged, with only the articular portion preserved. The second block contains most of the articulated postcranium, composed of nine trunk vertebrae (VIII-XVI), the three sacral, and the first nine caudal vertebrae. As also seen in the skull block, starting from cervical vertebrae VII, all vertebrae of the main postcranial block are covered by a pair of parasagittal osteoderms associated with each neural spine. Most ribs are articulated with the vertebrae in trunk elements VI-XIV; the gastralia is also preserved, and possible gastrolites are seen near its posterior portion. Only the right forelimb is articulated with the trunk, comprising radius, ulna, carpals, metacarpals, and phalanges of the five manual digits (the humerus was lost during the excavation of the specimen). The pelvic girdle is completely preserved and articulated with the rest of the body. Both ischia are still partially covered by matrix, and the pubes are displaced ventrally, reaching anteriorly the posterior portion of the gastralia. The right hindlimb is almost completely preserved, with all the bones exposed, except for digits I and II. The left hindlimb is also almost complete, but the originally articulated distal part of the pes was preserved in a smaller separate block (block six). The third block is small, preserving caudal vertebrae X-XV, all associated with osteoderms, as is the fourth block, which preserves nine more distal caudal vertebrae. It is not clear if these two tails segments are continuous, because the anteriormost vertebrae of the fifth block are very damaged. The fifth block includes the nearly complete left carpus and manus, and the sixth block includes the falanges of the left pes. Furthermore, the proximal part of the left humerus, nearly complete left radius and ulna, two very small caudal vertebrae, also

TABLE 1 New phylogenetic definitions for the main clades related to *Baurusuchus* following the requirements outlined by the International Code of Phylogenetic Nomenclature (PhyloCode) (De Queiroz & Cantino, 2020).

Clade name and registration	Phylogenetic definition, reference phylogeny, and composition
Baurusuchia A. D. Walker, 1968 [this work] converted clade name Registration Number: 410	Phylogenetic definition: The most inclusive clade containing *Baurusuchus pachecoi* Price, 1945, but not *Sebecus icaeorhinus* Simpson 1937 (Sebecidae), *Sphagesaurus huenei* Price 1950 (Sphagesauridae), *Araripesuchus gomesi* Price 1959 (Uruguaysuchidae), *Montealtosuchus arrudacamposi* Carvalho, Vasconcellos & Tavares 2007 (Peirosauridae), or *Crocodylus niloticus* Laurenti 1768 (Crocodylia). This is a maximum clade definition. Reference phylogeny: Hypothesis depicted in Pinheiro et al., (2018; Figure 11). Composition: based on the reference phylogeny, Baurusuchia includes *Baurusuchus*, *Stratiotosuchus*, *Pissarrachampsa*, *Campinasuchus*, and *Pabwehshi*.
Baurusuchidae L. I. Price, 1945 [this work] converted clade name Registration Number: 411	Phylogenetic definition: The least inclusive clade containing *Cynodontosuchus rothi* Woodward 1896, *Pissarrachampsa sera* Montefeltro, Larsson & Langer, 2011, and *Baurusuchus pachecoi* Price, 1945. This is a minimum-clade definition. Reference phylogeny: Phylogenetic hypothesis depicted in Figure 47 of this work. Composition: based on the reference phylogeny, Baurusuchidae includes *Cynodontosuchus*, *Gondwanasuchus*, Baurusuchinae, and Pissarrachampsinae.
Baurusuchinae F. C. Montefeltro, H. C. E. Larsson & M. C. Langer, 2011 [this work], converted clade name Registration Number: 412	Phylogenetic definition: The most inclusive clade containing *Baurusuchus pachecoi* Price, 1945, but not *Pissarrachampsa sera* Montefeltro, Larsson & Langer, 2011 (Pissarrachampsinae). This is a maximum clade definition. Reference phylogeny: Phylogenetic hypothesis depicted in Figure 47 of this work. Composition: based on the reference phylogeny, Baurusuchinae includes *Baurusuchus*, *Stratiotosuchus*, *Aplestosuchus*, and *Aphaurosuchus*.
Pissarrachampsinae F. C. Montefeltro, H. C. E. Larsson & M. C. Langer, 2011 [this work], converted clade name Registration Number: 413	Phylogenetic definition: The most inclusive clade containing *Pissarrachampsa sera* Montefeltro, Larsson & Langer, 2011, but not *Baurusuchus pachecoi* Price, 1945 (Baurusuchinae). This is a maximum clade definition. Reference phylogeny: Phylogenetic hypothesis depicted in Figure 47 of this work. Composition: based on the reference phylogeny, Pissarrachampsinae includes *Pissarrachampsa*, *Campinasuchus*, and *Wargosuchus*.

Definitions follows the recently published International Code of Phylogenetic Nomenclature (PhyloCode).

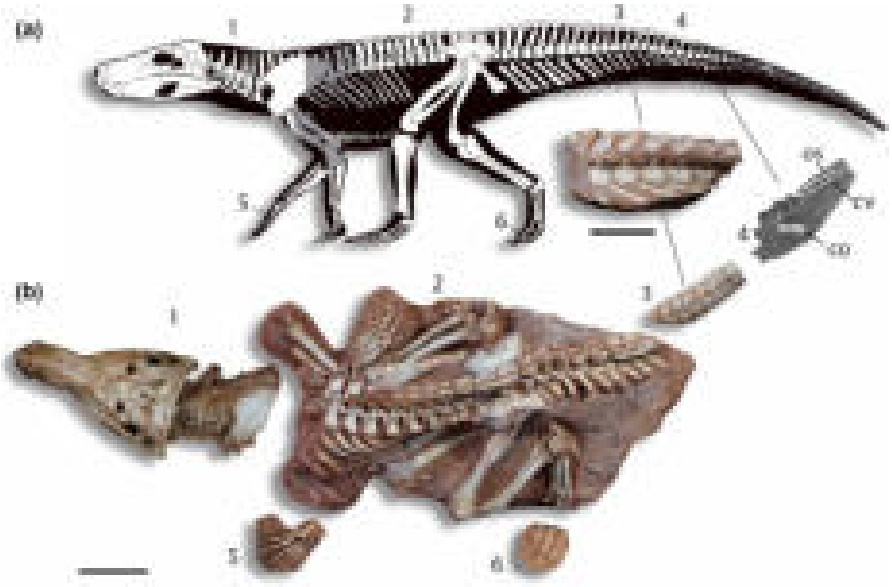

FIGURE 2 Cranial and postcranial elements of *Aphaurosuchus escharafacies*. (a) Drawing of preserved bones (in white) over a silhouette (modified from Carvalho et al., 2010). (b) Fossil elements positioned in anatomical position. Number indicates the different blocks: (1) Skull articulated with cervical vertebrae; (2) Largest block, containing most of the articulated postcranium; (3) Caudal vertebra X-XV; (4) CT scan of distal caudal vertebrae covered in matrix; (5) Left articulated carpal elements; (6) Pedal elements of left pes. Scale bar: 10 cm

bearing tiny osteoderms, were preserved isolated from the blocks, but surely belong to the same individual. Also, rib fragments are found isolated, but cannot be assigned to specific vertebrae.

3.3 | Etymology

The genus name is composed of the Greek words ἀφαυρός (aphauros), = feeble/powerless, and σοῦχος (souchos), = Egyptian name for crocodile, in reference to the week bite of the animal as demonstrated by Montefeltro et al., (2020). The species epithet is composed of ἐσχάρα (eschara), = Greek for scar, and facies, = Latin for face, in reference to the cut on the left jugal and dentary made by the rock saw during the collection of the specimen, which promptly gave the fossil its nickname "Scarface."

3.4 | Type locality

Furnas Farm, ca. 7 km south of Jales, São Paulo State, Brazil (Figure 1). The geographic coordinates were not taken during the fieldwork, but the digging spot was later identified in satellite images by the collectors as −20°20′25″S −50°32′54″W. These indicate about the same site as those discussed by Avilla et al., (2004) and Araújo Júnior and Silva Marinho (2013).

3.5 | Age and horizon

Adamantina/Vale do Rio do Peixe Formation, Bauru Group (Batezelli, 2005; Fernandes & Coimbra, 1996; Soares et al., 1980); Late Cretaceous (ca. Coniacian-Campanian) of the Bauru Basin (Castro et al., 2018).

3.6 | Diagnosis (autapomorphies marked with an asterisk)

Baurusuchidae with four premaxillary teeth and five maxillary teeth; depression on posterior portion of nasal, bearing a distinct longitudinal ridge*; contact of prefrontals restricted to midpoint of their medial surface; absence of a longitudinal crest on frontal surface*; squamosal dorsal surface slightly convex; squamosal prongs verticalized in lateral view, forming a right angle between the dorsal and occipital surfaces; lateral convexity of squamosal prongs leading to a more conspicuous participation in the lateral margin of the occipital wall*; posterolaterally bulged contact of squamosal prongs and paroccipital process in the occipital plane; jugal infraorbital ridge (*sensu* Montefeltro et al., 2011) extending on the anterior margin of lacrimal*; jugal foramina restricted to the ventral portion of antorbital area; reduced dorsal surface of parietals displaced posteriorly to the posterior portion of supratemporal fenestrae, forming a crest-like supratemporal rim; notch on the ventrolateral part of quadratojugal-quadrate contact; absence of well-marked depressions and ridges on the occipital surface of supraoccipital; choanal septum wide and flattened ventrally; "T-shaped" palatine, forming a triangular-shaped suborbital fenestrae; crested suture on the palatines contact; medial pharyngeal tube and pharyngotympanic tubes (*sensu* Duffeau & Witmer, 2015) of the same size; presence of an anterior wall at the pharyngotympanic tubes*; presence of a thin and conspicuous groove on the pterygoid posterodorsal surface.

3.6.1 | Differential diagnosis

The holotype of *Aph. escharafacies* (LPRP 0697) was recently examined in a revision of the osteoderm patterns in Baurusuchidae (Montefeltro, 2019) and was also modeled and studied with the Finite Element Analysis (FEA) of its skull (Montefeltro et al., 2020). Both works tentatively assigned the specimen to *Ba. pachecoi*, but did not back-up that inference with extensive anatomical data. However, *Aph. escharafacies* differs from *Ba. pachecoi* in a number of features, for example,: curved alveolar margin of the maxilla (in lateral view) posterior to the enlarged caniniform tooth; anterolateral anterolateral margins of the squamosal medially directed, not parallel to the skull longitudinal axis; posterior projections of the palatine aligned laterally ("T-shaped"), resulting in a subtriangular suborbital fenestra; and mandibular symphyseal area mediolaterally wider and rounded and less prominent anteriorly (Figure 3).

In addition, *Aph. escharafacies* differs from pissarrachampsines in having a concave choanal depression formed by the pterygoid and ectopterygoid wings, palatines not ventrally flattened, dorsoventrally flattened choanal septum, and lacking parachoanal fossae on the pterygoid. Particularly, it differs from *W. australis*, which does not preserve the palate, in lacking the frontal-nasal contact. Among non-baurusuchine and non-pissarrachampsine baurusuchids, *Aph. escharafacies* differs from *Cy. rothi* in presenting palatines that diverge laterodorsally from their ventromedial contact and enlarged premaxillary teeth, and from *G. scabrosus* in possessing a series of features, including outer and inner surfaces of the teeth lacking sulci, lack of a pair of foramina in the infratemporal ramus of the jugal, and bearing the anterior corner of the external mandibular fenestra vertically aligned with the anteriormost portion of the orbit in lateral view.

Among baurusuchines, *Aph. escharafacies* differs from *S. maxhecthi* in the participation of the frontal in the supratemporal fossa and supraorbital fenestra, and from *Ba. salgadoensis* in having a crested dorsal surface of the parietal, a crested lateral surface of the infra- and antorbital portions of the jugal, extending anteriorly to the anterior lacrimal border, and the posterior portion of the squamosal prongs participating in the occipital wall. Also, *Aph. escharafacies* differs from *Apl. sordidus* by the absence of the frontal

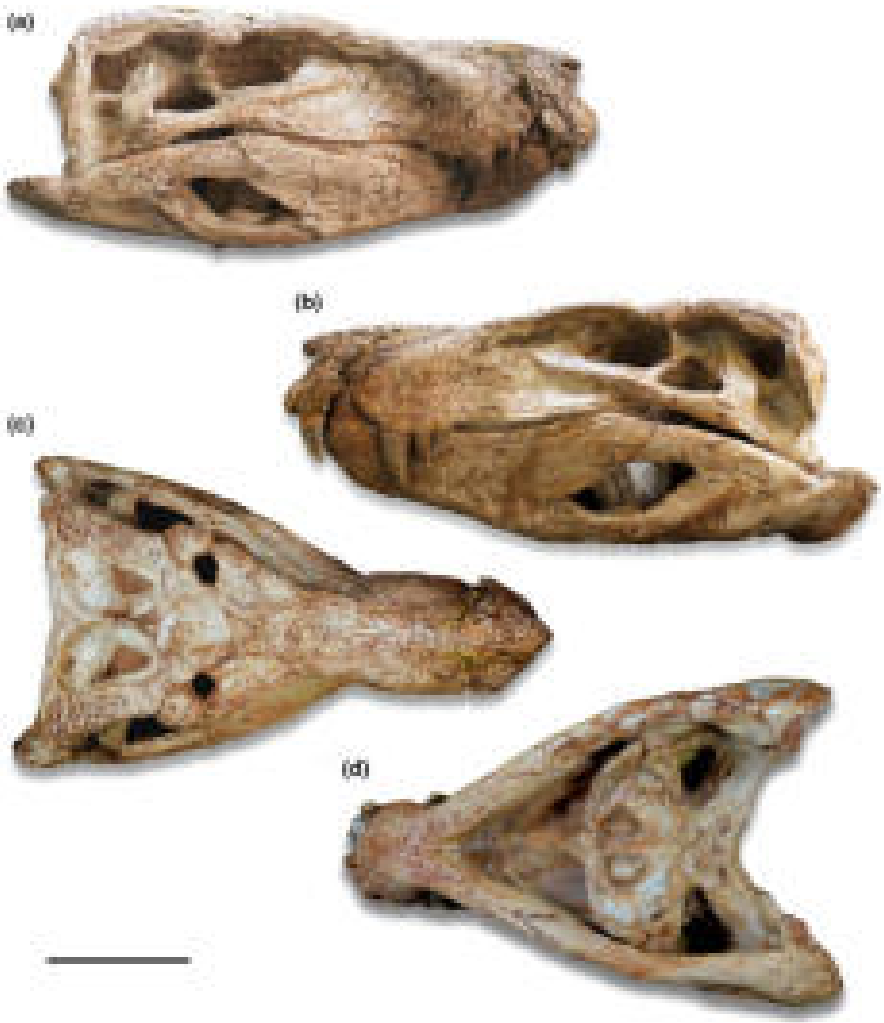

FIGURE 3 Skull of *Aphaurosuchus escharafacies* in (a) right lateral, (b) left lateral, (c) dorsal and (d) ventral views. Scale bar: 10 cm

longitudinal crest, by bearing a smooth choanal septum ventral surface, a posterior peg-like tuberosity on the mandibular symphysis, a depressed posterior portion of the nasal dorsal surface, and only one row of foramina on the lateral surface of the jugal. Finally, given the incompleteness of the skull of *Ba. albertoi*, *Aph. escharafacies* differs from that taxon only by the absence of a well-developed crest extending along the ventral portion of the quadrate until the basioccipital-otoccipital contact. Yet, differences between those taxa hinge on their postcranial anatomy, given the uniqueness of *Aph. escharafacies* (see Montefeltro, 2019) regarding the presence of a cervicodorsal gap between the nuchal and dorsal osteoderm shields and absence of a longitudinal keel on the nuchal osteoderms.

3.7 | Description

3.7.1 | General cranial morphology and openings

The skull of the holotype of *Aph. escharafacies* is well-preserved, exposing the bones that compose its lateral, dorsal, and ventral surfaces (Figures 4, 5). The snout is slightly damaged at the anterior contact between the premaxillae and nasals, so that it is not possible to clearly assess the nostril anatomy. The specimen falls within the short oreinirostral skull shape (*sensu* Busbey, 1995), with a deep rostrum, a convex upper margin, and rostral length less than 55 percent of basal skull length. The skull is lateromedially compressed, with a gradual lateral expansion posteriorly to the anterior portion of orbit.

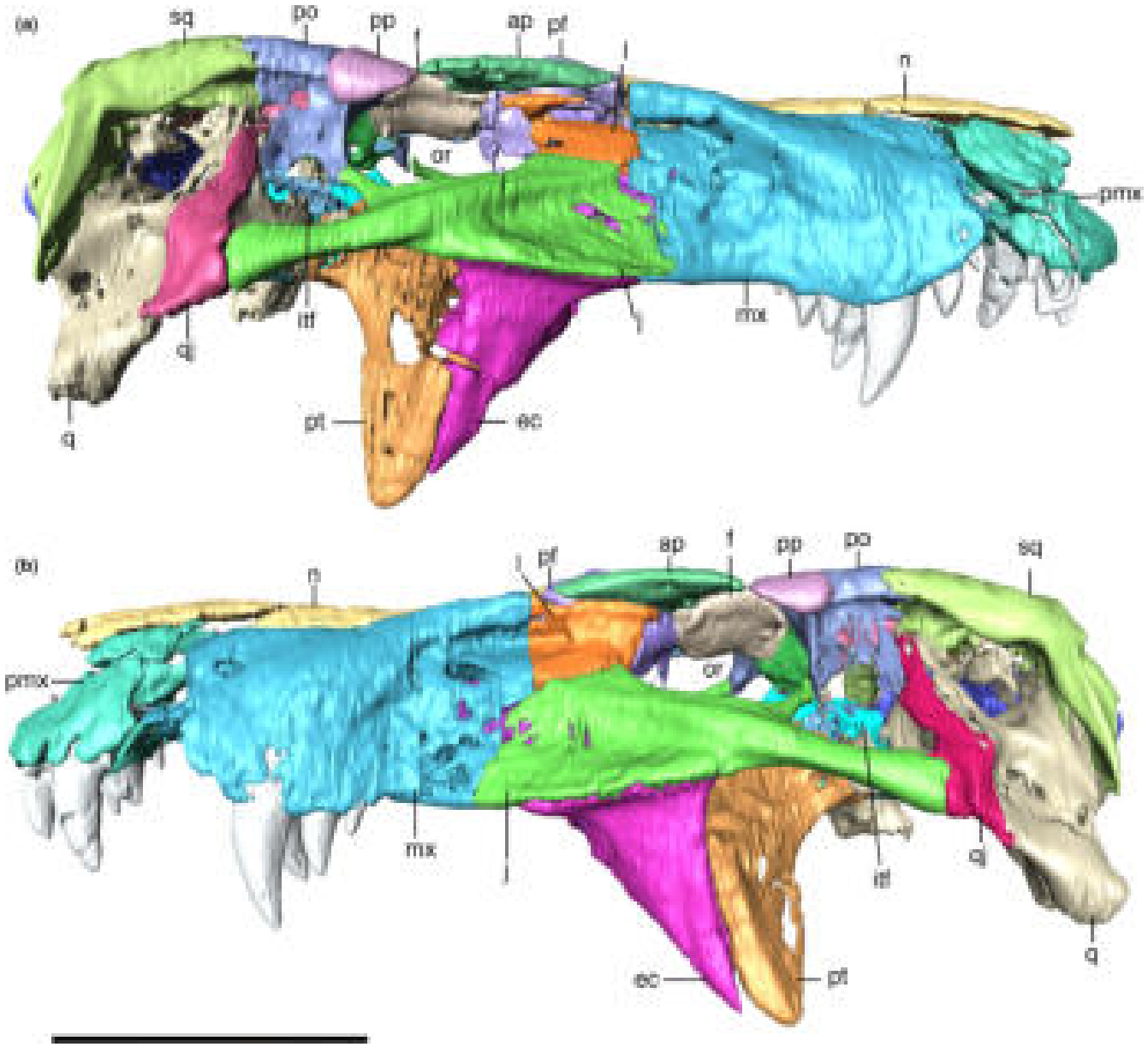

FIGURE 4 Digitally reconstructed skull of *Aphaurosuchus escharafacies* in (a) right lateral, and (b) left lateral views. ap, anterior palpebral; ec, ectopterygoid; f, frontal; itf, infratemporal fenestra; j, jugal; l, lacrimal; mx, maxilla; n, nasal; or, orbit; pf, prefrontal; pmx, premaxilla; po, postorbital; pp, posterior palpebral; pt, pterygoid; q, quadrate; qj, quadratojugal; sq, squamosal. Scale bar: 10 cm

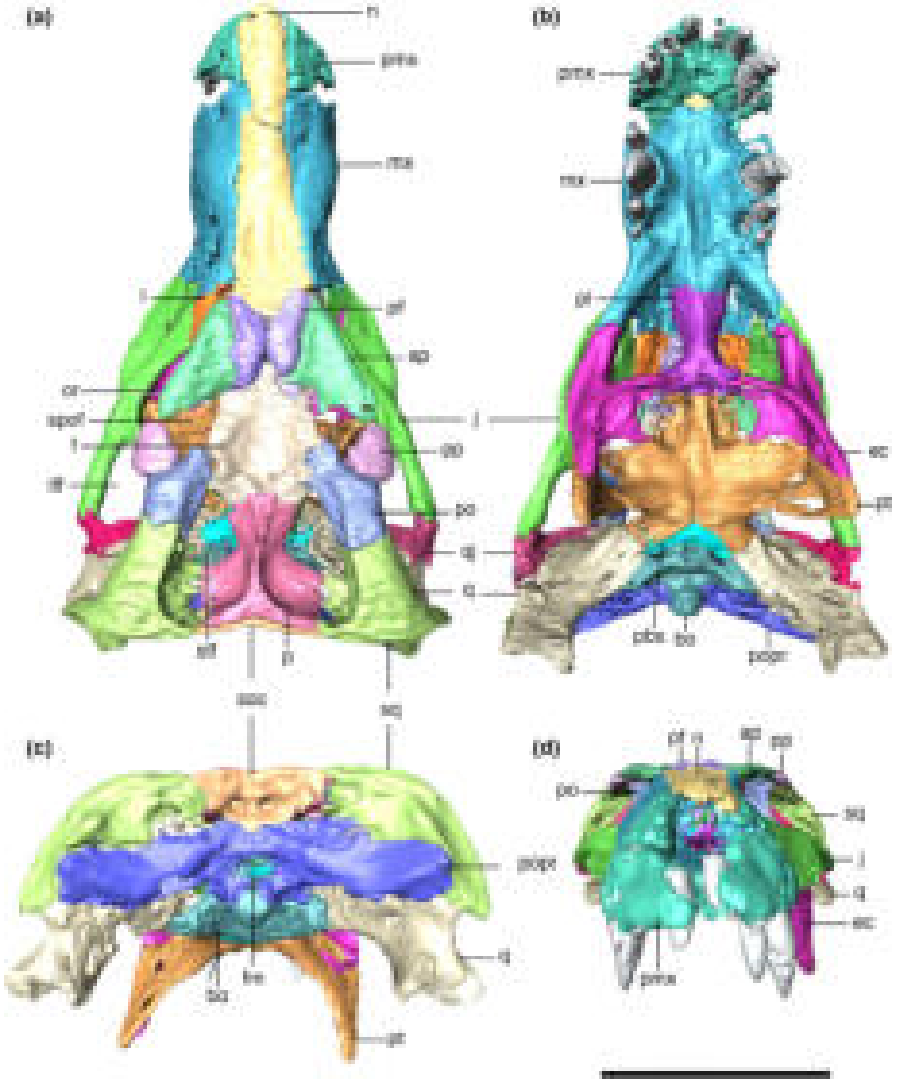

FIGURE 5 Digitally reconstructed skull of *Aphaurosuchus escharafacies* in (a) dorsal, (b) ventral, (c) posterior, and (d) anterior views. ap, anterior palpebral; bo, basioccipital; pbs, parabasisphenoid; ec, ectopterygoid; f, frontal; fm, foramen magnum; itf, infratemporal fenestra; j, jugal; l, lacrimal; mx, maxilla; n, nasal; or, orbit; p, parietal; pf, prefrontal; pl, palatine; pmx, premaxilla; po, postorbital; popr, paroccipital process; pp, posterior palpebral; pt, pterygoid; q, quadrate; qj, quadratojugal; soc, supraoccipital; spof, supraorbital fenestra; sq, squamosal; stf, supratemporal fenestra. Scale bar: 10 cm

The most compressed part of the snout is right posterior to the last maxillary teeth. The mandible is also lateromedially compressed at the portion between the third to fifth maxillary teeth. In lateral view, the retroarticular process projects dorsally, just posterior to the quadrate-mandible articulation. The antorbital fenestrae are completely absent.

The dorsal surface of the skull is highly ornamented, specially the dorsal portion of the maxilla, bordering the lateral margin of the nasals, where conspicuous thin grooves are present. However, an irregular ornamentation pattern is predominant along the entire cranial surface, more evident in some bones, such as the squamosals, nasals, premaxillae, maxillae, as well as in the mandible, and less in others, as the parietal, supraoccipital, quadrates, and quadratojugals.

Orbit

The orbit is oval in lateral view, with an anteroposteriorly directed long axis, and the anterior portion more dorsoventrally compressed. The ventral border of the orbit is more laterally positioned than the dorsal one, so that this opening faces dorsolaterally. In dorsal view, the orbital ventral border is laterally convex, and the aperture is anterolaterally directed. The orbit is dorsally covered by the anterior and posterior palpebrals, except for its lateralmost border and the circular supraorbital fenestra, formed between both palpebrals. The postorbital forms the dorsal portion of posterior margin of the orbit, whereas its ventral portion is formed by the dorsal ramus of the jugal. The jugal also forms the entire ventral border of orbit, sharing its anterior border with the lacrimal.

Supraorbital fenestra

The skull roof is pierced by the supraorbital fenestra, which is laterally enclosed by the posterolateral projection of the anterior palpebral and the anteromedial portion of the posterior palpebral. This contact arches laterally, forming a semi-circular medial gap, slightly compressed anteroposteriorly. The medial margin of the supraorbital fenestra is composed of a small lateral portion of the frontal and the anterolateral portion of the postorbital.

Supratemporal fenestr

The supratemporal fenestra is composed of the squamosal, parietal, postorbital, and frontal. The external supratemporal fenestra is subtriangular, longer anteroposteriorly than lateromedially, compressed lateromedially at its anterior portion. It bears elevated rims, except for the anterior margin, which is at the same level as the frontal. Anteriorly, the posterior portion of the frontal participates in a short portion of the external supratemporal fenestra. The postorbital forms its anterolateral margin, whereas the squamosal delimits the posterolateral margin of the aperture. The parietal forms the posteromedial corner and medial margin of the fenestra, separating the pair of supratemporal fenestrae by a thin crest. The internal supratemporal fenestra is formed by the same bones, but it is triangular and smaller than the external.

The supratemporal fossa comprises the region composed of unornamented bone surfaces immediately ventral to the supratemporal fenestrae (Holliday et al., 2020). The fossa presents two main orientation of its surface: the more dorsally exposed region, facing mostly dorsally, and the more internal region, the surface of which is more verticalized (infratemporal fossa *sensu* Holliday et al., 2020). The dorsally exposed region of the supratemporal fossa is more anterioposteriorly wide at its posterior half, near to the orbitotemporal foramen. The anterolateral surface of the fossa, formed by the medial surface of the postorbital, is markedly convex, gradually turning concave posteriorly towards the medial surface of the squamosal. The posterior portion of the fossa, formed by the squamosal and the parietal, is concave, bearing a few muscle scars and a conspicuous orbitotemporal foramen. This foramen is dorsoventrally short, mediolaterally elongated, and located at the squamosal-parietal suture. The medial portion of the supratemporal fossa is formed by the flattened surface of the parietal. All these margins converge towards the internal supratemporal fenestra, where they suffer a ventral inflexion, get more verticalized, and presents a smoother surface, lacking elevations or depressions.

Infratemporal fenestra

The infratemporal fenestra is triangular shaped, with rounded corners, smaller than the orbit, and dorsolaterally directed. In lateral view, the fenestra extends from the level of center of the posterior palpebral to slightly posterior to the postorbital-squamosal lateral suture. The anterodorsal margin of the fenestra is mostly formed by the dorsal ramus of the jugal, with its dorsalmost part formed by a small anteroventral portion of the postorbital. The posterodorsal border is formed by the ventral margin of the postorbital anteriorly, and posteriorly by the quadratojugal, which also forms the posterior end of the ventral margin of the fenestra. Finally, the fenestra is mostly bordered ventrally by the infratemporal process (or posterior ramus) of the jugal.

External and internal mandibular fenestrae

The external mandibular fenestrae are relatively large, representing the largest external fenestra of the skull (74.4 mm of anteroposterior length). Its dorsal border is formed by the dentary anteriorly and the surangular posteriorly. The dentary border faces anterodorsally, whereas the surangular margin is more horizontal, with a conspicuous ventral inflexion on its posterior end, near the ventral contact with the angular. The ventral border of the fenestra is sigmoidal and entirely composed of the angular, except for a small portion at its anterior tip, which is formed by the dentary. This anterior corner is conspicuously pinched dorsoventrally, whereas the posterior tip is more rounded due to the curvature of the surangular. The anterior tip is more ventrally positioned than the posterior.

The internal mandibular fenestra is ovoid, anteroposteriorly elongated, longer than the external, and dorsoventrally compressed, especially at its anterior corner. Its ventral margin is mostly formed by the angular, which also comprises its medial limit at the posterior portion. The rounded and dorsoventrally compressed anterior corner is formed exclusively by the splenial. Posterodorsally to that portion, the dentary and the surangular form the dorsal margin of the fenestra, the posteriormost portion of which is more laterally positioned in relation to the angular, at the posterior tip of the fenestra.

Choana

The choanal apertures (secondary choana *sensu* Witmer, 1995) are composed of the pterygoid, palatine, and vomer. The last two bones are tightly connected, forming the dorsal, lateral, and ventral margins of each aperture. Their medial margins are formed by the choanal septum of the pterygoid. The choanal apertures represent the posterior end of the nasopharyngeal duct (Fonseca et al., 2020), outside of which the choanal septum continues posteriorly, reaching the body of the pterygoid. This ventrally exposed part of the septum is laterally flanked by the parachoanal fenestrae, which are ovoid, mediolaterally compressed, and anteroposteriorly elongated. Each fenestra is limited anteriorly by the palatine, laterally by the ectopterygoid, posteriorly by the ectopterygoid wings of the pterygoid, and medially by a lamina of the latter bone. In fact, this lamina expands lateroventrally from the dorsal tip of the septum, leaving a depression immediately lateral to it, which corresponds to the choanal groove. Anteriorly, these sheets of bone contact the vomer above the choanal apertures.

3.7.2 | Cranial bones

Premaxilla

The premaxilla is subtriangular in lateral view, bordered posteriorly by the maxilla and dorsally by the nasal. The premaxillary process that

would presumably form the internarial bar is broken. Ornamentation on the premaxilla is concentrated on the posterodorsal part of the bone, composed of irregular ridges and thin posteroventrally to anterodorsally oriented grooves. The posteroventral margin of the premaxilla is projected posteriorly, forming the anterolateral margin of the semi-circular premaxilla-maxilla notch for the reception of the lower caniniform (D4) (Figure 6). There is a small concavity dorsal to the notch, from which an elongated groove extends anteroventrally, ending in a set of foramina slightly above the third premaxillary tooth. The perinarial fossa excavates the premaxilla posterolaterally to the external naris in the form of a smooth round concavity (Figures 7, 8). Due to preservational limitations, it is not possible to define the entire set of premaxillary foramina.

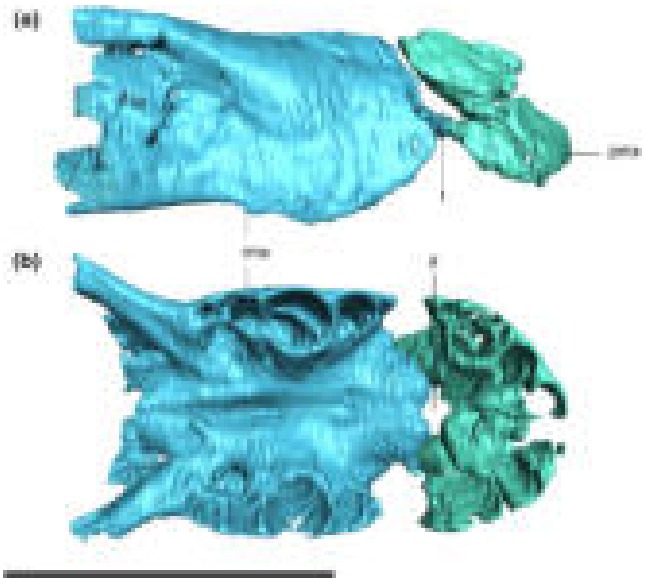

FIGURE 6 Digitally reconstructed articulation of the premaxillae and maxillae of *Aphaurosuchus escharafacies* in (a) lateral and (b) ventral views. f, foramen; if, foramen incisivum; pmx, premaxilla; rmx, posterior ramus of the maxilla. Scale bar: 10 cm

The premaxilla-maxilla suture is internalized in an anteroventrally to posterodorsally oriented notch. CT digital reconstructions of this area show the presence of a foramen laterally piercing the premaxilla-maxilla suture (Figure 6). Its exact shape is not clear due to the fragmentary preservation of this portion of the bone. In the ventral view, a rounded foramen incisivum is present on the midline contact between the premaxillae and maxillae (Figure 6). On the ventral surface, the premaxilla has a small pit posterior to the first tooth for the reception of the first dentary tooth (Figure 7).

Maxilla

The maxilla forms most of the lateral surface of the rostrum (Figures 9 and 10). It is sub-rectangular in lateral view, bordered by the jugal and the lacrimal posteriorly, by the nasal for mostly of its dorsal margin, and by the premaxilla anteriorly and anterodorsally.

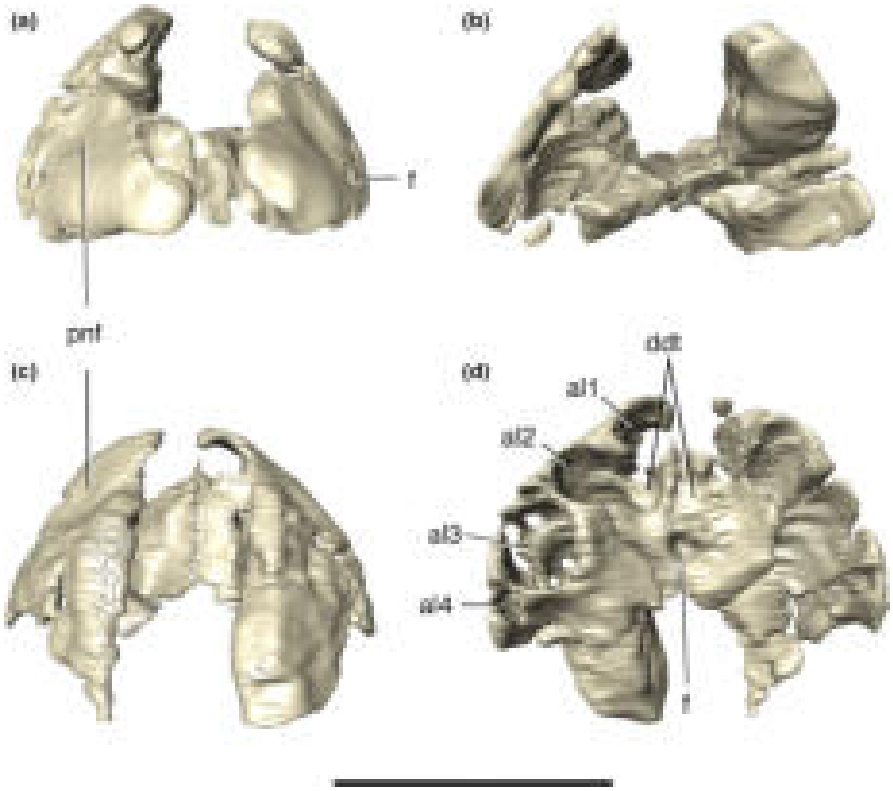

FIGURE 7 Digital reconstruction of the articulated premaxillae of *Aphaurosuchus escharafacies*. (a) anterior view. (b) posterior view. (c) dorsal view. (d). Ventral view. al1-4, alveoli; ddt, depressions for the insertion of the first dentary teeth; f, foramen; pnf, perinarial fossa. Scale bar: 5 cm

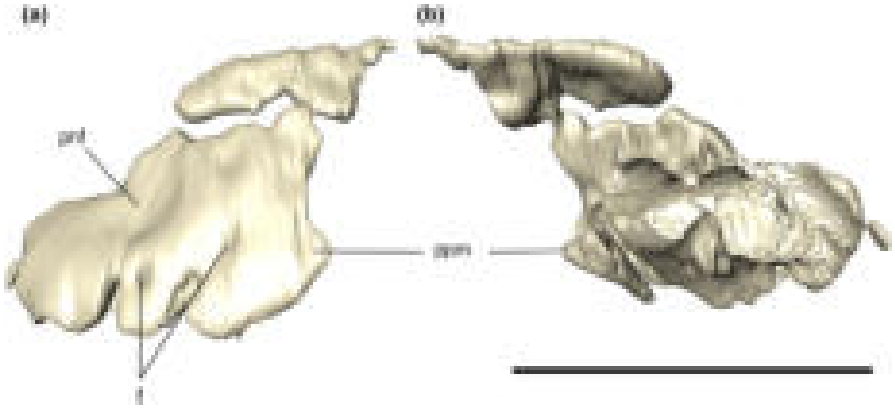

FIGURE 8 Digitally reconstructed left premaxilla of *Aphaurosuchus escharafacies* in (a) lateral and (b) medial views. f, foramen; pnf, perinarial fossa; ppm, posterior projection. Scale bar: 5 cm

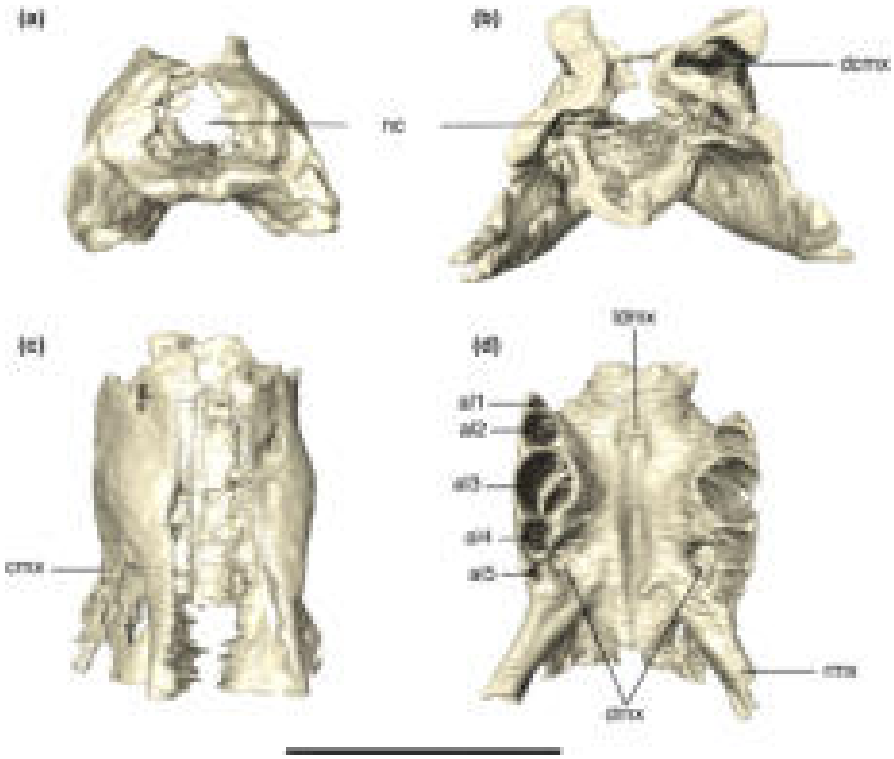

FIGURE 9 Digital reconstruction of articulated maxillae of *Aphaurosuchus escharafacies* in (a) anterior, (b) posterior, (c) dorsal, and (d) ventral views. al, alveoli; cmx, mediolateral maxillary constriction; dcmx, dorsal mediolateral maxillary constriction; dmx, depression for the insertion of dentary teeth; ldmx, midline longitudinal depression of maxillae; nc, nasal cavity; rmx, posterior ramus of maxilla. Scale bar: 10 cm

The ornamentation of the maxilla is composed of roughly vertical ridges, which extend dorsally from the small foramina near the alveolar margin. At the depressed posterior portion of the bone, the ridges are less conspicuous and more horizontally oriented, turning ventrally at their anterior ends. The maxilla-jugal suture is slightly anteroventrally to posterodorsally inclined, turning posteriorly on its ventral end. The maxilla is projected anteriorly and forms the posteroventral portion of the notch for the reception of the dentary caniniform. Posterior to the notch, the maxilla presents a bulged lateral surface that extends posterodorsally from the level of the third maxillary tooth. This is related to the alveolus of the large third maxillary tooth (m3). This bulged lateral surface extends onto the dorsal surface of the rostrum, forming a prominent lateral margin. The lateral alveolar margin possesses seven neurovascular foramina, forming a continuous line. Slightly posterior to the posteriormost maxillary tooth, the ventral portion of the bone is laterally depressed, forming a smooth surface, continuous to the jugal infraorbital depression (*sensu* Montefeltro et al., 2011).

The ventral surface of the maxilla is more lateromedially expanded at the alveolar portion. The palatal shelves of the maxillae

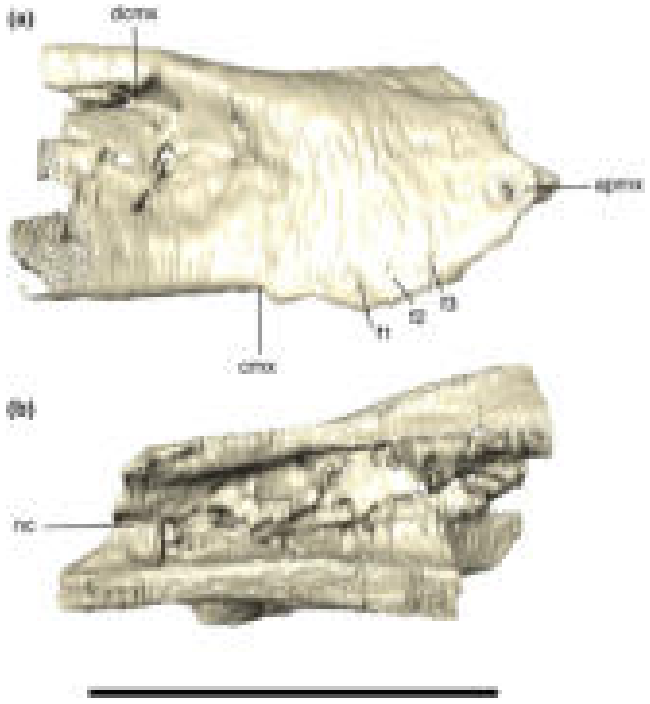

FIGURE 10 Digitally reconstructed right maxilla of *Aphaurosuchus escharafacies* in (a) lateral, and (b) medial views. apmx, anterior projection of the maxilla; cmx, mediolateral maxillary constriction; dcmx, dorsal mediolateral maxillary constriction; f, foramina; nc, nasal cavity. Scale bar: 10 cm

present a conspicuous midline longitudinal depression along the contact between both maxillae. This depression extends posteriorly to the contact with the palatines. Medial to the alveolar margin of the fourth and fifth maxillary teeth, there is a set of small circular pits for the insertion of the dentary teeth. The CT data show that the internal structure of the palatal shelves of the maxillae comprises a palatal bone, and the maxillary ramus is pneumatic at the level of the contact between the maxillae.

Nasal

The nasals are co-ossified, with no sign of suture between the paired bones (Figure 11). The pair forms a narrow and anteroposteriorly elongated element on the dorsal surface of the rostrum. Its lateral margins are roughly straight and its anterior tips are broken, but presumably formed, together with the premaxillae, the posterodorsal margin of the external nares. The nasal contacts the premaxillae, maxillae, anterior palpebrals, lacrimals, and prefrontals. Posteriorly, it is limited by the prefrontal pair, forming a small wedge between those bones. The sutures of the nasal with the prefrontals are obscured by the heavy ornamentation of the skull roof, but it is possible to see that the medial contact of the prefrontals prevents a nasal-frontal contact. In dorsal view, the anterior portion of the nasal is thinner than the posterior one, which gets wider posteriorly. The ornamentation of the nasal changes along its dorsal surface. Parallel and anteroposteriorly-directed thin grooves are present on

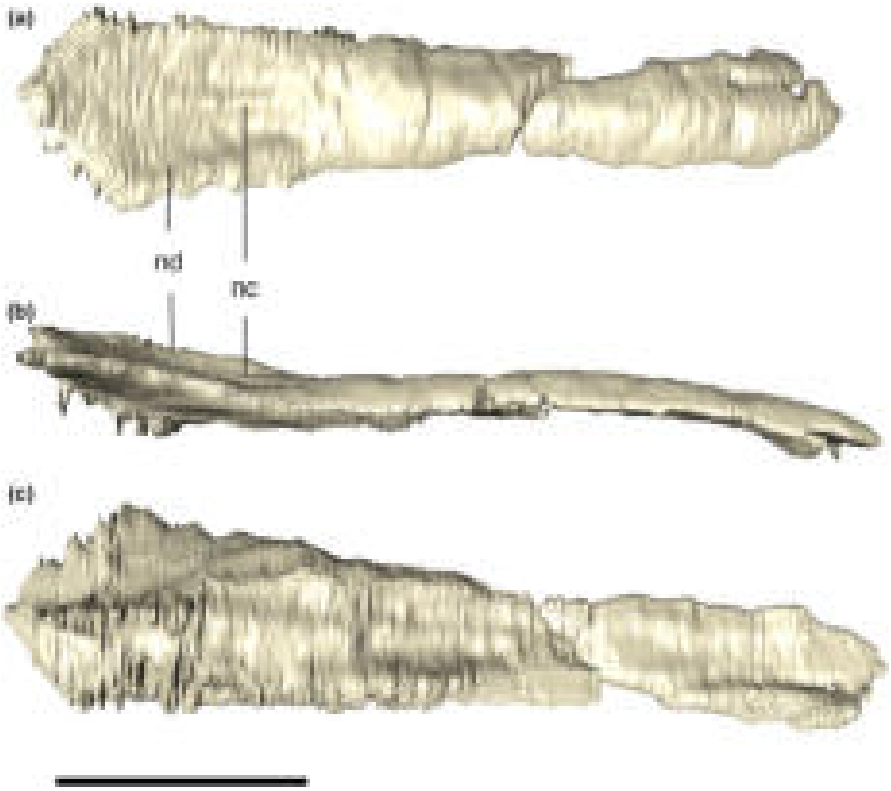

FIGURE 11 Digital reconstruction of the fused nasal of *Aphaurosuchus escharafacies* in (a) dorsal, (b) lateral, and (c) ventral views. nc, nasal crest; nd, nasal depression. Scale bar: 5 cm

its anterior portion, whereas irregular grooves are seen posteriorly. However, at the posteriormost portion of the bone, near the contact with the prefrontals, the grooves converge to the midline area of the bone. This area is marked by a short, elongated, and anteroposteriorly directed ridge, (i.e., nasal medial crest), both sides of which are flanked by an anteroposteriorly elongated depression.

The nasal is also exposed in lateral view, where the dorsal margin of the anterior portion of the bone is straight to slightly convex. The dorsal surface of the bone is posteriorly followed by a depression approximately at a level immediately posterior to the last maxillary teeth. In lateral view, posterior to the depression, near the contact with the prefrontals, the dorsal outline of the skull turns dorsally in a gradual fashion. This region is one of the highest portions of the skull roof, together with the anterior portion of the nasal and the sagittal crest formed by the parietals.

Anterior palpebral

The anterior palpebral is dorsoventrally flattened, almost triangular in dorsal view, with its lateral expansion covering most of the orbit dorsally (Figure 12). The bone lies upon the lacrimal and the prefrontal, and possesses a thin lateromedial anterior portion that contacts the posterolateral corner of the nasal. The medial margin of the anterior palpebral is rounded, covering the lateral platform for its reception, formed by the lateral expansion the prefrontal and the anterolateral margin of the frontal. Its posterior margin is slightly concave, forming the anterior border of the supraorbital fenestra, with its rounded lateral tip contacting the anteriormost portion of the posterior palpebral. The dorsal surface of anterior palpebral is slightly depressed along its medial margin. The dorsal ornamentation of the bone is stronger on its medial portion with short, smooth and lateromedially-directed grooves. The CT data reveal small canals along the lateral margin of the palpebral (better observed on the right anterior palpebral). Apart from that, the overall inner structure of the bone is solid.

Posterior palpebral

The posterior palpebral is smaller than the anterior one, and forms the posterolateral margin of the supraorbital fenestra. The bone is rounded in dorsal view, covering the posterior portion of the orbit. Its lateral portion is more anteroposteriorly expanded than its medial portion and it is also slightly inclined ventrally (Figure 13). The posterior palpebral contacts the postorbital posteriorly, fitting into the concave anterolateral surface of that bone. The posterior palpebral ornamentation consists of irregular grooves on the dorsal and lateral surfaces. As in the anterior palpebral, the CT scan shows the posterior palpebral as a solid bone, with four main internal canals, two of which are close to one another, and the remaining two positioned at the lateral surface of the bone.

Prefrontal

The prefrontal is roughly triangular in dorsal view, with its dorsal surface convex, and forming one of the highest portions of the skull roof, reaching the same level of the sagittal crest of the parietal. Its posterior portion is lateromedially compressed and tapering to a tip (Figure 14). The medial margin of the prefrontal converges towards its anteroposterior midline, touching its antimere and preventing the frontal-nasal contact at midline. The lateral portion of the prefrontal forms, together with the lacrimal, the platform that supports the anterior palpebral. On its entire

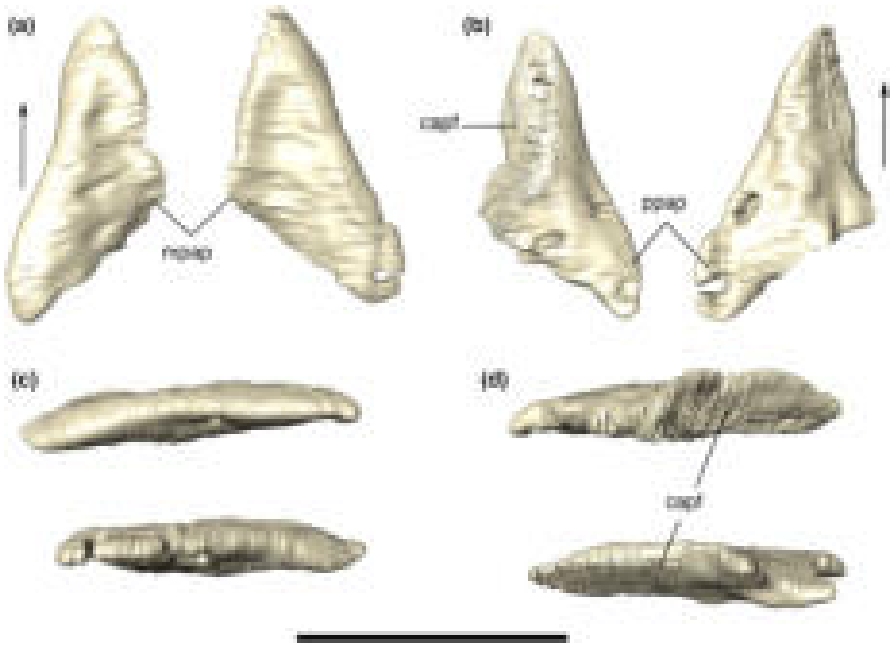

FIGURE 12 Digital reconstruction of the left and right anterior palpebrals of *Aphaurosuchus escharafacies* in (a) dorsal, (b) ventral, (c) lateral, and (d) medial views. Arrows indicate anterior direction. capf, contact area with the prefrontal; mpap, medial projection of the anterior palpebral; ppap, posterior projection of anterior palpebral. Scale bar: 5 cm

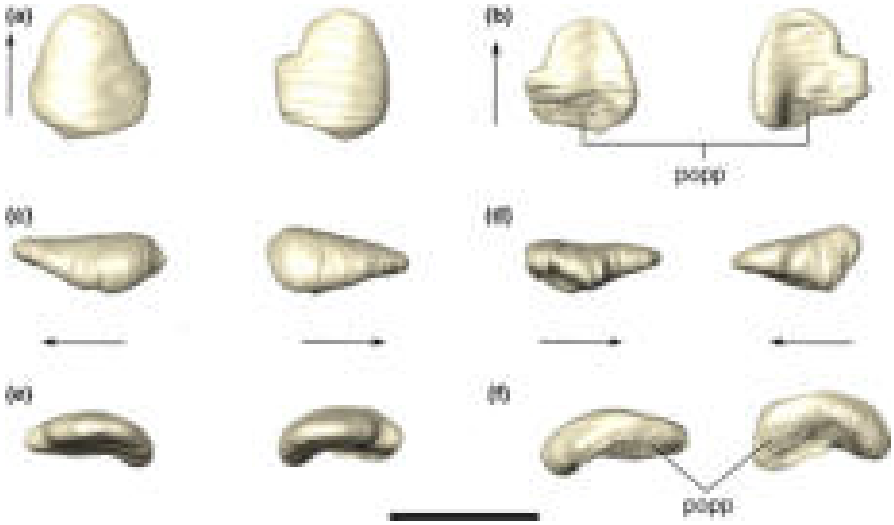

FIGURE 13 Digital reconstruction of the left and right posterior palpebrals of *Aphaurosuchus escharafacies* in (a) dorsal, (b) ventral, (c) lateral, (d) medial, (e) anterior, and (f) posterior views. Arrows indicate anterior direction. popp, postorbital contact area with the posterior palpebral. Scale bar: 3 cm

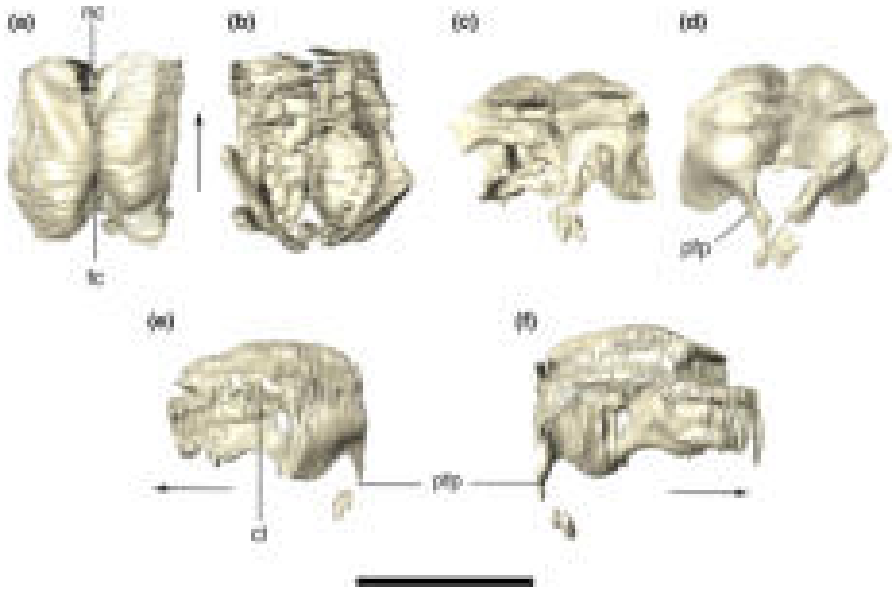

FIGURE 14 Digital reconstruction of the left and right prefrontals of *Aphaurosuchus escharafacies* in (a) dorsal, (b) ventral, (c) anterior, (d) posterior, (e) left lateral, and (f) left medial views. Arrows indicate anterior direction. cl, contact with the lacrimal; fc, area of contact with the frontal; nc, area of contact with the nasal; pfp, prefrontal pillar. Scale bar: 5 cm

dorsal surface, the prefrontal is highly ornamented by irregular grooves. CT data allow the visualization of the prefrontal pillar. This element projects medioventrally from the ventrolateral portion of the prefrontal (e.g., anterior inner surface of the orbit). The ventralmost tip of the prefrontal pillar faces slightly laterally, giving the structure a medially curved outline. Also, this tip contacts ventrally a small anterodorsal portion of the pterygoid.

Lacrimal

The lacrimal has a subrectangular shape in lateral view, with smooth ornamentations mainly covering its posterodorsal surface. The lacrimal fits into the anterior portion of the anterior process of the jugal, forming the anterior and anterodorsal borders of the orbit. It contacts the maxilla anteriorly, via an almost straight and interdigitated suture. This lacrimal-maxillary suture is inclined posteriorly at its dorsalmost portion. Dorsally, the lacrimal forms the lateral portion of the platform for the support of the anterior palpebral (Figure 15). The anterior margin of the lacrimal is ridged, as an anterodorsal extension of the crested portion of the jugal. The posterior margin of the lacrimal forms the anterior margin of the orbit. The CT data reveal a small and circular lacrimal duct positioned just above the posterior part of the jugal suture. Furthermore, a medial contact between the lacrimal and the laterodorsal portion of the prefrontal pillar is also revealed by the CT data.

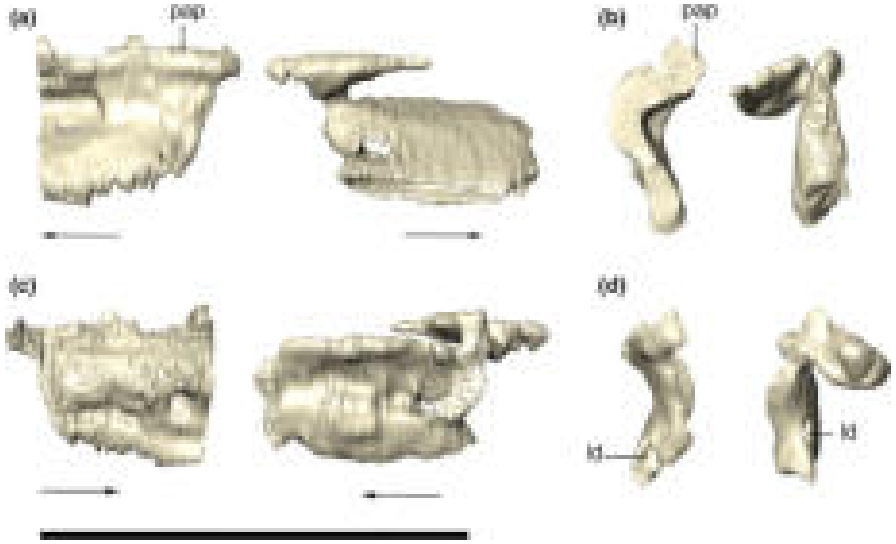

FIGURE 15 Digital reconstruction of the left and right lacrimals of *Aphaurosuchus escharafacies* in (a) lateral, (b) anterior, (c) medial, and (d) posterior views. Arrows indicate anterior direction. ld, lacrimal duct; pap, platform for the anterior palpebral. Scale bar: 5 cm

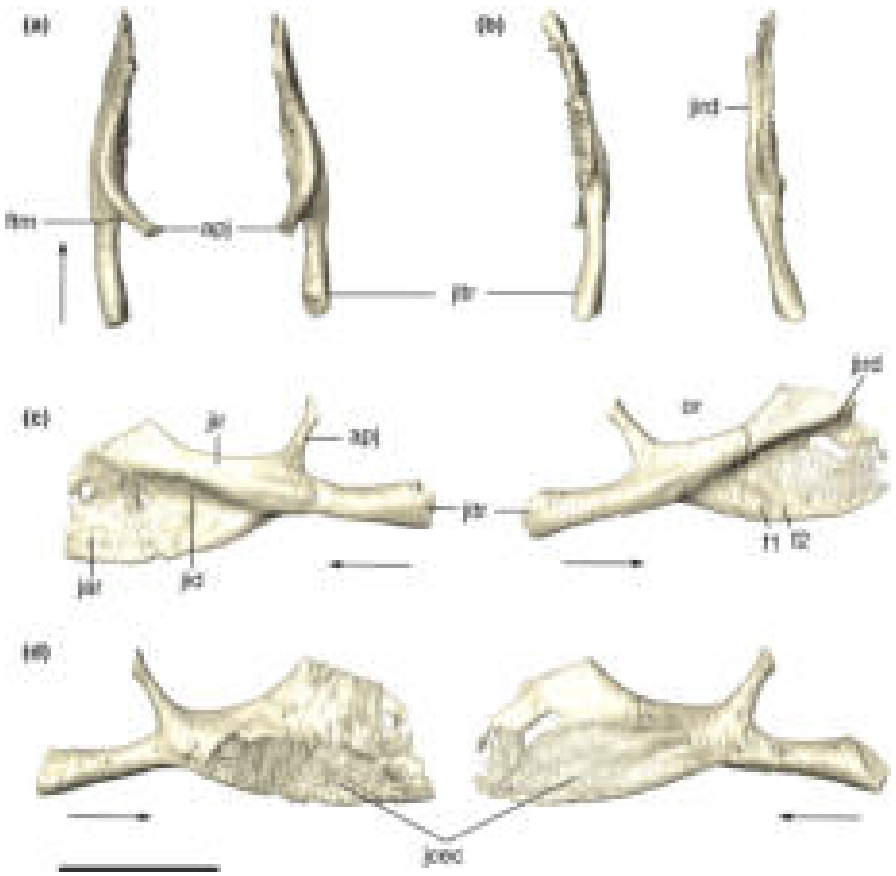

FIGURE 16 Digital reconstruction of the left and right jugals of *Aphaurosuchus escharafacies* in (a) dorsal, (b) ventral, (c) lateral, and (d) medial views. Arrows indicate anterior direction. apj: ascending process of the jugal; f1-2, foramina; ftm, foramen for the maxillary ramus of the cranial trigeminal nerve; jar, jugal antorbital ramus; jcec, jugal medial contact with ectopterygoid; jid: jugal infraorbital depression; jir, jugal infraorbital ramus; jird, jugal infraorbital ridge; jitr: jugal infratemporal ramus; or, orbit. Scale bar: 5 cm

Jugal

The jugal is a triradiated and heavily ornamented bone, forming part of the borders of the orbit and the infratemporal fenestra. In dorsal view, the lateral outline of the jugal is convex, with the posterior portion more laterally positioned (Figure 16). The anterior (infraorbital) ramus of the jugal forms the ventral margin of the orbit and contacts the posterior margin of the maxilla. This forms an anteriorly convex suture, in the ventral portion of which, the jugal briefly

overlaps the maxilla laterally. Dorsal to that, there is a triple contact between jugal, lacrimal, and maxilla. The infraorbital ramus of the jugal gradually expands dorsoventrally as it extends anteriorly, so that the antorbital portion is twice the depth of the posterior (infratemporal) ramus, in lateral view. A longitudinal infraorbital ridge extends posteroventrally from the lacrimal suture until the infraorbital ramus of the jugal, separating the body of the bone into dorsal and ventral portions. The dorsal portion is lateromedially narrow and somewhat continuous to the infratemporal portion of the bone. Ventral to the jugal infraorbital ridge, there is a well-marked jugal infraorbital depression (Montefeltro et al., 2011). At this region, the jugal has its most lateromedially-flattened portion. This surface is slightly concave dorsoventrally and ornamented with elongated anteroventrally directed thin grooves. These grooves tend to become shorter and closer to one another posteriorly. The ventralmost surface of the infraorbital ramus bears a series of foramina, varying from small circular openings to oval and anteroposteriorly elongated ones.

The ascending process of the jugal is cylindrical, extending dorsomedially from the main body of the bone and turning slightly posteriorly at is dorsalmost portion. It lacks any kind of ornamentation and connects with the ventral process of the postorbital. This forms the postorbital bar, which separates the orbit from the infratemporal fenestra. The foramen for the entrance of the maxillary ramus of the cranial trigeminal nerve pierces the posteroventral portion of the ascending process of the jugal (Figure 16a).

The infratemporal ramus, of the jugal is cylindrical, composing almost the entire ventral border of infratemporal fenestra and posteriorly articulating with the quadratojugal via a verticalized, interdigitated suture. Its dorsal surface bears large, transversally elongated grooves. The shape of this ramus is somehow maintained forward, along the dorsal portion of the anterior ramus of the bone, reaching the lacrimal suture anteriorly. The transition between the ventral margins of the infratemporal and infraorbital rami is marked by a gradual increase of the dorsoventral depth of the latter ramus anteriorly. CT data show the medial contact with the ectopterygoid, which occurs along the entire medial antorbital surface of the jugal, forming a slightly upper lifted ventrolateral border. There is a series of foramina along the entire internal surface of the jugal, except forits antorbital portion, especially on the cylindrical portion or the posterior ramus.

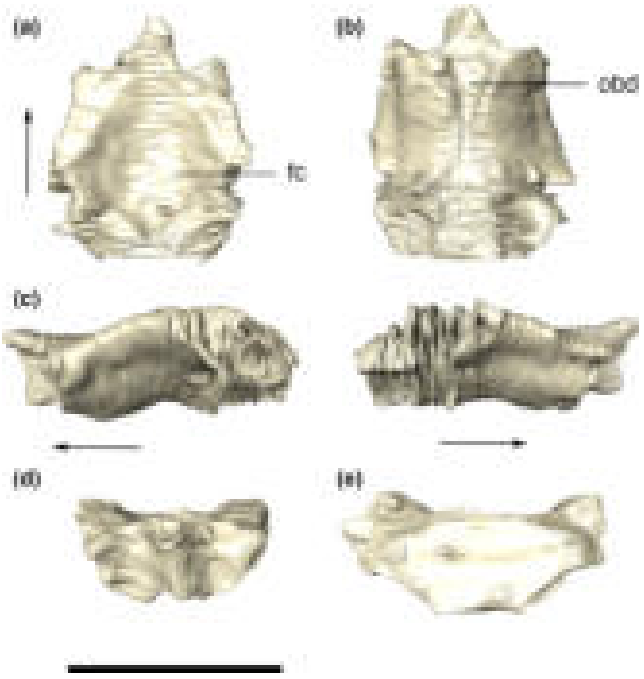

FIGURE 17 Digital reconstruction of the fused frontals of *Aphaurosuchus escharafacies* in (a) dorsal, (b) ventral, (c) left and right lateral, (d) anterior, and (e) posterior views. Arrows indicate anterior direction. fc, frontal concavity; obd, olfactory bulb depression. Scale bar: 5 cm

Frontal

The frontals are fused into a single element that forms an overall dorsally concave structure. The bone contacts the posterior portion of the prefrontals anteromedially, and the anterior palpebrals laterally. It also participates in the external supraorbital fenestrae and fossae posteriorly. The frontal contacts the anteromedial margin of the postorbitals posterolaterally and its posterior margin contacts the parietal. The anterior part of the dorsal surface of the bone, near the contact with the prefrontals, is elevated in relation to the posterior portion. Also, this anterior portion is narrower lateromedially. In dorsal view, the frontal gradually widens posteriorly, reaching its maximum width at the anteriormost contact with the postorbitals. At its posteriormost contacts with the postorbitals, the frontal forms a posterior wedge, which enters the anteromedial supratemporal fossae. Along the sagittal line, the dorsal surface of the frontal is mostly smooth, and lacks a longitudinal crest, presenting instead reduced, inconspicuous and scattered pebbled ornamentations (Figure 17).

The borders of the frontal are elevated in relation to its central portion and the ornamentation of its dorsal surface is not as conspicuous as that of the remaining bones of the skull roof. However, irregular grooves are present on the elevated portions of the bone, bordering the central portion. The CT data reveal that the ventral surface of the frontal has a sagittal depression traversing the bone, which is inferred to represent the depression for the crista cranii and olfactory bulbs.

Postorbital

The postorbital is subtriangular in dorsal view, participating in the anterolateral border of the supratemporal fossae and fenestrae. The bone is composed of two portions: a rugose dorsal part, forming the anterolateral corner of the skull roof, and a smooth ventral ramus that participates in the meatal chamber (Figure 18). The dorsal surface of the former is slightly convex, highly ornamented, as in the pattern of grooves and ridges present on the squamosal, and gradually changing the pattern for a smooth ornamentation more anteriorly. The ventral surface of the dorsal portion is markedly concave and continuous to the quadrate anterodorsal process in the meatal

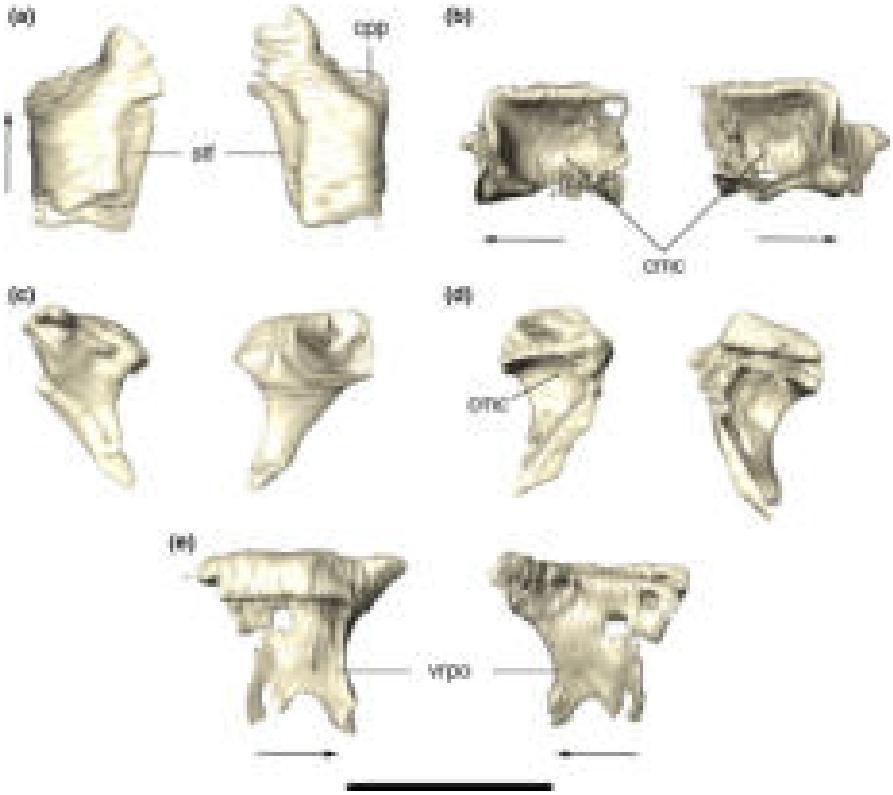

FIGURE 18 Digital reconstruction of the left and right postorbitals of *Aphaurosuchus eschrafacies* in (a) dorsal, (b) ventral, (c) anterior, (d) posterior, and (e) right postorbital in lateral and medial views. Arrows indicate anterior direction. cmc, ventral concavity of postorbital composing the meatal chamber; cpp, contact area with posterior palpebral; stf, anterolateral margin of the supratemporal fenestra; vrpo, ventral ramus of postorbital. Scale bar: 5 cm

chamber. Posteriorly, the postorbital-squamosal suture is slightly curved anteriorly, and both bones form the posterolateral margin of the skull roof. The anterolateral corner of the postorbital is slightly concave to receive the posterior palpebral. Anteromedially, the postorbital is connected to the frontal by an interdigitated suture at the anterior border of supratemporal fenestra. A restricted portion of the supraorbital fenestra margin is formed by an anterolateral extension of the dorsal surface of the postorbital. In lateral view, the ventral ramus of the postorbital extends ventrally and bifurcates, in which its anterior ramus contacts the ascending process of the jugal, forming the dorsal portion of the postorbital bar between the orbit and the infratemporal fenestra. The posterior part of the bifurcation meets the quadratojugal, forming the posterior border of the infratemporal fenestra. The contact with the quadratojugal extends along the entire posterior margin of the ventral ramus of the postorbital. CT data reveal that the postorbital is lateromedially traversed by a number of aligned canals. Some of these invade the surrounding bones, such the squamosal and the frontal, and likely represent passages of nerves and blood vessels.

Quadratojugal

The quadratojugal occupies the posterolateral surface of the skull, positioned posterior to the infraorbital fenestra and partially covered dorsally by the laterodorsal expansions of the postorbital and squamosal. The main body of the quadratojugal in posterior view is ventrolaterally to dorsomedially inclined, and shorter anteroposteriorly than dorsoventrally in lateral view (Figure 19). Ornamentation is restricted to the most lateralized portion of the bone, mainly near the contact with the posterior process of the jugal, where elongated sub horizontal, and thin grooves are present. The grooves gradually bow dorsally at the posterior margin of the infratemporal fenestra. The suture with the jugal is interdigitated and verticalized, whereas the suture with the quadrate is irregular, but also verticalized, extending dorsally until the postorbital-squamosal suture. The anterodorsal suture with the ventral ramus of the postorbital is posteriorly convex, reaching the infratemporal fenestrae ventrally, posteriorly to the dorsal tip of the fenestra.

The ventral portion of the quadratojugal is posteriorly expanded, with a pointed posteroventral corner. It does not form a continuous ventral margin with the quadrate, but a notch is instead seen at the contact between those bones. The lateral surface of the base of the quadratojugal bears an anteroventral extension of the quadrate depression (Figure 20). Right above this smooth depression, the quadratojugal becomes convex on its lateral ornamented surface. The ornamentation of this area could be related to the insertion of *m. leavator bulbi* (Larsson & Sues, 2007; Montefeltro et al., 2011). Dorsal to this area, the anterior part of the bone turns anteromedially, where it forms part of the posterior margin of the infratemporal fenestra, contacts the posteroventral ramus of the postorbital and enters the meatal chamber. This area becomes

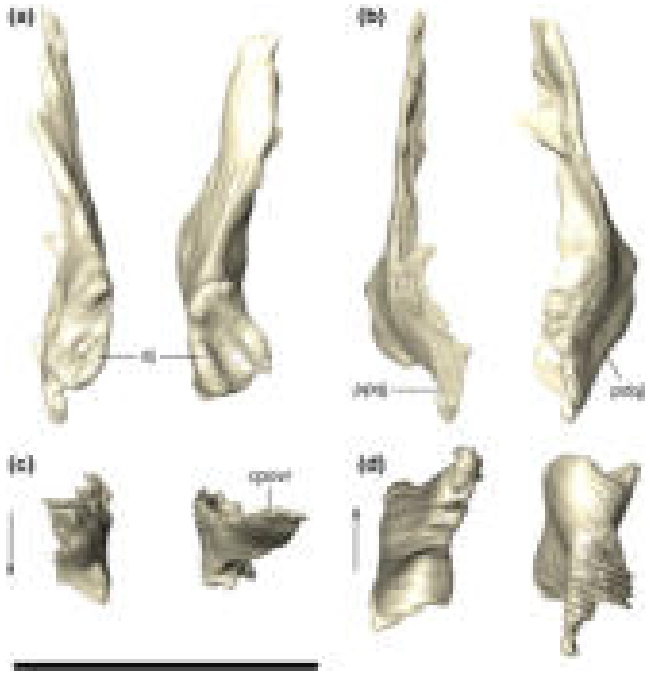

FIGURE 19 Digital reconstruction of the left and right quadratojugals of *Aphaurosuchus escharafacies* in (a) anterior, (b) posterior, (c) dorsal, and (d) ventral views. Arrows indicate anterior direction. aj, articulation area with the jugal; cpovr, contact with the ventral ramus of the postorbital; ppqj, posteroventral pointed tip of the quadratojugal; pdqj, posteroventral depression of the quadratojugal. Scale bar: 5 cm

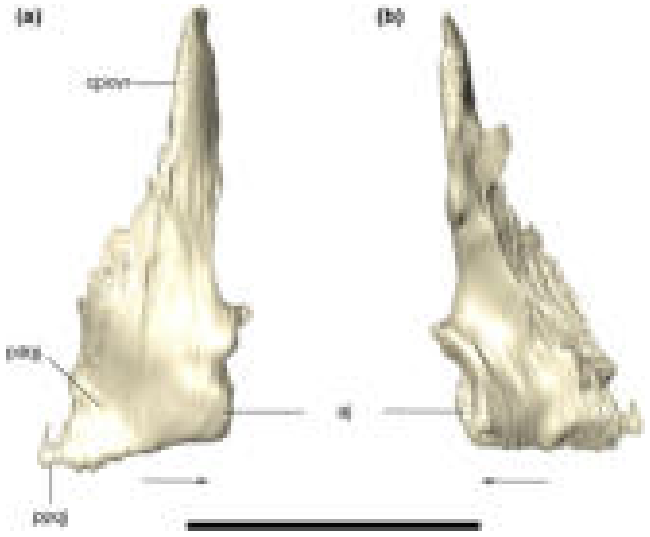

FIGURE 20 Digitally reconstructed right quadratojugal of *Aphaurosuchus escharafacies* in (a) lateral, and (b) medial view. Arrows indicate anterior direction. aj, articulation area with the jugal; cpovr, contact with the ventral ramus of the postorbital; ppqj, posteroventrally-pointed tip of the quadratojugal; pdqj, posteroventral depression of the quadratojugal. Scale bar: 5 cm

lateromedially flatter and the outer ornamentation is inconspicuous. The quadratojugal also forms the posteroventral corner of the infratemporal fenestra.

The CT data reveal that the quadratojugal is a pneumatized bone, bearing three conspicuous ventrally located diverticulae. The largest one is at the ventralmost portion of the bone, near the contact with the quadrate, and seems to be an extension from this diverticulum in the quadrate. The smaller diverticulae, are more superficial and possibly continuous to the foramina seen at posterior ramus of the jugal. The laminar (i.e., mediolaterally thin) ascending portion of quadratojugal entering the meatal chamber is not pneumatic.

Quadrate

The quadrate is verticalized, longer dorsoventrally than anteroposteriorly, slightly inclined medially at the dorsal portion, and forming the posterolateral margin of the skull. It participates on the jaw joint, contacting the articular ventrally via two articular condyles. In posterior view, the lateral condyle is more expanded ventrally and the surface between the two condyles is concave, dorsal to which the quadrate forms the stout structure that extends dorsally and attaches to the lateral wall of the neurocranium, squamosal, and paroccipital process. The quadrate-squamosal contact extends laterally which is anterodorsally to posteroventrally oriented along the entire posterodorsal margin of the quadrate. In lateral view, there is a notch at the contact with the posteroventral portion of the quadratojugal (Figures 3 and 4).

The lateral surface of the quadrate lacks ornamentation and most of its ventral portion is occupied by the quadrate depression (sensu Montefeltro et al., 2011), which also expands forward into the quadratojugal. Dorsally, in the meatal chamber, the lateral surface of the quadrate is marked by the bony otic aperture (sensu Montefeltro et al., 2016). Anteriorly to that, the bone is as laterally expanded, with this surface narrowing anteroposteriorly, as it is dorsally. Posterior to that narrower portion, the bone surface slightly turns medially, comprising an internalized periotic fossa. This fossa is pierced by a small and elliptical subtympanic foramen, in the left quadrate, anterodorsally to the otic incisure, whereas in the right element, a slightly larger foramen can be observed more ventrally, which probably represents a different subtympanic foramen. (Figure 21).

The ventral portion of the quadrate forms the posterolateral part of the basicranium, contacting the paroccipital process, basioccipital, parabasisphenoid, and pterygoid via interdigitated sutures, and represents an attachment surface for the mandibular adductor muscles (Iordansky, 1973; Montefeltro et al., 2020). Unlike the contact with the paroccipital process, the quadrate suture with the basioccipital is marked by a crest, which does not continues ventrally along the medial surface of the quadrate. Other quadrate crests described by Iordansky (1973) are also recognized in *Aph. escharafacies*. Crest A corresponds to an elongated straight crest that extends along the anteromedial surface of the bone, parallel and slightly posterior to the quadratojugal suture and associated to the insertion of the *m. adductor mandibulae externus superficialis*. Two other roughly parallel crests are seen on the anterolateral contact of the quadrate with the pterygoid, the crest B is more marked medially and merges gradually with the remaining surface of the quadrate laterally, while the crest B' is more conspicuous and extends dorsally to the most

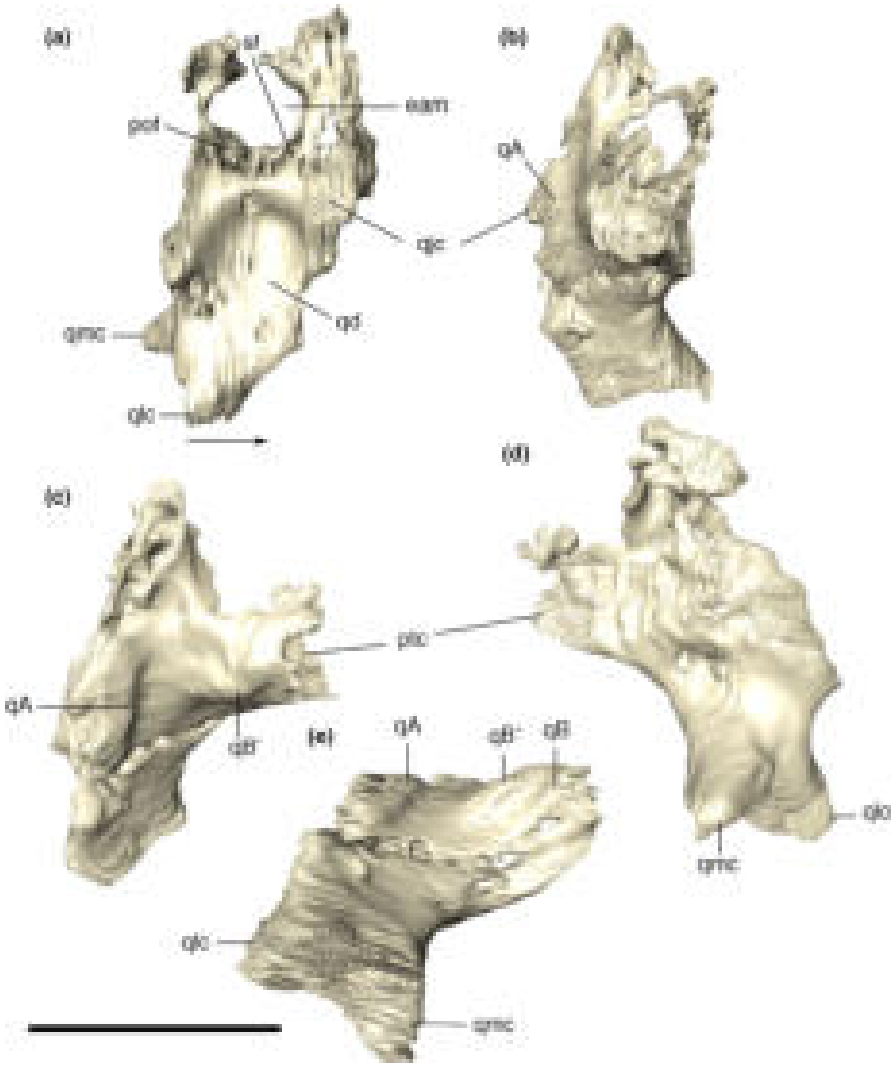

FIGURE 21 Digitally reconstructed right quadrate of *Aphaurosuchus escharafacies* in (a) lateral, (b) medial, (c) anterior, (d) posterior, and (e) ventral views. Arrow indicates anterior direction. eam, external auditory meatus; pof, periotic fossa; ptc, pterygoid contact; qA, ventral quadrate crest (crest A) for the insertion of *M. adductor mandibula externus superficialis*; qB, ventral quadrate crest (crest B) for the insertion of *M. ad. mand. ext. medialis*; qB', ventral quadrate crest (crest B') for the insertion of *M. ad. mand. posterior*; qd, quadrate depression; qjc, quadratojugal contact; qlc, quadrate lateral condyle; qmc, quadrate medial condyle; sf, subtympanic foramen. Scale bar: 5 cm

lateral portion of crest B. These crests are related to the insertions of *mm. adductor externus medialis* and *adductor mandibulae posterior*, respectively.

CT data show that the internal surface of the quadrate is highly pneumatic, except for the more massive condylar portion of the bone. The images also reveal aspects of the meatal chamber, such as the internalized subtympanic foramina, which are ventrally displaced relative to the dorsalmost one, which is visible externally. Finally, an anteroposteriorly reduced dorsal otic incisure is also observed, and the posterior limit of the bony otic aperture is positioned near the squamosal suture.

Squamosal

The squamosal is an "L-shaped" bone composed of a main anteroposteriorly elongated body and the verticalized squamosal prong, which projects ventrally from the posterior part of the main body. The bone occupies the posterodorsal portion of lateral surface of the skull and the laterodorsal portion of the occipital wall. In dorsal view, the posterior portion of the squamosal is more mediolaterally expanded. In lateral view, it has a sigmoid ventral outline and a slightly convex dorsal margin. Anteriorly, the squamosal contacts the posterior portion of the postorbital via a slightly anteriorly convex (in lateral view) suture. The dorsomedial portion of the squamosal forms the posterolateral wall of the supratemporal fenestra, contacting the parietal medially via a sigmoid (in posterior view) suture (Figure 22). At the posterior portion of the supratemporal fossa, the lateromedially elongated tempororbital foramen is positioned at the squamosal-parietal suture. In dorsal view, posterior to the supratemporal fossa, the squamosal-parietal suture is anteromedially to posterolaterally oriented.

The ventral margin of the anterior ramus of the squamosal is sigmoid, and enclosing the meatal chamber dorsally. At the posterior

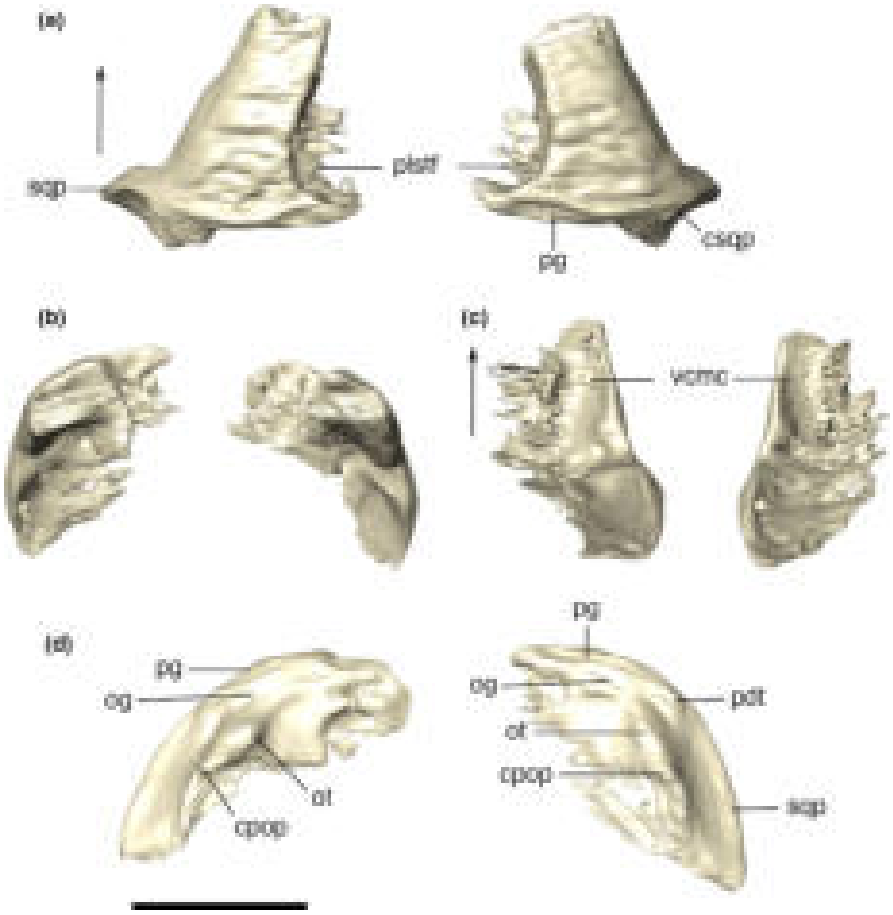

FIGURE 22 Digital reconstruction of the left and right squamosals of *Aphaurosuchus escharafacies* in (a) dorsal, (b) anterior, (c) ventral, and (d) posterior views. Arrows indicate anterior direction. cpop, contact with the paroccipital process; csqp, posterior concavity of the squamosal prong; og, occipital groove; ot, occipital tuber; pdt, posterodorsal tuber; pg, posterodorsal groove; plstf, posterolateral wall of the supratemporal fenestra; sqp, squamosal prong; vcmc, ventral concavity of the meatal chamber. Scale bar: 5 cm

portion, the squamosal has a marked ventral inflexion, forming the squamosal prong. The prong forms a right angle with the anterior ramus of the bone, corresponding to the posterior margin of the skull in lateral view.

The posterior surface of the squamosal forms most of the lateral portion of the occipital wall, due to the main lateromedial orientation of the prong (Figure 23). That surface is somewhat concave and its ventralmost portion expands laterally beyond the level of the lateral extension of the dorsal portion. In posterior view, the medial suture of the prong with the supraoccipital and the paroccpital process starts sub horizontal, ventral to the lateral half of the dorsal margin of the supraoccipital, then extending ventrally until the ventral triple contact among squamosal, supraoccipital, and the paroccipital process. Lateral to this point, the suture extends as a nearly straight line to the ridged and bulged area at the dorsolateral corner of the paroccipital process. From this bulged area, the suture extends ventrally until it reaches the contact with quadrate.

In the transition from the dorsal to the posterior surface of the squamosal, there is a horizontal rugose groove with elevated borders, the posterodorsal groove, starting lateral to the upper limit of the squamosal-supraoccipital suture. This groove is slightly curved posteriorly and it ends up laterally in a small, posteriorly-pointed posterodorsal tuber. Another depression is present on the posterior surface of the squamosal prongs, the occipital groove. It is smoother and positioned right below the posterodorsal groove. In posterior view, the occipital groove arches dorsally, ending laterally in a conspicuous occipital tuber. The surface below the occipital groove is flattened, whereas lateral to that, the lateralmost portion of the posterior surface of the squamosal prongs is depressed, and becomes gradually more convex ventrally (Figure 22b). The lateral surface of the squamosal prong is dorsoventrally convex and gradually becomes anteroposteriorly narrower ventrally.

CT data the medial participation of the squamosal in the margin of the supratemporal fenestra, which extends ventrally until the contact with the medial portion of the quadrate. There is a series of foramina on the dorsal part of the internal surface of the bone, right below a conspicuously more solid portion.

Parietal

The parietals are fused to one another, forming the posterior portion of the skull roof and the medial margin of the external and internal supratemporal fenestrae (interfenestral bar). The CT scan

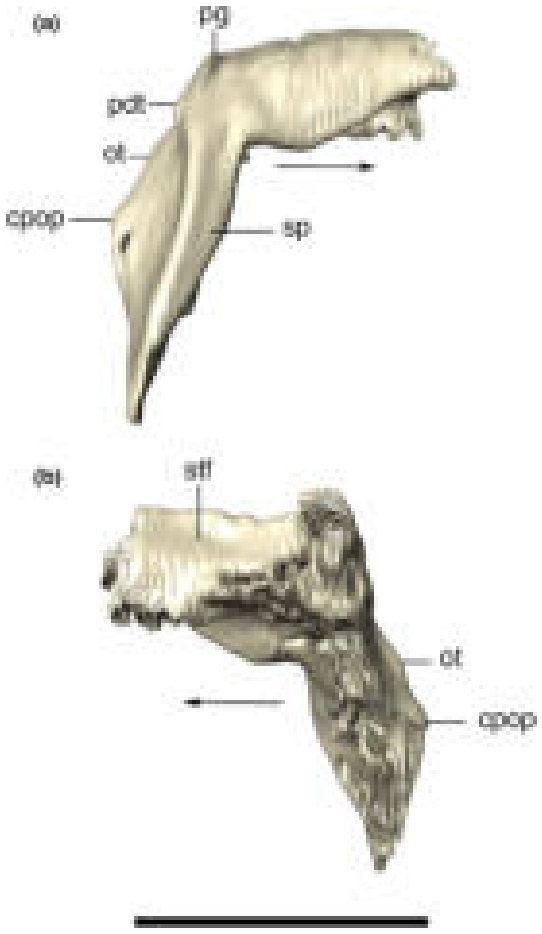

FIGURE 23 Digital reconstruction of the right squamosal of *Aphaurosuchus escharafacies* in (a) lateral, and (b) medial views. Arrows indicate anterior direction. cpop, contact with the paroccipital process; ot, occipital tuber; pdt, posterodorsal tuber; pg, posterodorsal groove; sp, squamosal prong; stf, supratemporal fenestra. Scale bar: 5 cm

images show a solid bone lacking foramina. Along its posterior margin, the parietal contacts the supraoccipital on a nearly straight line. Laterally, the parietal contacts the squamosals via irregular sutures that extend anteroposteriorly on the posterior part of the supratemporal fossae, in which a dorsoventrally compressed and mediolaterally elongated tempororbital foramen (see Squamosal) is present on each side. Anterolaterally, the parietal contacts the postorbitals at the anteromedial surface of the supratemporal fossae. The dorsal surface of the parietal is "T-shaped," with an ornamentation composed of small and inconspicuous grooves. It is thin and crest-shaped along its entire anteroposterior extension, lacking a conspicuous sagittal sulcus (Figure 24). The lateral surfaces of the parietal that compose the supratemporal fossae is smooth, lacking ornamentations except for thin irregular ridges located below the interfenestral bar and towards the tempororbital foramina.

Laterosphenoid

The laterosphenoid is a solid, but relatively slender bone only accessible with the CT data. It is located ventral to the frontal-parietal contact and meets the dorsal surface of the pterygoid. Each laterosphenoid is obliquely oriented, with the capitate process more laterodorsally-positioned in relation to the constricted ventral midline portion that contacts the pterygoid. This process contacts the ventrolateral portion of the frontal, so that the laterosphenoid pair has a general "V shape" in anterior view (Figure 25). The ventral surface is lateromedially constricted and covers the anterior portion of the olfactory bulb, anteriorly, and contacts the dorsal surface of the parabasisphenoid ventrally. From the lateral margin of the capitate process, each laterosphenoid possesses a ventrally expanded lateral bridge (*sensu* Holliday & Witmer, 2009), which is slightly curved anteriorly at its ventralmost tip, forming an anterior bulge. Each bulge is positioned almost parallel to its pair and posteroventral to the lateral margin of the cultrifom process of the parabasisphenoid. Posteriorly to this portion, the lateral bridge forms the anterodorsal margin of the trigeminal foramen. The posterior margin of the foramen is formed by a bone surface that we interpret as part of the prootic, which consists in a marked change in lateral surface slope extending dorsally from the posterior margin of the trigeminal aperture, arguably making the contact between the bones. Although no clear suture is observed in *Aph. escharafacies*, in modern crocodylians, the prootic is known to extend posteriorly from the posterior margin of the trigeminal foramen (Iordansky, 1973).

Supraoccipital

The supraoccipital is an anteroposteriorly restricted bone, with a subtriangular outline in posterior view, and forming the dorsomedial part of the occipital wall. The CT data reveals two parasagittal internal spaces that extend inside the supraoccipital, and gradually reduce in size until its complete closure at the anterior contact with the parietal. We suggest that these parasagittal spaces are pneumatic diverticula, which we tentatively homologize here to the ottocipital diverticulum present in extant forms (Dufeau & Witmer, 2015). However, we were not able to assess the possible presence of an intertympanic diverticulum (*Antrum mastoideum*) anteriorly connecting to the intertympanic sinus. The dorsal surface of the supraoccipital shows similar ornamentation of small pits present in the posterior portion of the parietal. The supraoccipital posterior surface is mostly flat and ornamented by thin, dorsoventrally-directed ridges and (Figure 26), as well as a few additional irregular ridges and grooves. The occipital surface of the supraoccipital bears an inconspicuous crest that almost reaches the ventral margin of the bone, which probably served for the insertion of nuchal ligaments.

The supraoccipital contacts the parietal anteriorly via a slightly posteriorly concave suture. It contacts the squamosal posterolaterally via a suture that, as seen in posterior view, extends lateromedially at its medial portion and turns ventrally towards the triple contact between these bones and the paroccipital process. In posterior view, the supraoccipital tappers ventrally and contacts the dorsal portion of the vertical suture that separates both paroccipital processes.

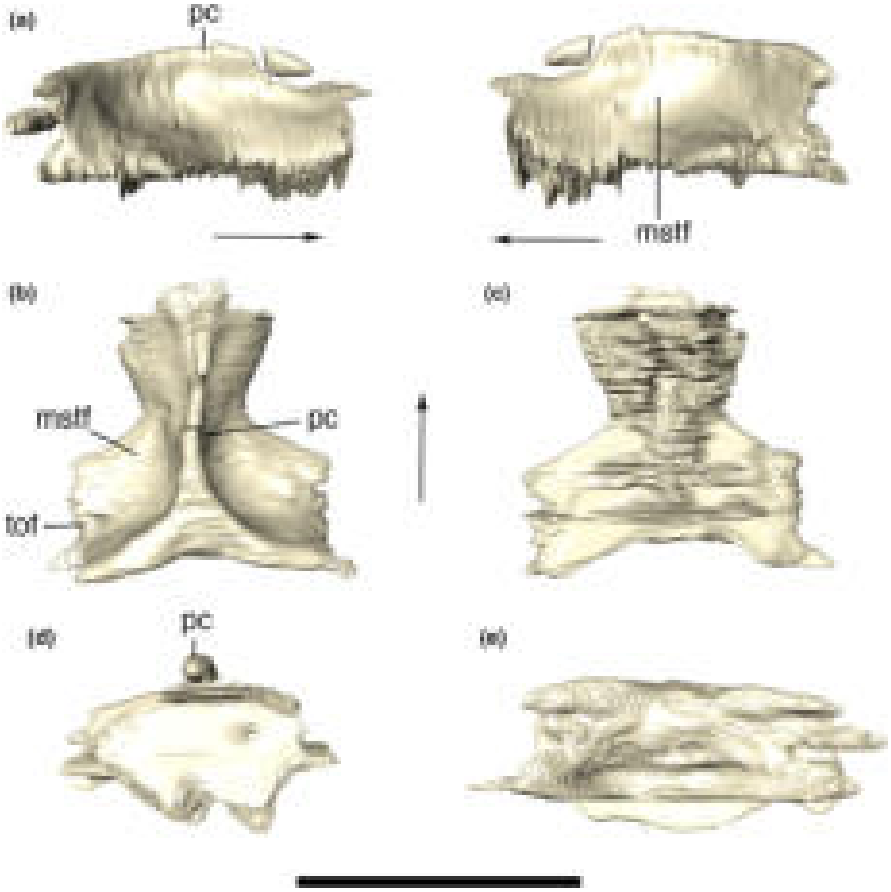

FIGURE 24 Digital reconstruction of the fused parietals of *Aphaurosuchus escharafacies* in (a) right and left lateral, (b) dorsal, (c) ventral, (d) anterior, and (e) posterior views. Arrows indicate anterior direction. mstf, medial wall of the supratemporal fossa; pc, parietal crest; tof, temporoorbital foramen. Scale bar: 5 cm

Otoccipital and Paroccipital process

The exoccipital and opisthotic are fused into the otoccipital bone, which forms a lateromedially elongated portion of the occipital wall. Each element meet one another at the midpoint above the foramen magnum, via a vertical suture and expands dorsolaterally from that suture, attaching to the ventral limit of the supraoccipital (Figure 27). Lateral to the suture, each otoccipital forms a subtriangular dorsal tip, lateral to which the elements remain sutured laterodorsally to the supraoccipital and the squamosals. Internally, the ottocipital, including the paroccipital process, is highly pneumatic, which we tentatively homologized to expansions of the ottocipital diverticulum. The bone is compact at its posteriormost portion, which forms the occipital wall. The ottocipital extends laterally forming the paroccipital process, which contacts the quadrate and squamosal. Ventral to the lateralmost contact with the squamosal (by the occipital tuber), the suture between these two bones continues vertically until the contact with the quadrate. From that point on, the suture with the quadrate extends ventromedially, until it reaches the triple contact between both bones and the basioccipital. The contact with the basioccipital is marked by a small protuberance. From this point on, the suture continues dorsomedially, where the otoccipital participates in the dorsolateral surface of the occipital condyle (Figure 28).

Basioccipital

The basioccipital composes the ventralmost portion of the occipital wall at its midline. Its dorsal portion forms the condylar neck, which represents most of the occipital condyle, also participates in the ventral margin of the foramen magnum and the cranial cavity floor. The anterior portion of the basioccipital is firmly attached to the posterior edge of the parabasisphenoid. In this region, the basioccipital slopes anteroventrally, forming an angle of approximately 30° relative to the skull roof plane. The anterior edge of the basioccipital, together with the parabasisphenoid, encloses the pair of pharyngotympanic tubes (=lateral Eustachian canals) and the median pharyngeal tube (=median Eustachian canal) (Figure 29). The openings of the pharyngotympanic tubes are laterally and slightly posterior to the median opening. The lateral openings are only slightly larger than that for the pharyngeal tube. All three openings are oval and bounded anteriorly by a wall formed by the contact between the basioccipital and the parabasisphenoid. Laterally, the basioccipital is attached to the quadrates, via a ridged suture. In ventral view, the basioccipital bears a shallow sulcus extending towards its anteroventral margin, which continues on the quadrate. This sulcus gradually becomes shallower posterolaterally, ending anterior to the point of the maximal posterior inflexion of the lateral portions of the basioccipital.

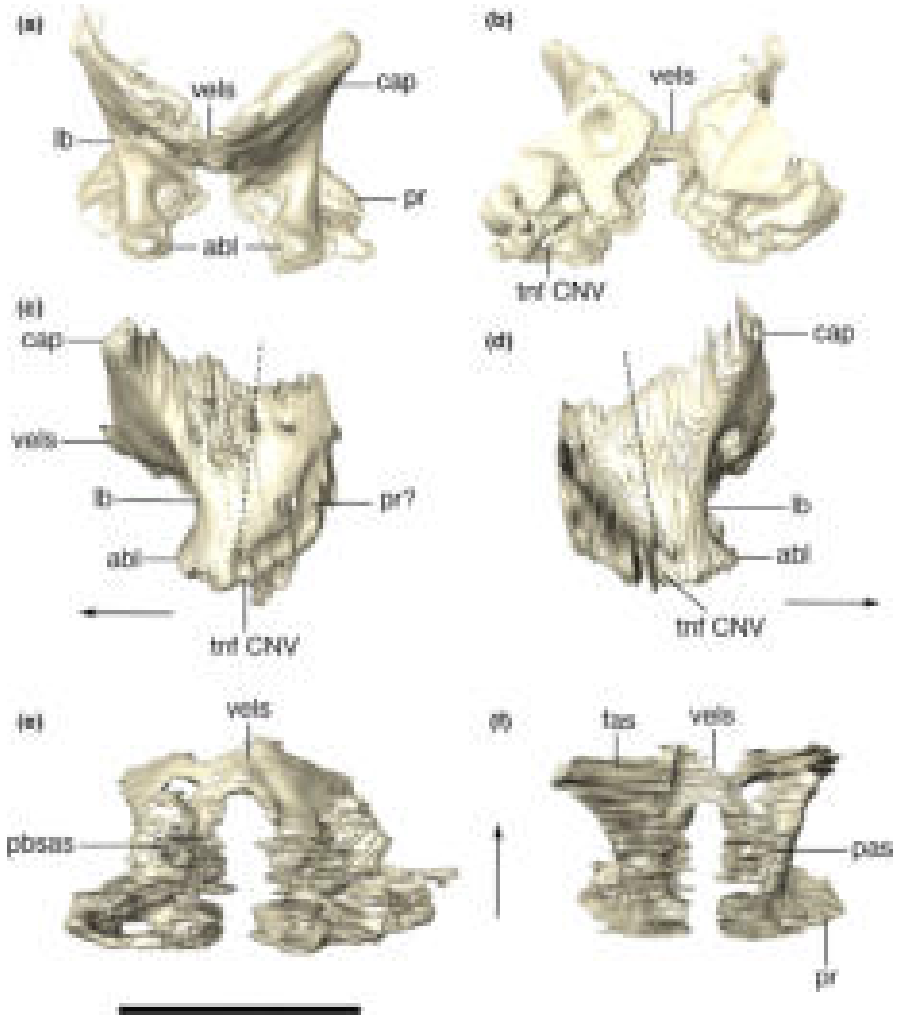

FIGURE 25 Digitally reconstructed right and left laterosphenoids of *Aphaurosuchus escharafacies* in (a) anterior, (b) posterior, (c) left lateral, (d) right lateral, (e) ventral, and (F) dorsal views. Dashed lines indicate the inferred laterosphenoid-prootic contact. abl, anterior bulge of laterosphenoid; Arrows indicate anterior direction. pbsas, parabasisphenoid articular surface; cap, capitate process; fas, frontal articular surface; lb, lateral bridge; pas, parietal articular surface; pr?, prootic; tnf CNV, trigeminal nerve foramen; vels, ventral enclosure of laterosphenoid. Scale bar: 5 cm

In lateral view, the basioccipital gradually slopes anteriorly from the occipital condyle, forming the ventral bony support of the rhombocephalum region of the endocast. The bone ends immediately anterior to the lateral suture with the otoccipital, at the level of the inferred posterior margin of the mesencephalum (Fonseca et al., 2020). At this portion, the basioccipital forms a slightly dorsoposteriorly-inclined anterior surface, where is locate the passages of the pharyngotympanic and the medial pharyngeal tubes.

Basisphenoid

The basisphenoid is fused together with the dermal parasphenoid in *Aph. escharafacies*. Accordingly, we refer to these bones as parabasisphenoid throughout our description. The parabasisphenoid is a midline bone located at the posterior portion of the ventral surface of the skull and subtriangular in ventral view. The ventral exposure of the parabasisphenoid is similar anteroposteriorly to that of the basioccipital. It contacts the basioccipital posteriorly, the quadrate laterally, and the pterygoid anterolaterally. The ventral surface of the parabasisphenoid is inclined anteroventrally to posterodorsally, following the slope of the basioccipital. The anteriormost contact with the pterygoid is internalized into the narrow and conspicuous sagittal groove, which extends anteriorly into the pterygoid at the posterior wall of the choana. From this anterior groove, the parabasisphenoid diverges posterolaterally, following the medial margin of the quadrate ramus of the pterygoid, with which it articulates via a ridged suture. The parabasisphenoid contacts the quadrate at its posterolateral and dorsal portions, and the posterior margin of the bone attaches to the basioccipital roughly transversally in respect to the main anteroposterior axis of the skull. This suture is not visible along its entire course, and part of it is internalized into the medial pharyngeal and the pharyngotympanic tubes. At this contact, the parabasisphenoid presents a crest following the same disposition of its suture with the basioccipital, enclosing the pneumatic apertures present in the region. The basioccipital forms most of these apertures edges,

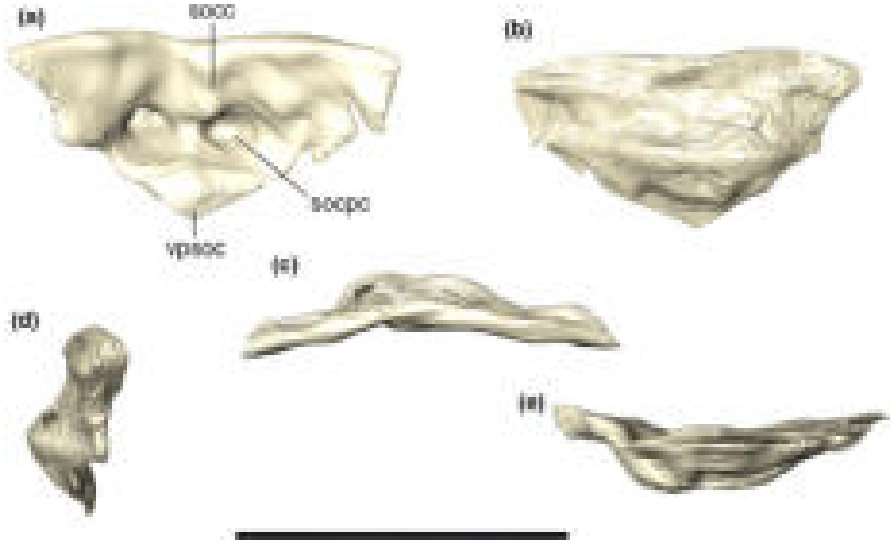

FIGURE 26 Digital reconstruction of the supraoccipital of *Aphaurosuchus escharafacies* in (a) posterior, (b) anterior, (c) dorsal, (d) left lateral, and (e) ventral views. socc, supraoccipital crest; socpc, supraoccipital parallel canals; vpsoc, ventrally projected tip of the supraoccipital. Scale bar: 5 cm

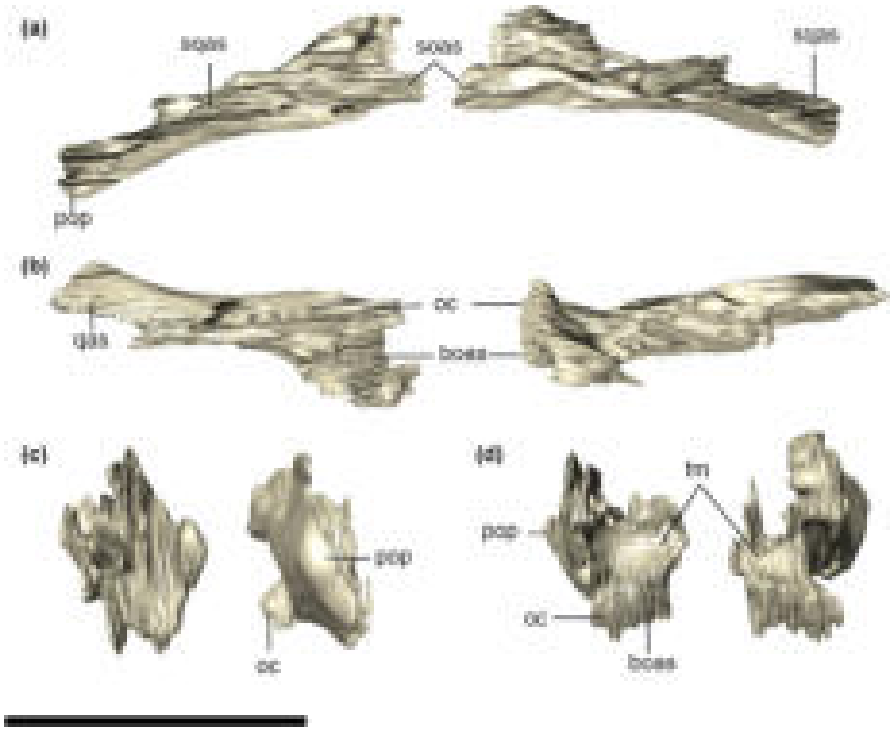

FIGURE 27 Digital reconstruction of the left and right otoccipitals of *Aphaurosuchus esharafacies* in (a) dorsal, (b) ventral, (c) lateral, and (d) medial views. boas, basioccipital articular surface; fm, foramen magnum; oc, occipital condyle; pop, paroccipital process; qas, quadrate articular surface; soas, supraoccipital articular surface; sqas, squamosal articular surface. Scale bar: 5 cm

but the parabasisphenoid has a greater contribution to the medial pharyngeal tube. The ventral surface of the parabasisphenoid has a pair of well-defined parasagittal crests. The crests delimit a deep groove between them, which is divided by another transverse but less marked crest, and is pierced by a small circular foramen at its midline. Laterally, the parabasisphenoid forms a dorsal surface which is separated from the ventral surface of the quadrate and pterygoid by a well-developed step. As a consequence, the parabasisphenoid central region projects ventrally in respect to its lateral region (Figure 30).

The CT data reveal that the anteriormost portion of the parabasisphenoid is more constricted lateromedially and displaced dorsally, forming the cultriform process (Figures 30 and 31), which contacts dorsally the ventral portion of the

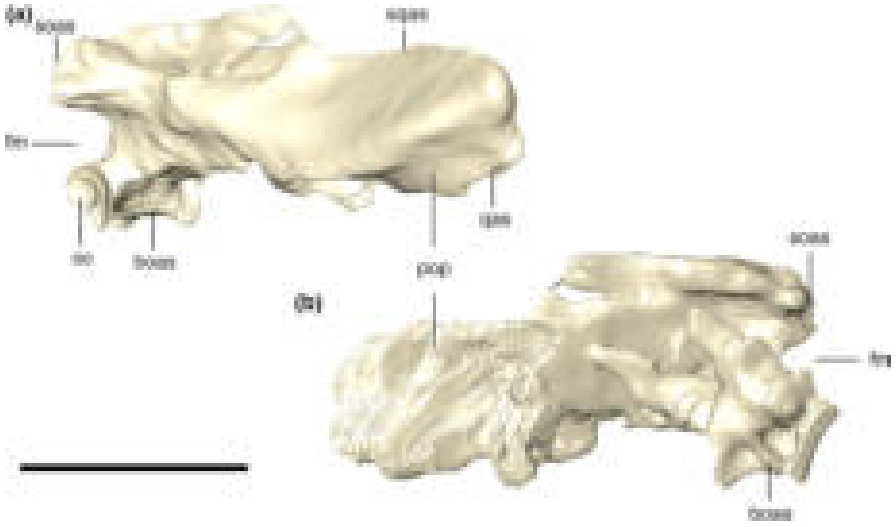

FIGURE 28 Digitally reconstructed right otoccipital of *Aphaurosuchus escharafacies* in (a) lateral, and (b) medial views. boas, basioccipital articular surface; fm, foramen magnum; oc, occipital condyle; pop, paroccipital process; qas, quadrate articular surface; soas, supraoccipital articular surface; sqas, squamosal articular surface. Scale bar: 5 cm

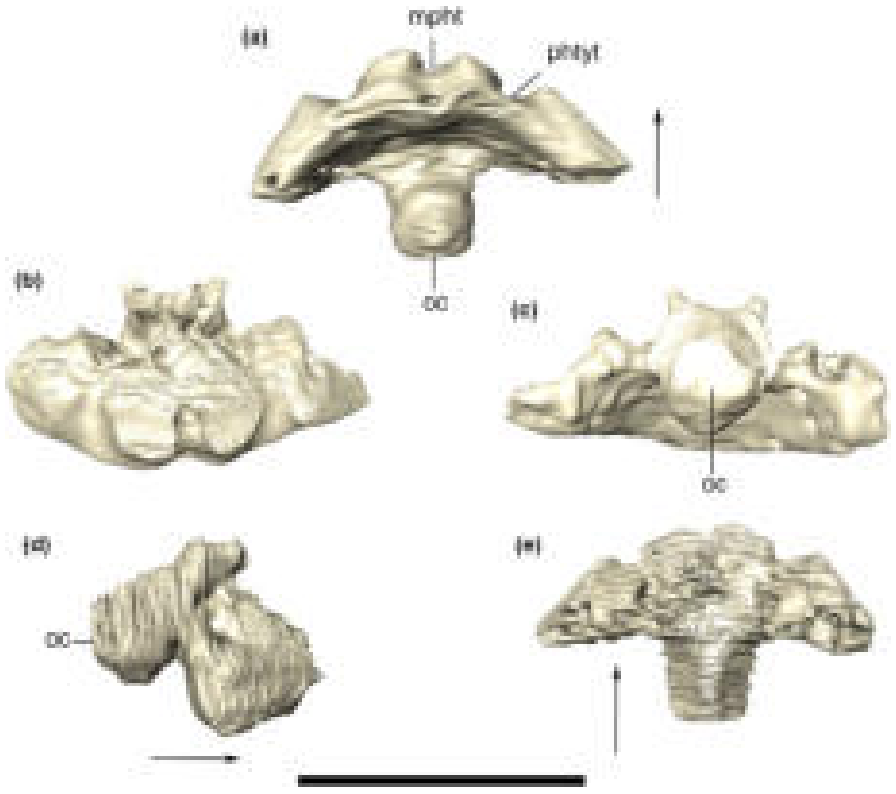

FIGURE 29 Digital reconstruction of the basioccipital of *Aphaurosuchus escharafacies* in (a) ventral, (b) anterior, (c) posterior, (d) right lateral, and (e) dorsal views. Arrows indicate anterior direction. mpht, medial pharyngeal tube; oc, occipital condyle; phtyt, pharyngotympanic tube. Scale bar: 5 cm

laterosphenoids and prootics (Figure 30). The cultriform process in *Aph. escharafacies* is a stout structure that gradually tapers anteriorly from the rest of the bone. The parabasisphenoid forms the floor of the median pharyngeal sinus, which extends internally from the median tube. An anterior extension of this pneumatic recess might represent the floor of the parabasisphenoid diverticulum. Anterior to the pneumatic recess, the dorsal surface of the parabasisphenoid is marked by a deep hypophyseal fossa that occupies most of the bone posteriorly to the cultriform process. However, due to limitations of the resolution of the CT data, we cannot assess the exit of the abducens nerve and the cavernous dural venous sinuses.

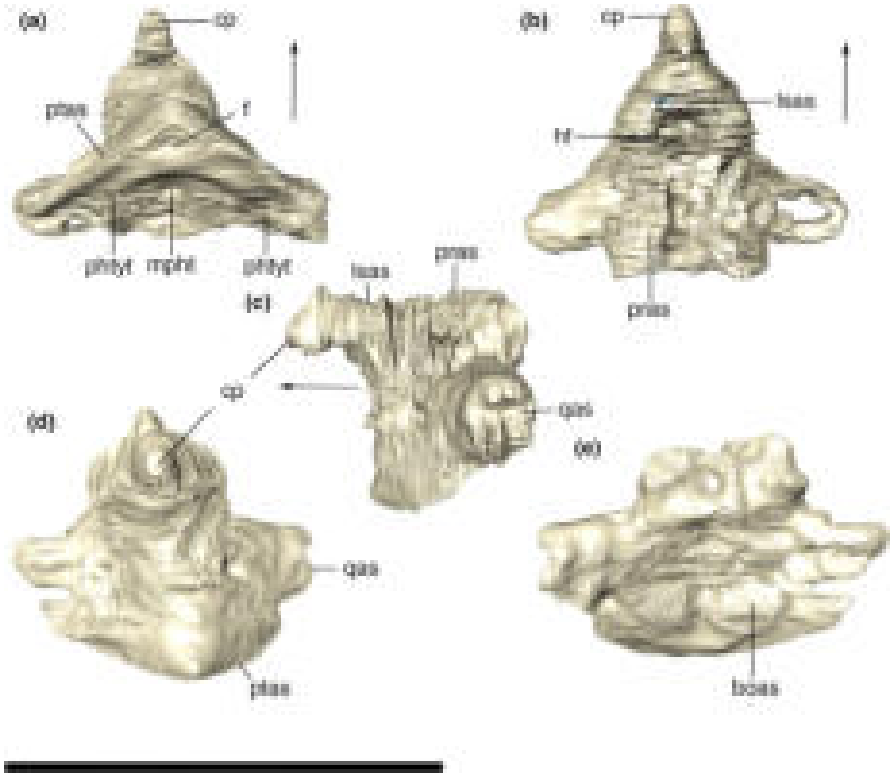

FIGURE 30 Digitally reconstructed parabasisphenoid of *Aphaurosuchus escharafacies* in (a) ventral, (b) dorsal, (c) lateral, (d) anterior, and (e) posterior views. Arrows indicate anterior direction. boas, basioccipital articular surface; cp, cultriform process; f, foramen; hf, hypophyseal fossa; lsas, laterosphenoid articular surface; mpht, medial pharyngeal tube; phtyt, pharyngotympanic tube; pras, prootic articular surface; ptas, pterygoid articular surface; qas, quadrate articular surface. Scale bar: 5 cm

Pterygoid

The pterygoids are fused into a large, highly pneumatized, and complex bones forming most of the posterior portion of the palate. It contacts the ectopterygoids and palatines anteriorly, the parabasisphenoid posteriorly, and the quadrates lateroposteriorly (Figure 32). The pterygoid wings are ventrally projected; when in articulation, with the jaws occluded, the element projects below the level of the ventral border of the lower jaw. In the anterior part of the bone, the choanal septum and the parachoanal fenestrae are located in a recessed, dorsally arching part of the palate. There is a conspicuous ventral concavity in the center of each pterygoid wing, continuous to a similar depression in the ectopterygoid, which is separated from it only by the slightly ridged suture between these bones. In this configuration, the ventral tips of the wings are blunt and heavily ornamented, as is the adjacent portion of the ectopterygoids. The medial portion of the pterygoid wing is thin, but becomes thicker laterodistally. In its medal portion, the pterygoid wings form only the posteromedial edge of the parachoanal fenestrae. The sagittal portion of the ventral surface of the pterygoid is smooth, with a longitudinal concavity extending from the contact with the parabasisphenoid to the posteriomost portion of the choanal septum. The choanal septum is formed entirely by the pterygoids. The septum is robust and ventrally flattened, possessing only small and inconspicuous ornamentation at its posterior portion. The septum is confluent with the posterior surface of the choana so there is no step between the choanal depression and the outer surface of the septum. In each side of the septum, a laterally expanded flattened sheet of bone is present, roofing the air passage in this region. The lateralmost borders of the sheet of bones project ventrally and their ventral surface is smooth. These bony sheets border the parachoanal fenestrae medially. The CT data show that those bony sheets converge medially towards their dorsal portions. So that, the roof of the choanal aperture, dorsal to the choanal septum is subtriangular. Both the bony sheets and the choanal septum are anteriorly continuous with, respectively, the vomer and the palatine. The postchoanal surface of the pterygoid forms a broad surface on the palatal surface of the skull. This surface gradually slopes dorsally, making the pterygoid more ventrally projected at its posterior portion, reaching the same level of the ventral surface of the palatine anteriorly. Between the base of both pterygoid wings, there is a narrow sagittal groove continuous to the one present at the ventral surface of the parabaisphenoid. Lateral to this groove, the ventral surface of the pterygoid, has conspicuous rugosities that continue slightly laterally into the base of the posterior margins of the pterygoid wings. These rugosities are associated with the attachment of the *m. pterygoideus ventralis* (Montefeltro et al., 2020). The posterodorsal process of the pterygoid extends until it firmly attaches to the quadrate, at the level of the parabasisphenoid lateral extension. The outer surface of the posterodorsal process of the pterygoid presents a separated muscle scar that is roughly spherical and highly ornamented, which laterally

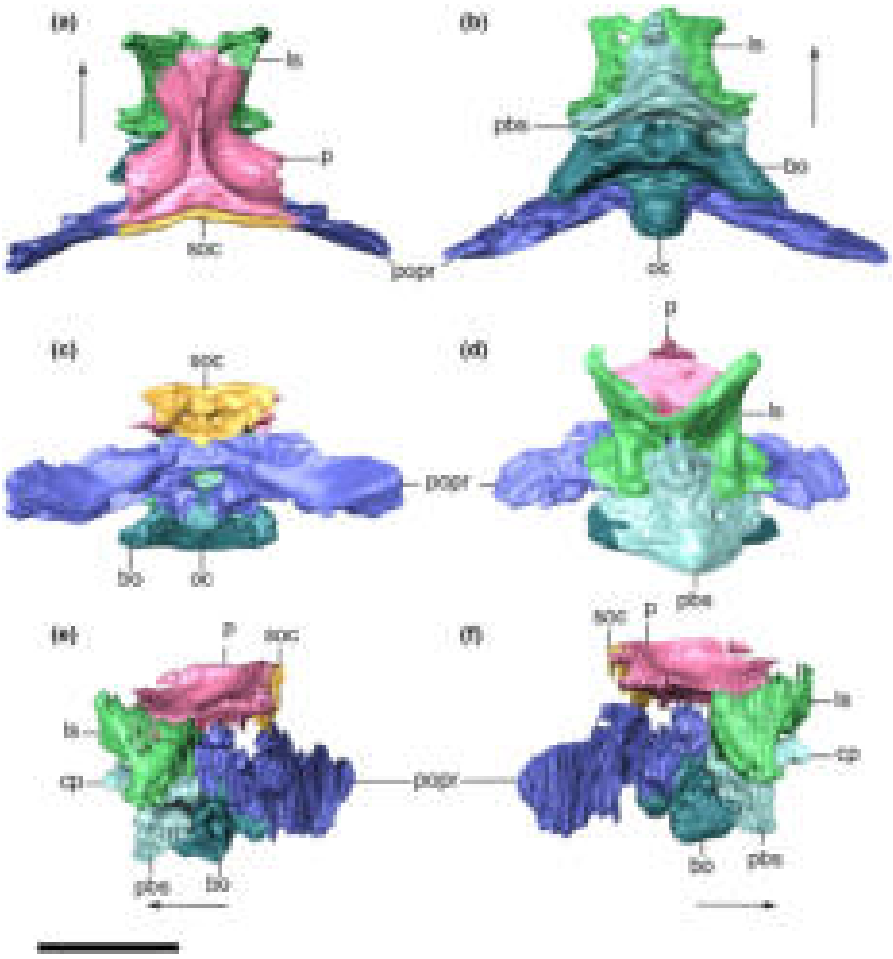

FIGURE 31 Digitally reconstructed braincase of *Aphaurosuchus escharafacies* (a) dorsal, (b) ventral, (c) anterior, (d) posterior, (e) left, and (f) right lateral views. Arrows indicate anterior direction. bo, basioccipital; pbs, parabasisphenoid; cp, cultriform process; fm, foramen magnum; ls, laterosphenoid; p, parietal; popr, paroccipital process; soc, supraoccipital. Scale bar: 5 cm

contacts the anteroventral surface of the parabasisphenoid. This region was suggested as for the attachment area for the *m. adductor mandibulae posterior* (Montefeltro et al., 2020). Posterolaterally (and also slightly dorsally) from this muscle scar, the contact with the posterodorsal process of the parabasisphenoid is marked by an interdigitated suture that reaches the level of the triple contact between pterygoid, quadrate, and the lateral edge of the pharyngotympanic tube. The lateralmost portion of the quadrate ramus bears a conspicuous muscle scar, that is, crest B (Iordanski, 1973).

Ectopterygoid

The ectopterygoid is formed by two main parts: the dorsolateral ramus and the posteroventrally projected flange, or ectopterygoid wing (Figure 33). It has a solid internal structure, contrasting with the condition seen in the pterygoid. The dorsolateral ramus has an elongate elliptical cross-section, with its long axis directed anteromedially to posterolaterally. This ramus contacts the medial surface of the jugal laterally and the maxilla anteriorly. The posterolateral contact with the jugal occurs at the ventromedial surface of that bone and their suture is not accessible in lateral view. The dorsolateral ramus of the ectopterygoid forms the posterior half of the lateral edge of the suborbital fenestra and most of its posterior edge. The lateral surface of this process is only assessable in the CT scan images, which reveals a smooth surface, lacking foramina. Medial to the jugal contact, the lateral surface of the ectopterygoid is concave, until the origin of the pterygoid wing. At this point, the ectopterygoid emits a stout anteromedial process (the anteromedial portion of the ectopterygoid wing) that firmly attaches to the palatine posterolateral process forming the anterior margin of the parachoanal fenestra. Its more laminar posterior extension forms the lateral margin of that aperture and overlaps the pterygoid ventrally at its posterior margin.

The ectopterygoid wing is robust, covers the anteroventral edge of the pterygoid wing, and forms most of the posterolateral portion of the palate. This structure is convex dorsolaterally and concave ventromedially, so that its ventral portion, along with that of the pterygoid wings, it is mostly verticalized. The concave ventromedial surface bears a depression, which is continuous to that present on the ventral surface of the pterygoid (Figure 34). In the ectopterygoid, this depression is divided by a slightly ridged thin crest, setting the lateral limit for a restricted concavity lateral to the suture with the palatine. The tip of the ectopterygoid wing is ornamented by small punctures more ventrally and very thin grooves more dorsally,

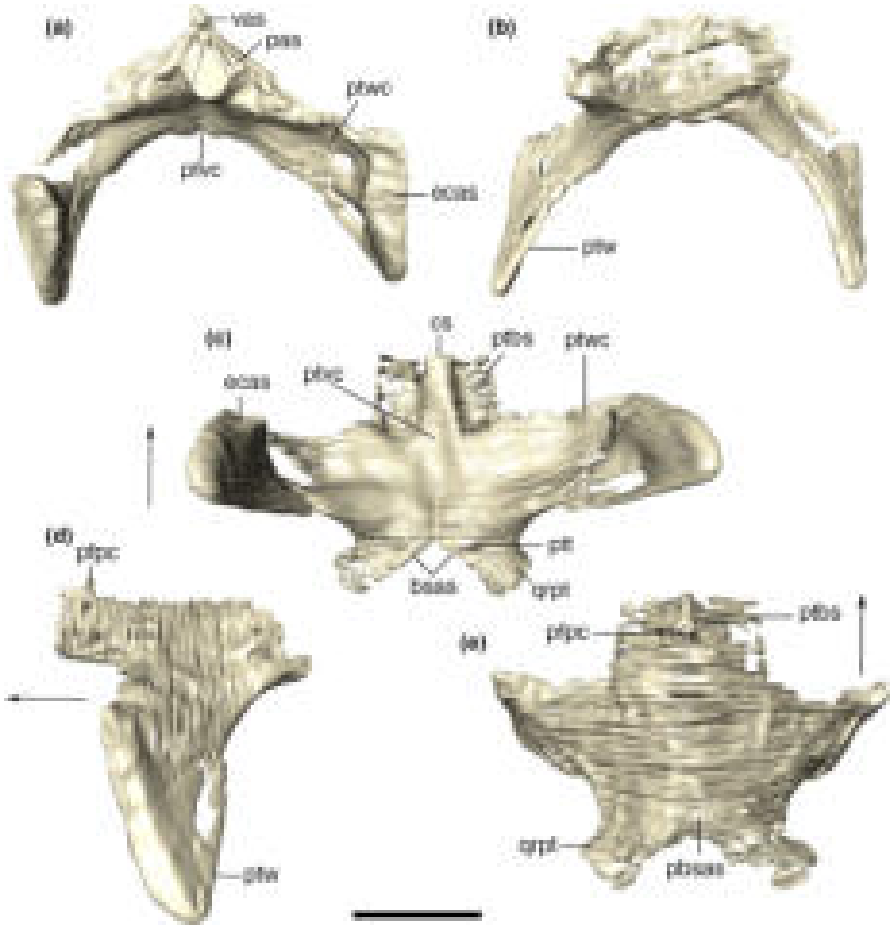

FIGURE 32 Digitally reconstructed fused pterygoids of *Aphaurosuchus escharfacies* in (a) anterior, (b) posterior, (c) ventral, (d) lateral, and (e) dorsal views. Arrows indicate anterior direction. pbsas, parabasiphenoid articular surface; cs, choanal septum; ecas, ectopterygoid articular surface; pas, palatine articular surface; pfpc, prefrontal pillar contact; ptbs, pterygoid bony sheets; ptt, pterygoid tuberosity; ptvc, pterygoid longitudinal ventral concavity; ptw, pterygoid wing; ptwc, pterygoid wing concavity; qrpt, quadrate ramus of pterygoid; vas, vomer articular surface. Scale bar: 5 cm

which are related to the insertion of *m. pterygoideous ventralis*. This attachment area continues to the posterior edge of the pterygoid wing (Montefeltro et al., 2020).

Palatine

The palatines are strongly sutured together, forming a tubular elongated structure (nasopharyngeal duct) that occupies the midline of the skull between the suborbital fenestrae. The nasopharyngeal duct is posteroventrally to anterodorsally inclined. It represents the longest air passage from the primary choana (*sensu* Witmer, 1995), at the anterior contact with the maxillae, to the opening of the secondary choana posteriorly. The anterior extension of the palatine does not reach the level of the anterior margin of the suborbital fenestra. As such, this bone is only excluded from the anterior most medial margin of the suborbital fenestrae. The tubular portion of each palatine diverges posterolaterally in front of the choanal depression, and contacting the anteromedial portion of the ectopterygoid laterally. This posterolateral ramus is oriented roughly perpendicular to the sagittal line, so that the palatine pair is "T-shaped" in ventral view (Figure 35). At its posterolateral limit, the palatine forms the posteromedial corner of the suborbital fenestra. The ventral surface of the palatine is not flattened, but forms a crested sagittal suture with its antimere, limiting the ventral surface of the palatine to a thin crest. A broad and flat ventral surface is only present posteriorly, near the posterolateral processes. In this more expanded region, the ventral surface of the palatine is pierced by few foramina, which seem to form a continuous series extending anteriorly to the midline ridge. The posterior surface of the palatine, ventral to the choanal septum of the pterygoid, is verticalized. At the edge between the ventral and posterior limit of this region, a small foramen bordered ventrally by a small transverse crest. The verticalized posterior margin of the palatine encompasses the posterior limit of the air passage. This opening faces roughly posteriorly, into the choanal depression, at the level of the anterior limit of the parachoanal fenestrae.

Vomer

The vomers can only be assessed via the CT data. It is positioned dorsal to the palatine, but sutures between the vomer and palatine are not visible. We suggest that the vomers are fused to one another and to the palatines ventrally (Figures 35 and 36). Considered as a

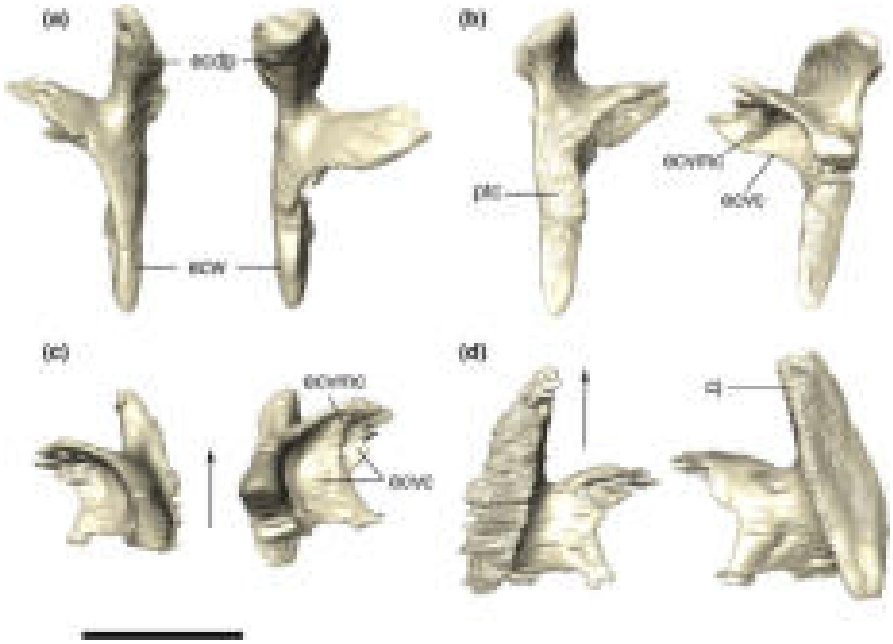

FIGURE 33 Digital reconstruction of the left and right ectopterygoids of *Aphaurosuchus escharafacies* in (a) anterior, (b) posterior, (c) ventral, and (d) dorsal views. Arrows indicate anterior direction. cj, area of contact with the jugal; ecdp, ectopterygoid dorsal process; ecvc, ectopterygoid ventral concavity; ecvmc, ecpterygoid ventromedial crest; ecw, ectopterygoid wings; ptc, pterygoid contact. Scale bar: 5 cm

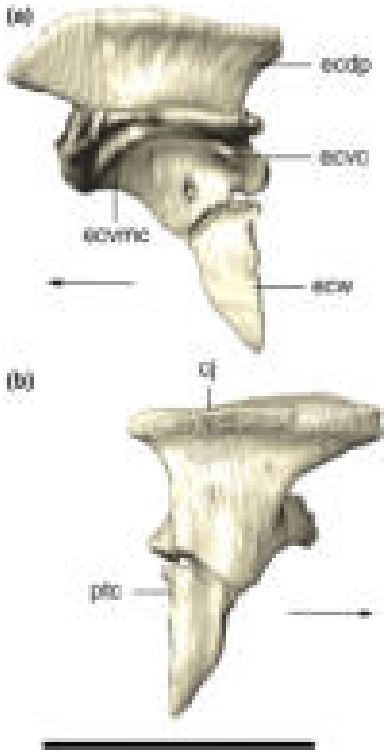

FIGURE 34 Digitally reconstructed right ectopterygoid of *Aphaurosuchus escharafacies* in (a) medial, and (b) lateral view. Arrows indicate anterior direction. cj, area of contact with the jugal; ecdp, ectopterygoid dorsal process; ecvc, ectopterygoid ventral concavity; ecvmc, ecpterygoid ventromedial crest; ecw, ectopterygoid wings; ptc, pterygoid contact. Scale bar: 5 cm

single unit, the vomer has a subtriangular cross section (Figure 37) and is mediolaterally constricted dorsally. The dorsal surface of the vomer is dorsoventrally flattened, with a smooth longitudinal depression. This dorsal surface ends posteriorly at the contact with the pterygoid. The vomer covers dorsolaterally the nasopharyngeal duct by lateromedially thin bony walls, restricting the ventral area of the nasal cavity for air passage, at the primary choana (*sensu* Witmer, 1995).

3.7.3 | Mandible

Dentary

The dentary bone forms the greatest part of the anterior and lateral regions of the lower jaw. The dentary forms the anterior, dorsal, and ventral borders of the external mandibular fenestra. Its outer ornamentation is formed by conspicuous irregular ridges and grooves. In addition, there is a longitudinal, thin and deep sulcus that extends along the dorsolateral surface of the dentary, from the fourth dentary tooth to the dentary-surangular suture (Figure 38). Laterodorsally, the dentary contacts the surangular via a posteriorly convex suture, at the level of the highest dorsoventral extension of the external mandibular fenestra. It contacts the angular posteroventrally, near the anterior tip of the fenestra, via an anteroventrally to posterodorsally inclined suture. The dentary is lateromedially constricted at the level of the seventh tooth. This constriction divides the bone into the symphyseal area anteriorly, and a posterior portion forms part of the mandibular rami. The

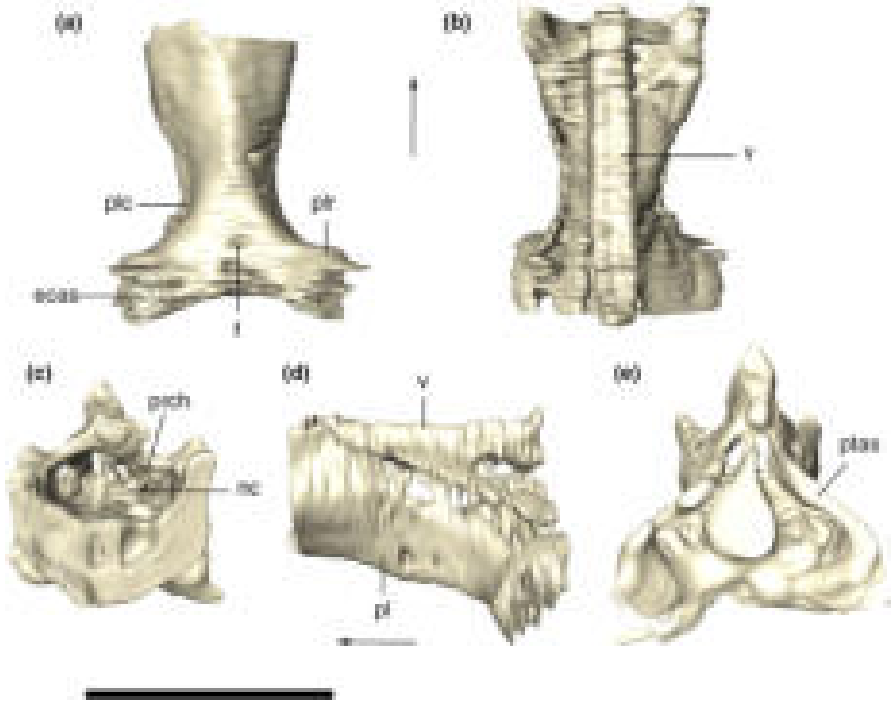

FIGURE 35 Digitally reconstructed fused palatines and vomers of *Aphaurosuchus escharafacies* in (a) ventral, (b) dorsal, (c) anterior, (d) lateral, and (e) posterior views. Arrows indicate anterior direction. ecas, ectopterygoid articular surface; f, foramen; nc, nasal cavity; pl, palatine; plc, palatine lateromedial constriction; plr, palatine posterolateral ramus; prch, primary choana; ptas, pterygoid articular surface; v, vomer. Scale bar: 5 cm

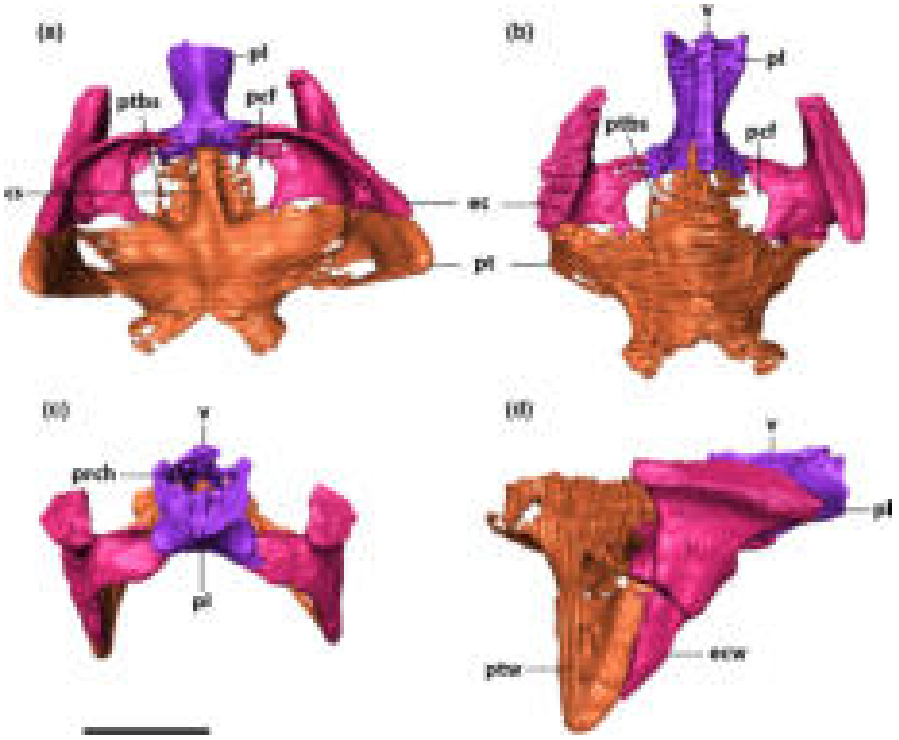

FIGURE 36 Digitally reconstructed choanal region bones of *Aphaurosuchus escharafacies* in (a) ventral, (b) dorsal, (c) anterior, and (d) right lateral views. cs, choanal septum; ec, ectopterygoid; ecptc, ectoperygoipterygoid ventral concavity; ecw, ectopterygoid wing; pcf, parachoanal fenestra; pl, palatine; prch, primary choana; pt, pterygoid; ptbs, pterygoid bony sheets; ptw, pterygoid wing; v, vomer. Scale bar: 10 cm

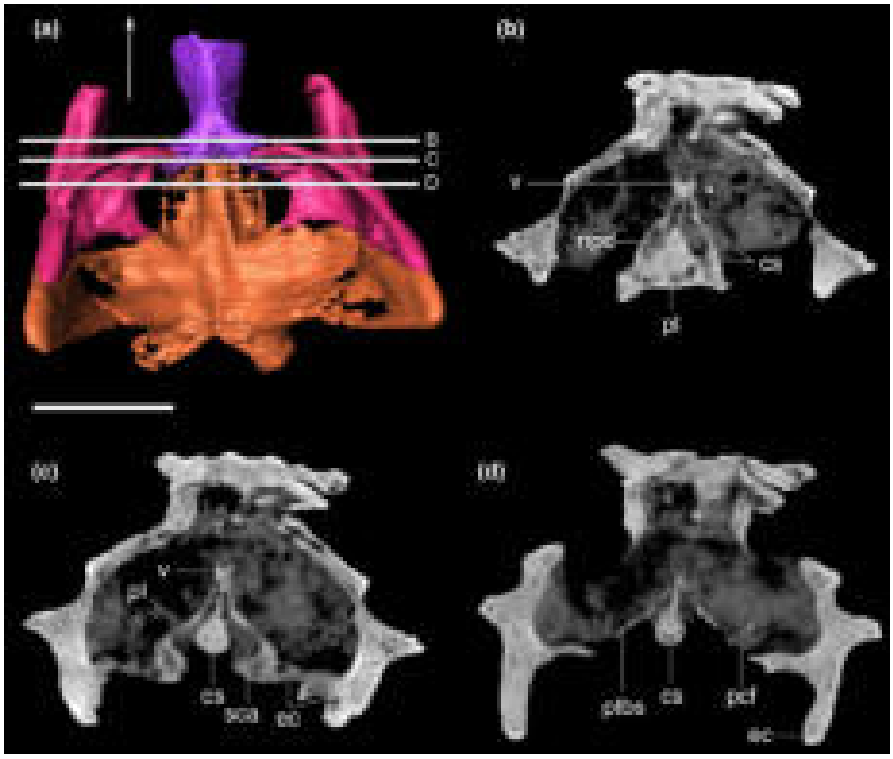

FIGURE 37 Digitally reconstructed choanal region bones (a) in ventral view. White lines represent different slices through the posterior portion of the secondary choana aperture and pterygoid bony sheets, illustrated in the following CT image stacks (b, c, and d) in coronal view. Arrow indicates anterior direction. cs, choanal septum; ec, ectopterygoid; pcf, parachoanal fenestra; pl, palatine; ptbs, pterygoid bony sheet; npd, nasopharyngeal duct; sca, secondary choana aperture; v, vomer; Scale bar: 10 cm

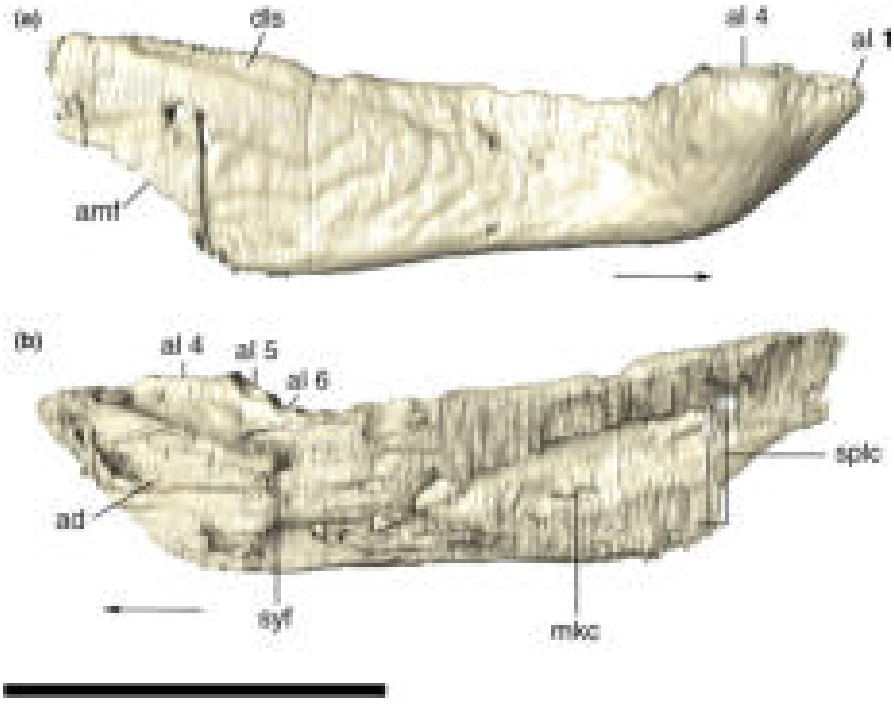

FIGURE 38 Digitally reconstructed right dentary of *Aphaurosuchus escharafacies* in (a) lateral, and (b) medial views. Arrows indicate anterior direction. al1-6, alveoli; ad, articulation area with the left dentary; amf, anterior margin of the mandibular fenestra; dls, dorsal longitudinal sulcus of the dentary; mkc, Meckelian cavity; splc, splenial contact area; syf, symphyseal fossa. Scale bar: 10 cm

dentary pair is "v-shaped" in dorsal/ventral view (Figure 39). The lateral surface of the symphyseal area is rounded at the level of the large fourth tooth, becoming more lateromedially constricted anteriorly. The CT data show that, the occlusal symphyseal surface is concave. The mandibular symphysis is anterodorsally to posteroventrally inclined, so that the anteroventral margin of the jaw is convex in lateral view. Posteriorly to the symphyseal area, the dentary is mediolaterally restricted and diverges lateroposteriorly into the mandibular rami. Furthermore, along the medial surface of the dentary, it is possible to observed the Meckelian cavity positioned between the dentary-splenial contact. The Meckelian cavity is dorsoventrally wider posteriorly close to the posterior border of the dentary, turning more constricted anteriorly near the mandibular symphysis, at approximately the level of the seventh dentary tooth. The dentary bears ten teeth (d1-d10) of different sizes, but similar shape. The fourth mandibular tooth is the largest of the dentary, fitting dorsally into the premaxilla-maxilla notch.

Splenial

The splenial is a lateromedially flattened bone on the medial surface of the mandible, but its ventral surface also participates in the symphyseal region. CT data reveal a thin, solid bone that forms the medial wall of the Meckelian canal and the anterior margin of the internal mandibular fenestra (Figure 40). Its ventral surface is not rounded as that of the dentary, but flattened, with a shallow longitudinal depression. This depression (i.e., the 'splenial depression' of Montefeltro et al., 2011) is medial to the splenial-dentary suture at the symphyseal portion. The splenial depression is better delimited medially, by the ridged medial contact between both splenial. This ridged suture forms a marked peg like protuberance at the posterior surface of the symphysis. Just behind the posterior end of the symphysis, at the medial surface, the foramen *intramandibularis oralis* is visible. This foramen is relatively small (approximately 10 mm in its longest axis), elliptical and anteroposteriorly elongated. The splenial ornamentation is restricted to superficial small dots and tiny grooves at its ventralmost surface, near the contact with the dentary. The medial surface of the splenial is smooth, lacking ornamentations. Posteriorly, where the posterior portion of the bone is forked, it forms the anterior margin of the internal mandibular fenestra.

Surangular

The surangular forms the posterodorsal portion of the mandible, contacting the dentary anteriorly, via an interdigitated suture, and the angular posteroventrally, forming the posterodorsal border of the external mandibular fenestra. It is a solid bone, with only a few foramina piercing its surface. It is mostly lateromedially compressed,

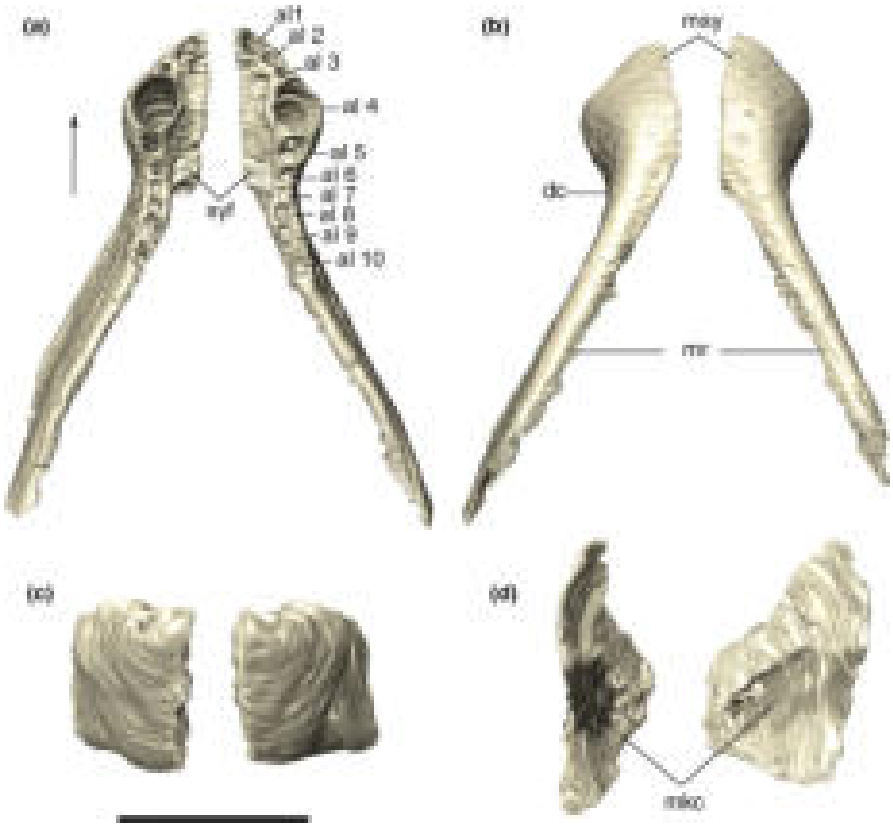

FIGURE 39 Digital reconstruction of the left and right dentaries of *Aphaurosuchus escharafacies* in (a) dorsal, (b) ventral, (c) anterior, and (d) posterior views. Arrow indicates anterior direction. al1-10, alveoli; dc, dentary mediolaterally constriction; mkc, Meckelian cavity; mr, mandibular rami; msy, mandibular symphysis; syf, symphyseal fossa. Scale bar: 10 cm

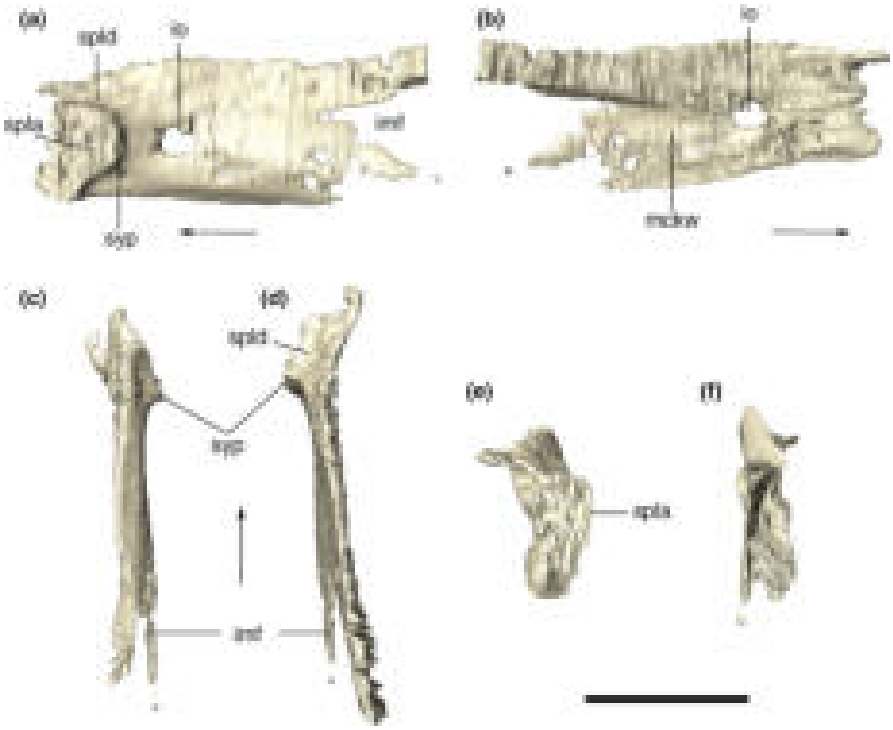

FIGURE 40 Digitally reconstructed right splenial of *Aphaurosuchus escharafacies* in (a) medial, (b) lateral, (c) ventral, (d) dorsal, (e) anterior and (f) posterior views. Arrows indicate anterior direction. imf, internal mandibular fenestra; io, foramen *intramandibularis oralis*; mckw, Meckelian cavity medial wall; spla, splenial articulation area; spld, splenial depression; syp, mandibular symphysis peg projection. Scale bar: 5 cm

but it is convex on its lateral surface. The surangular major axis is oblique, with the anterior portion of the bone more dorsally positioned than the posterior (Figure 41). The ornamentation is restricted to its lateral surface, composed of anteroposteriorly-directed thin grooves anteriorly, as well as irregular and more inconspicuous grooves and ridges posteriorly. The posterior portion of the bone is flattened and dorsoventrally high. At this portion, the surangular contacts the dorsal surface of the angular via a sinuous suture, being concave ventrally and slightly pointed posterodorsally. The medial surface of the bone forms the posterodorsal and posterior borders of the internal mandibular fenestra. CT data reveal that this portion of the surangular is dorsoventrally expanded and laterome-dially thin, extending posteriorly between the angular and the articular in lateral view. The anteroventral portion of this expanded surface is slightly pointed and extends anteriorly to the anterior tip of the articular. This surface also extends posteriorly to the level of the anterior portion of the glenoid fossa, where it gradually becomes dorsoventrally constricted.

Angular

The angular is an anteroposteriorly oriented bone, which composes most of the posterior half of the mandible ventral surface, including the entire ventral border of the external and internal mandibular fenestrae. Anteriorly, it contacts the posterior portion of the dentary and splenial. This contact is better seen in the CT images stacks, which shows a thin anterior extension of the angular wedged between the posterior portion of those bones (Figure 42). The dorsal surface of this anterior extension of the angular is lateromedially concave, forming the floor of the Meckelian canal, from the level of the tenth dentary tooth anteriorly to its posterior most extension. Posterodorsally, the outer contact of the angular with the surangular occurs via a sinuous suture, extending from the posterior corner of the external mandibular fenestrae towards the posteriormost tip of mandibular ramus. At its posterior limit, in lateral view, the dorsal margin of the angular is concave and forms the posteriormost limit of the mandible, including the lateral and ventral surfaces of the retroarticular process. The angular posterior edge is dorsoventrally expanded, forming a convex posterolateral surface, which contacts the lateral surface of the articular. The entire ventral and lateral surfaces of the angular are ornamented, comprising irregular thin grooves lateroanteriorly, and more dorsoposteriorly to anteroventrally-direct ornamentation closer to the retroarticular process. Parallel to the posteroventral border of external mandibular fenestra, a robust crest marks the anterior extension for the insertion of *m. pterygoideous ventralis* (Montefeltro et al., 2020).

The medial surface of the angular lacks ornamentations and is dorsoventrally convex anteriorly. The ventral margin of the internal mandibular fenestra possesses a subtriangular dorsal projection, positioned slightly anterior to the center of the fenestra, which marks the anterior limit of the attachment of the *m. adductor mandibulae posterior* (Montefeltro et al., 2020). Such projection gently slopes anteriorly, being steeper posteriorly. In lateral view, the dorsal portion of this projection is rounded, but medially concave below that. At the dorsal surface of the angular, between its lateral and medial

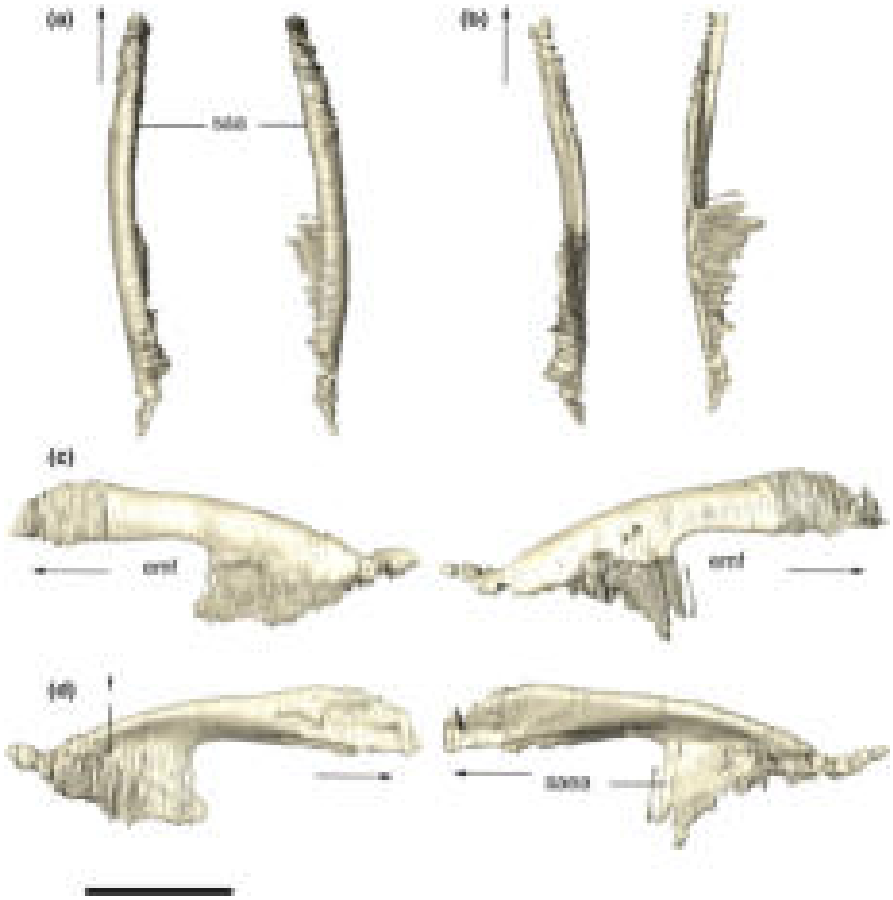

FIGURE 41 Digital reconstruction of the left and right surangulars of *Aphaurosuchus escharafacies* in (a) dorsal, (b) ventral, (c) lateral, and (d) medial views. Arrows indicate anterior direction. emf, external mandibular fenestra; f, foramen; saa, surangular major axis; saea, surangular expanded area. Scale bar: 5 cm

elevated borders, lies the Meckelian groove (floor of the Meckelian canal). It extends from the posterior contact with the articular to the anteriorly-projected portion of the bone between the dentary and the splenial.

Articular

The articular contacts the angular anteroventrally and, along the lateral half of its ventral margin, it forms most of the retroarticular process. The bone is subtriangular in dorsal view, with an anterior projection and a mediolaterally-wider posterior portion. The anterior projection is dorsoventrally thinner anteriorly, becoming wider posteriorly. The dorsal and ventromedial surfaces of the bone are orthogonally related (Figure 43). The anterior part of the dorsal surface is flattened and inclined posterodorsally to anteroventrally. The glenoid fossa for articulation with the quadrate is located right posterior to that flat area. The CT data reveal that the glenoid fossa is divided into two distinct articular surfaces for the medial and lateral condyles of the quadrate. The retroarticular process is lateromedially compressed, with a rounded dorsolateral extension. The transition from the posterior margin of the subhorizontal glenoid fossa to the subvertical posteromedial surface of the articular is well-marked (Figure 44). The retroarticular process expands posteriorly and is laterally covered by the angular. In this configuration, the retroarticular forms the posteriormost tip of the mandible.

3.7.4 | Dentition

Upper jaw dentition

Four regularly spaced teeth are present in the premaxilla (pm1-pm4). The first tooth is positioned at the anteriormost portion of the bone, being incomplete in both sides. However, it is possible to assert that the first tooth is conical in shape and distally curved at the apical end. It also has a serrated mesial carina, as seen in all other premaxillary teeth. The second tooth is relatively thinner and more elongated. The third tooth is the largest premaxillary tooth. It is also more rounded in cross section. The fourth tooth is the smallest, placed at a more dorsal position in the premaxilla (Figure 45).

There are five maxillary teeth (m1-m5). The third one corresponds to a hypertrophied caniniform, whereas the first and fifth maxillary teeth are smaller. All maxillary teeth possess labiolingualy compressed crows and have more rounded roots in cross section, with serrated carinae in both mesial and distal margins (i.e., ziphodont morphology *sensu* Prasad & de Broin, 2002). The teeth are slightly curved distally, except for the m1. With the jaws occluded,

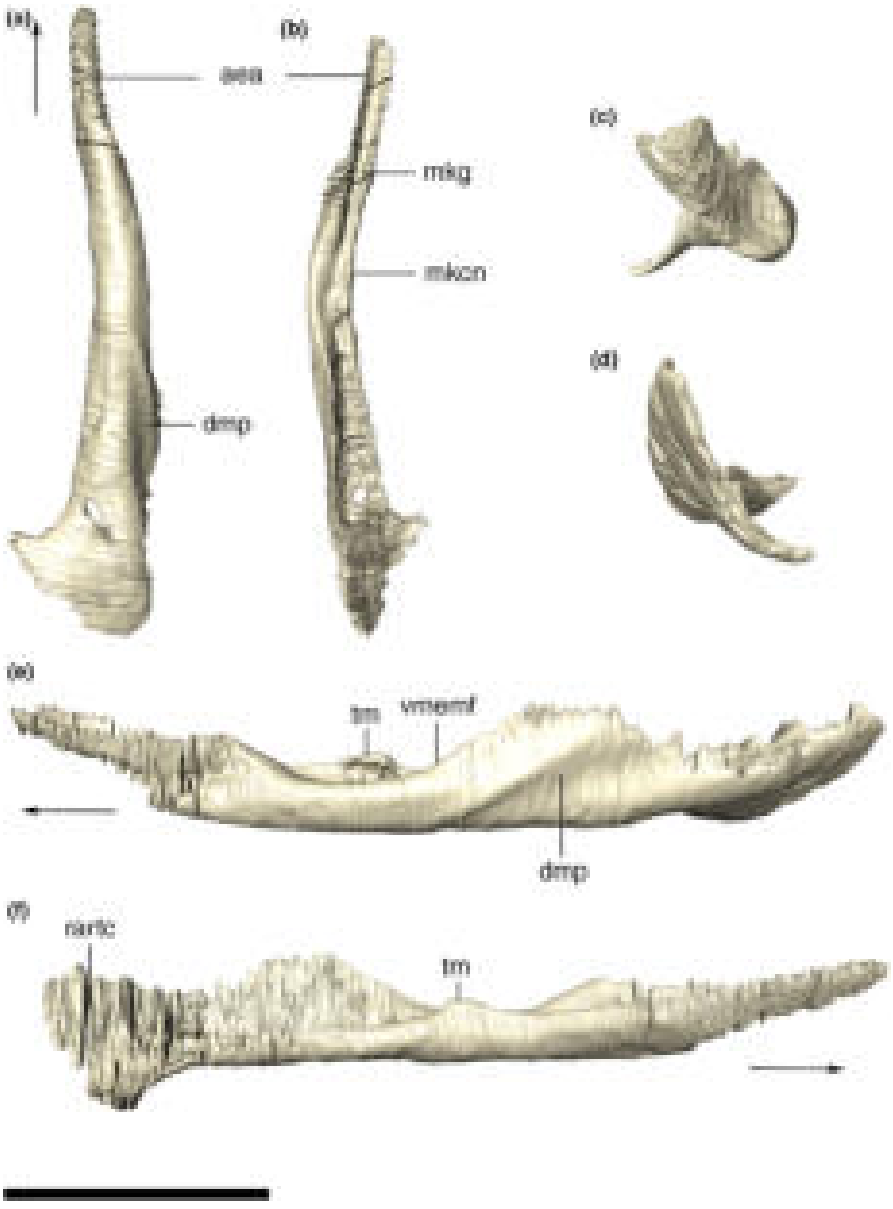

FIGURE 42 Digitally reconstructed left angular of *Aphaurosuchus escharafacies* in (a) ventral, (b) dorsal, (c) anterior, (d) posterior, (e) lateral, and (f) medial views. Arrows indicate anterior direction. aea, anterior expansion of the angular; dmp, depression for the insertion of *M. pterygoideous*; mkcn, Meckelian canal; mkg, Meckelian groove; rartc, retroarticular contact; tm, torose margin; vmemf, ventral margin of the external mandibular fenestra. Scale bar: 10 cm

the hypertrophied caniniform almost reaches the level of the ventral margin of dentary. The fourth and fifth maxillary teeth are subtriangular in lingual and labial views, less distally curved (the fifth almost straight), and reduced in size.

Lower jaw dentition

The lower jaw tooth row is composed of ten dentary teeth (D1-D10). D1 is procumbent, that is, anteriorly inclined, more rounded in cross section, and not as pointed as the remaining teeth. D4 is the largest dentary tooth and is typically ziphodont with a distally curved crown, and serrations on both mesial and distal carinae. It also presents the largest root, which almost reaches the level of the ventral surface of the dentary internally. D9 is approximately of the same size as D1, but less curved distally at its apex. The remaining teeth are smaller, subtriangular in shape, slightly labiolingualy compressed, with a more rounded cross section (Figure 46).

4 | DISCUSSION

4.1 | Phylogenetic position of *Aphaurosuchus escharafacies*

The scoring of *Aph. escharafacies* in the expanded version of the data-matrix of Godoy et al., (2014) resulted in a single Most Parsimonious Tree (MPT) with 143 steps, in which the new species is recovered as

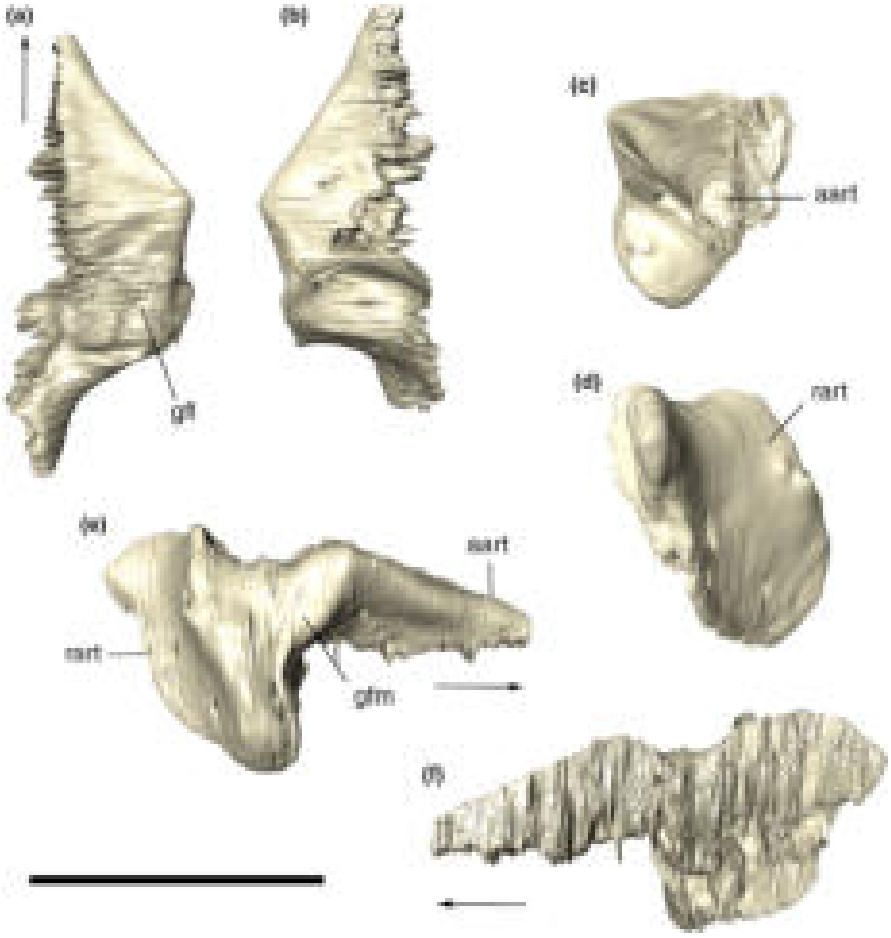

FIGURE 43 Digitally reconstructed left articular of *Aphaurosuchus escharafacies* in (a) dorsal, (b) ventral, (c) anterior, (d) posterior, (e) lateral, and (f) medial views. Arrows indicate anterior direction. aart, anterior projection of the articular; gfl, glenoid fossa for the articulation of the lateral quadrate condyle; gfm, glenoid fossa for the articulation of the medial quadrate condyle; rart, retroarticular process. Scale bar: 5 cm

the sister taxon to all other baurusuchines (Figure 47). *Baurusuchus* is recovered as monophyletic, with *Ba. albertoi* as the sister taxon of the *Ba. pachecoi* +Ba. *salgadoensis* clade. In addition, *S. maxhechti* and *Apl. sordidus* are recovered as the successive sister-taxa to *Baurusuchus*. These results differ from Godoy et al., (2014), which did not recover a monophyletic *Baurusuchus*. In their topology, *Ba. albertoi* clustered with *Apl. sordidus* in a clade supported by a well-developed row of foramina dorsal to the ectopterygoid-jugal suture.

Our results led to a revaluation of the character states that diagnose the two main Baurusuchidae clades (Godoy et al., 2014; Montefeltro et al., 2011). A notched ventral border of the quadrate-quadratojugal contact is excluded as synapomorphy of Pissarrachampsinae, as this condition is also present in *Aph. escharafacies*, and was reinterpreted as a plesiomorphy of the Pissarrachampsinae +Baurusuchinae clade. Yet, three additional Pissarrachampsinae synapomorphies were recognized: a frontal longitudinal ridge extending anteriorly to the frontal mid-length, a sculpture on the outer surface of the dentary and the splenial, and a rounded dorsal margin of mandibular fenestra. Also because of *Aph. escharafacies*, two features are no longer recovered as Baurusuchinae synapomorphies: a dorsal extension of the quadratojugal not surpassing the dorsal margin of the laterotemporal fenestra, and a ridged ventral surface of the choanal septum (*Aph. escharafacies* has a smooth ventral surface of the choanal septum and the quadratojugal extends dorsally from the dorsal tip of laterotemporal fenestra). Additional synapomorphies were identified for Baurusuchinae, that is, a jugal with the antorbital portion deeper than the infraorbital one, a relatively straight dorsal skull profile, and a well-developed row of foramina dorsal to ectopterygoid-jugal suture. Accordingly, the latter feature is no longer regarded as a sinapomorphy of the *A. sordidus* + *Ba. albertoi*.

The phylogenetic position of *Aph. escharafacies* as the sister taxon to all other Baurusuchinae is supported by the presence of the following traits: posterodorsal surface of nasal depressed (vs. rounded or flat), ventral surface of the choanal septum smooth (vs. ridged), and absence (vs. presence) of a series of foramina in the angular below the mandibular fenestra. The *Baurusuchus* clade is supported by two of the new characters proposed here: a higher angulation (more than 100°) of the squamosal prongs in lateral view and the more lateralized position of the posterolateral surface of the squamosal prongs in posterior view (Figure 2 and Figure 3 of SI 2).

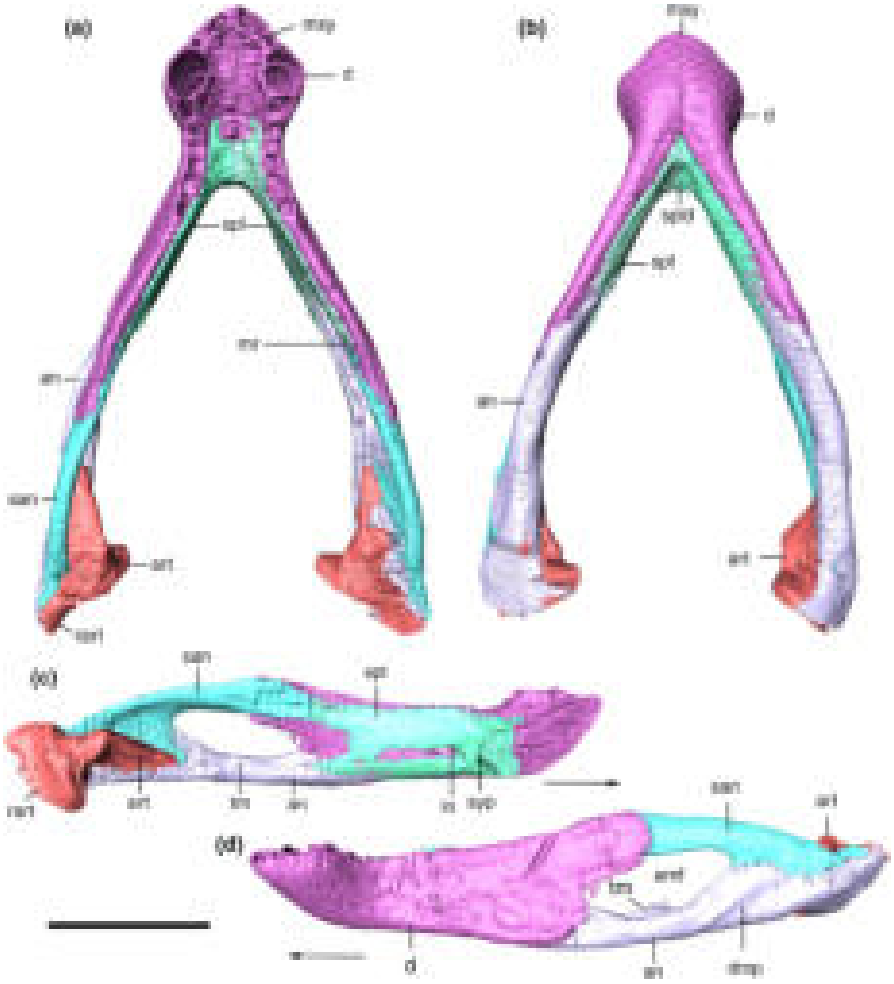

FIGURE 44 Digitally reconstructed and articulated mandible bones of *Aphaurosuchus escharafacies* in (a) dorsal, (b) ventral view. Left mandible is reconstructed in (c) medial, and (d) lateral views. Arrows indicate anterior direction. an, angular; art, articular; d, dentary; dmp, depression for the insertion of *M. pterygoideous*; emf, external mandibular fenestra; io, foramen *intramandibularis oralis*; mr, mandibular ramus; msy, mandibular symphysis; rart, retroarticular; san, surangular; spl, splenial; spld, splenial depression; syp, mandibular symphysis peg projection; tm, torose margin. Scale bar: 10 cm

4.2 | Implications for early baurusuchid evolution

Among the morphological traits originally referred as diagnostic for Baurusuchinae and Pissarrachampsinae (Montefeltro et al., 2011), *Aph. escharafacies* bears all the baurusuchine features except for the extensive medial contact of the prefrontals and the ridged ventral surface of the choanal septum. At the same time, *Aph. escharafacies* bears two of the three Pissarrachampsinae diagnostic features (*sensu* Montefeltro et al., 2011): posterior portion of the nasal bearing a broad depression and a restricted medial approximation of the prefrontals. However, it is worth mentioning that the medial contact of the prefrontals occurs more anteriorly among pissarachampsines, whereas in *Aph. escharafacies* it is more restricted and positioned at the anteroposterior mid-point.

Nascimento (2014, page 180) defined the "*Baurusuchus* choanal pattern," in which the ectopterygoid and pterygoid are ventrally concave and not pneumatized, and the "*Pissarrachampsa* choanal pattern," in which the ectopterygoid bears the parachoanal fossae, the pterygoid wings are pneumatized and have a straight ventral surface. For Nascimento (2014), baurusuchids with the latter pattern also usually present an up-lifted anterior border of the supratemporal fenestra, two parasagittal sulci on the ventral surface of the palatine, and the pharyngeal tube apertures (lateral "Eustaquian foramina") larger than the intertympanic foramen (medial "Eustaquian foramen"). The results of the comparative analysis conducted here mostly agree with the general patterns proposed by Nascimento (2014).

However, we recognized additional diagnostic features related to the choanal regions of Pissarrachampsinae and Baurusuchinae. The Pissarrachampsinae choanal pattern also includes the flattened ventral surface of the palatine with a pair of conspicuous longitudinal row of foramina, straight palatine-maxilla suture, ectopterygoid and pterygoid wings posteriorly directed, ectopterygoid mediolaterally flattened, pterygoid forming parachoanal fossae, choanal septum lateromedially thin, and postchoanal portion of the pterygoid anteroposteriorly short and dorsally recessed at the contact with the

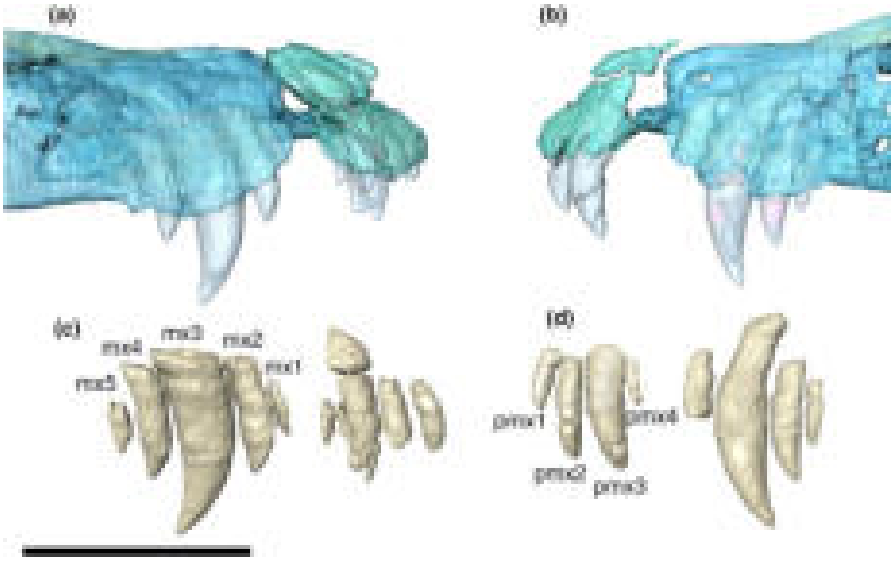

FIGURE 45 Upper jaw dentition of *Aphaurosuchus escharafacies*. (a) and (b) shows right and left lateral views of the semitransparent premaxillae and maxillae, (c) and (d) show the isolated teeth from each bone, respectively. Numbers indicate the tooth number of each the premaxilla (pm1-4) and maxilla (mx1-5). Scale bar: 10 cm

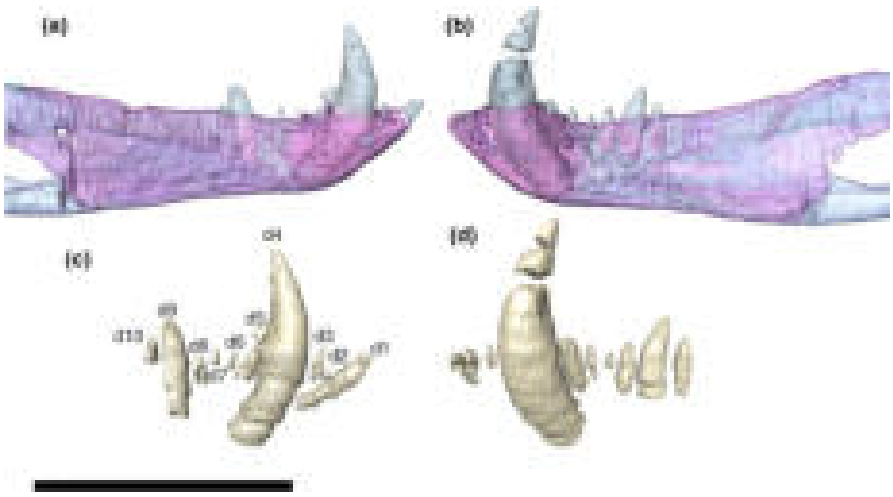

FIGURE 46 Lower jaw dentition of *Aphaurosuchus escharafacies*. (a) and (b) shows right and left lateral views of the semitransparent mandible, with the dentary in pink. (c) and (d) show the isolated teeth from each dentary. d1-10, dentary teeth. Scale bar: 10 cm

parabasisphenoid. As for the Baurusuchinae choanal pattern, we additionally recognized the palatine inclined dorsolaterally from the ventral suture with its antimere, the palatine-maxilla suture anteriorly convex, ectopterygoid and pterygoid wing ventrally projected and with depressed areas on their ventral surfaces, and pterygoid anteroposteriorly expanded on its postchoanal portion near the contact with the parabasisphenoid.

It is clear that *Aph. escharafacies* bears typical traits of both Baurusuchinae and Pissarrachampsinae, and this condition is somehow represented in our phylogenetic hypothesis by the placement of the taxon close to that dichotomy, along the baurusuchine branch. Accordingly, that evolutionary segment may be within a "zone of variability" sensu Bever et al., (2011), when plesiomorphies persist across speciation/cladogenetic events and are read as homoplasies (e.g., "pissarrachampsine traits" of *Aph. escharafacies*) given the incompleteness of the fossil record. Indeed, baurusuchids have a restricted geographical range, with undisputed taxa occurring only in the South American Adamantina/Vale do Rio do Peixe and Bajo de la Carpa formations. Further, the former unit congregates most of that diversity, including all formally described baurusuchines. In fact, the entire diversity of baurusuchids of the Adamantina/Vale do Rio do Peixe Formation may be coeval, restricted to the probably short time span –somehow fitting within the Coniacian to Campanian time span (Castro et al., 2018) – in which that stratigraphic unit was deposited. Moreover although diverse, baurusuchids have a very similar body plan, related to their role as medium to large sized terrestrial predators (Montefeltro et al., 2020). In fact, the acquisition of novel anatomical traits allowed baurusuchids expanding into a niche rarely explored by crocodyliforms and, in the absence of a reported preceding extinction event, this is the most likely factor that promoted

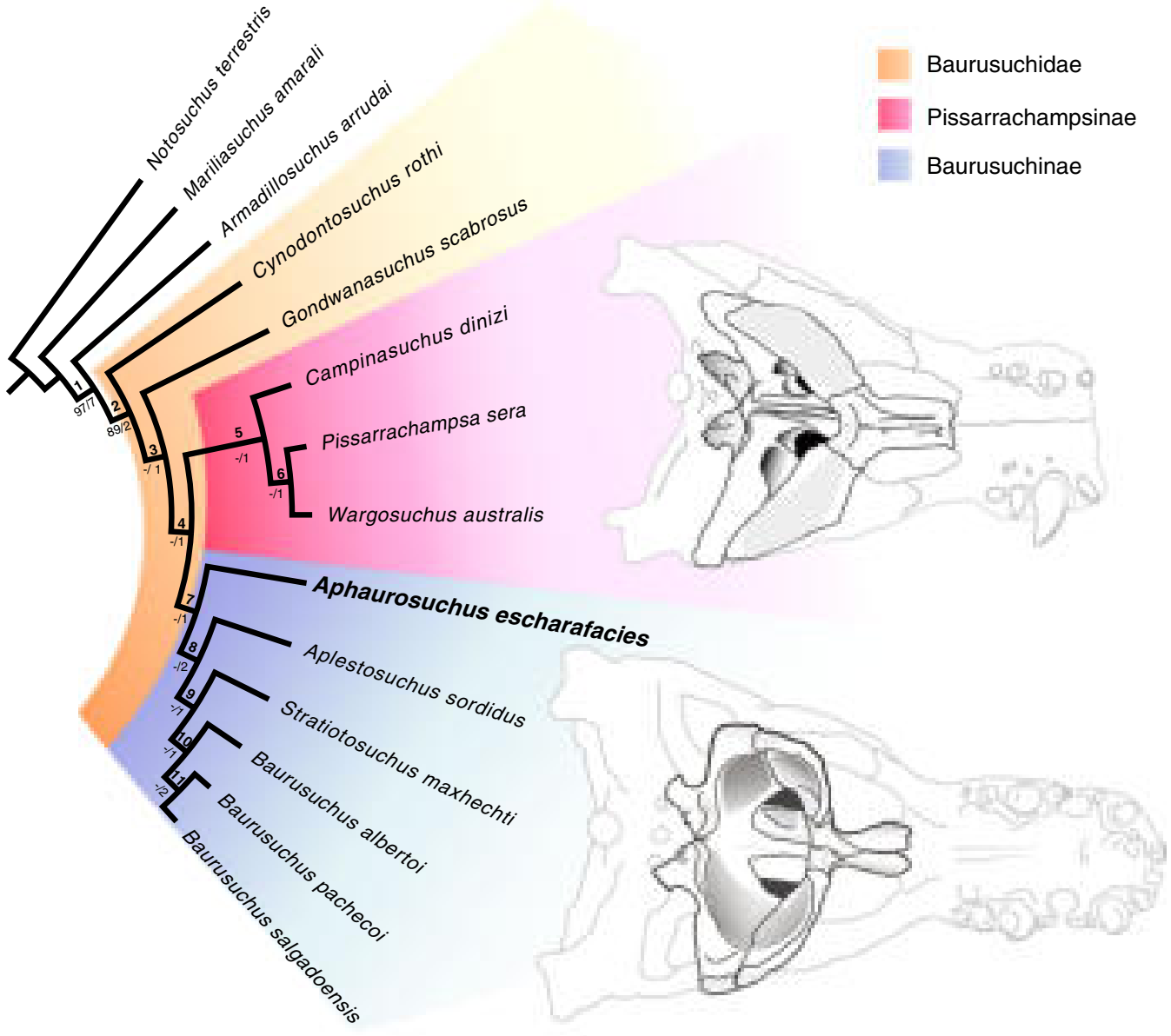

FIGURE 47 Phylogenetic position of the species *Aphaurosuchus escharafacies* within Baurusuchidae at the base of Baurusuchinae clade. The single most parsimonious tree (total length = 143 steps) recovered after an implicit enumeration analysis using the software TNT. The bootstrap (50% cut) and decay values are shown below the nodes. Silhouettes illustrates the 'choanal pattern' of Pissarrachampsinae (*Pissarrachampsa sera*, LPRP 0019) and Baurusuchinae (*Aphaurosuchus escharafacies*, LPRP 0697)

their adaptive radiation (Simpson, 1949). Yet, instead of a more common 'early burst' evolutionary pattern, in which disparity increases more rapidly during the initial occupation of recently opened niches (Harmon et al., 2010), the fossil record of baurusuchids shows the rise of a highly taxonomic diverse clade, but with a similar body plan persisting among the species. Similar cases have been reported in other groups such as therian mammals (Grossnickle & Newham, 2016) and early sauropodomorphs (Langer et al., 2019), and specifically for the last, consisting in a radiation of which was also not preceded by major extinction events. Further investigations are needed to contextualize the origin of Baurusuchidae within such macroevolutionary models.

5 | CONCLUSIONS

Aphaurosuchus escharafacies represents the 11th described baurusuchid species. CT data allowed a tridimensional analysis and description of most of the skull bones of the holotype and only known specimen (LPRP/USP 0697), including the first virtual reconstruction of individualized bones for a baurusuchid. This allowed the description of hardly accessible bones, such as the vomer and the laterosphenoid, revealing that the former seems to be fused to its pair and to the dorsal surface of the palatine, composing the roof of the nasopharyngeal duct. The laterosphenoid in very close contact with the prootic and presents an anteroventral enclosure below the anterior portion of the

olfactory bulb, as well as anterior projections from the ventralmost expansion of the lateral bridge. Furthermore, most braincase bones were identified and reconstructed, revealing the morphology of important elements, such as the cultriform process and the hypophyseal fossa. The palatal area was also fully reconstructed, revealing structures such as the pterygoid bony sheets expanding laterally from the dorsal margin of the choanal septum, forming a continuation of the nasopharyngeal duct. Our morphological and phylogenetic analyses reveal an interesting combination of morphological features that place *Aph. escharafacies* as the sister-taxon to all other Baurusuchinae, but bearing some key features of Pissarrachampsinae. This suggests that the early radiation of these groups occurred fast, geographically restricted, related to the exploration of a new ecological niche for notosuchians, and within a possible zone of variability.

ACKNOWLEDGMENTS

This research was funded by the Coordenação de Aperfeiçoamento de Pessoal de Nível Superior (CAPES - Finance Code 001) and Fundação de Amparo à Pesquisa do Estado de São Paulo (FAPESP 2019/06311-4) to GD. The authors thank Sandra Tavares (MPMA), Ismar Carvalho (UFRJ), Rafael Costa da Silva (CPRM), and Thiago Marinho (CCCP/UFTM) for access to specimens in order to conduct the comparative analysis, and to F. J. Oliveira and M. K. Santos (Hospital das Clínicas de Ribeirão Preto) for the CT scanning of *Aph. escharafacies*. Finally, the authors thank the reviewer, Pedro Lorena Godoy, for his constructive comments and suggestions during the review phase. The authors do not have any conflict of interest related to the publication of this paper to declare.

AUTHOR CONTRIBUTIONS

G.D described the species, worked on 3D images, and analyzed the phylogenetic data. M.C.L and F.C.M. read and revised all versions of the article, contributing with essential suggestions and modifications along the text. All authors wrote, read, contributed to the manuscript, and approved its final version.

DATA AVAILABILITY STATEMENT

The fossil specimen described in the present study in formally deposited at the paleontological collection of the Laboratório de Paleontologia de Ribeirão Preto, Faculdade de Filosofia, Ciências e Letras da Universidade de São Paulo, over the registration number: LPRP/USP 0697.

ORCID

Gustavo Darlim https://orcid.org/0000-0001-7735-2483
Felipe C. Montefeltro https://orcid.org/0000-0001-6519-8546
Max C. Langer https://orcid.org/0000-0003-1009-4605

REFERENCES

Araújo Júnior, H.I. & da Silva Marinho, T. (2013) Taphonomy of a Baurusuchus (Crocodyliformes, Baurusuchidae) from the Adamantina Formation (Upper Cretaceous, Bauru Basin), Brazil: implications for preservational modes, time resolution and paleoecology. *Journal of South American Earth Sciences*, 47, 90–99.

Arruda, J.T., Carvalho, I.S. & Vasconcellos, F.M.V. (2004) Baurusuquídeos da Bacia Bauru (Cretáceo Superior, Brasil). *Anuário do Instituto de Geociências*, UFRJ, Rio de Janeiro, 27, 64–74.

Avilla, L.S., Fernandes, R. & Ramos, D.F. (2004) Bit marks on a crocodylomorph from the Upper Cretaceous of Brazil: evidence of social behavior? *Journal of Vertebrate Paleontology*, 24, 971–973.

Batezelli, A., Gomes, N.S. & Perinotto, J.A.D.J. (2005) Petrografia e evolução diagenética dos arenitos da porção norte e nordeste da Bacia Bauru (Cretáceo Superior). *Revista Brasileira de Geociências*, 35(3), 311–322.

Batezelli, A. & Ladeira, F.S.B. (2016) Stratigraphic framework and evolution of the Cretaceous continental sequences of the Bauru, Sanfranciscana, and Parecis basins, Brazil. *Journal of South American Earth Sciences*, 65, 1–24.

Bever, G.S., Gauthier, J.A. & Wagner, G.P. (2011) Finding the frame shift: digit loss, developmental variability, and the origin of the avian hand. *Evolution & development*, 13(3), 269–279.

Bremer, K.R. (1994) Branch support and tree stability. *Cladistics*, 10(3), 295–304.

Busbey, A.B. (1995) The structural consequences of skull flattening in crocodilians. *Functional morphology in vertebrate paleontology*, 173–192.

Campos, D.A., Suarez, J.M., Riff, D. & Kellner, A.W.A. (2001) Short note on a new Baurusuchidae (Crocodyliformes, Metasuchia) from the Upper Cretaceous of Brazil. *Boletim do Museu Nacional, Nova Série, Geologia.*, 57, 1–7.

Carvalho, I.S. & Bertini, R.J. (1999) *Mariliasuchus amarali*: um novo Crocodylomorpha (Notosuchia) do Cretáceo da Bacia Bauru, Brasil. *Geologia Colombiana*, 24, 83–105.

Carvalho, I.S., Campo, A.C.A. & Nobre, P.H. (2005) *Baurusuchus salgadoensis*, a new Crocodylomorpha from the Bauru Basin (Cretaceous), Brazil. *Gondwana Research*, 8(1), 11–30.

Carvalho, I.S., de Vasconcellos1b, F.M., da Silva Marinho, T., Nobre, P.H., de Arruda Campos, A.C., & Arruda, J.T. (2010) Répteis Fósseis de General Salgado, SP. Sítio Geológicos e Paleontológicos do Brasil, 053.

Carvalho, I.S., Teixeira, V.P., Ferraz, M.L., Ribeiro, L.C.B., Martinelli, A.G., Neto, F.M. et al. (2011) *Campinasuchus dinizi* gen. et sp. nov., a new Late Cretaceous baurusuchid (Crocodyliformes) from the Bauru Basin, Brazil. *Zootaxa*, 2871(2011), 19–42.

Castro, M.C., Goin, F.J., Ortiz-Jaureguizar, E., Vieytes, E.C., Tsukui, K., Ramezani, J. et al. (2018) A Late Cretaceous mammal from Brazil and the first radioisotopic age for the Bauru Group. *Royal Society Open Science*, 5(5), 180482.

De Queiroz, K. & Cantino, P.D. (Eds) (2020) *International Code of Phylogenetic Nomenclature (PhyloCode)*. CRC Press.

Dias-Brito, D., Musachio, E.A., Castro, J.C., Maranhão, M.S.S., Suárez, J.M. & Rodrigues, R. (2001) Grupo Bauru: uma unidade continental do Cretáceo no Brasil- concepções baseadas em dados micropaleontológicos, isótopos e estratigráficos. *Revue Paléobiologique, Géneve*, 20(1), 245–304.

Dufeau, D.L. & Witmer, L.M. (2015) Ontogeny of the middle-ear air-sinus system in *Alligator mississippiensis* (Archosauria: Crocodylia). *PLoS One*, 10(9), e0137060.

Fernandes, L.A. (1998) *Estratigrafia e evolução geológica da parte oriental da Bacia Bauru (Ks, Brasil*. (Doctoral dissertation, Universidade de São Paulo).

Fernandes, L.A. (2004) Mapa litoestratigráfico da parte oriental da bacia bauru (pr, sp, mg), escala 1:1.000.000. *Boletim Paranaense de Geociências*, 55.

Fernandes, L.A. & Coimbra, A.M. (1996) Bacia Bauru (Cretaceo superior, Brasil). *Anais da Academia Brasileira de Ciencias*, 68(2), 195–205.

Fernandes, L.A. & Ribeiro, C.M.M. (2015) Evolution and palaeoenvironment of the Bauru Basin (upper Cretaceous, Brazil). *Journal of South American Earth Sciences*, 61, 71–90.

Fonseca, P.H.M., Martinelli, A.G., da Silva Marinho, T., Ribeiro, L.C.B., Schultz, C.L. & Soares, M.B. (2020) Morphology of the endocranial cavities of *Campinasuchus dinizi* (Crocodyliformes: Baurusuchidae) from the Upper Cretaceous of Brazil. *Geobios*, 58, 1–16.

Godoy, P.L., Montefeltro, F.C., Norell, M.A. & Langer, M.C. (2014) An additional baurusuchid from the Cretaceous of Brazil with evidence of interspecific predation among Crocodyliforms. *PLoS One*, 9, e97138.

Goloboff, P.A., Farris, J.S. & Nixon, K.C. (2008) TNT, a free program for phylogenetic analysis. *Cladistics*, 24(5), 774–786.

Grossnickle, D.M. & Newham, E. (2016) Therian mammals experience an ecomorphological radiation during the Late Cretaceous and selective extinction at the K-Pg boundary. *Proceedings of the Royal Society B: Biological Sciences*, 283(1832), 20160256.

Harmon, L.J., Losos, J.B., Jonathan Davies, T., Gillespie, R.G., Gittleman, J.L., Bryan Jennings, W.B. et al. (2010) Early bursts of body size and shape evolution are rare in comparative data. *Evolution: International Journal of Organic Evolution*, 64(8), 2385–2396.

Holliday, C.M., Porter, W.R., Vliet, K.A. & Witmer, L.M. (2020) The frontoparietal fossa and dorsotemporal fenestra of archosaurs and their significance for interpretations of vascular and muscular anatomy in dinosaurs. *The Anatomical Record*, 303(4), 1060–1074.

Holliday, C.M. & Witmer, L.M. (2009) The epipterygoid of crocodyliforms and its significance for the evolution of the orbitotemporal region of eusuchians. *Journal of Vertebrate Paleontology*, 29(3), 715–733.

Iordansky, N.N. (1973) The skull of the Crocodilia. *Biology of the Reptilia*, 4, 201–262.

Langer, M.C., McPhee, B.W., Marsola, J.C.A., Roberto-da-Silva, L. & Cabreira, S.F. (2019) Anatomy of the dinosaur *Pampadromaeus barberenai* (Saurischia—Sauropodomorpha) from the Late Triassic Santa Maria Formation of southern Brazil. *PLoS One*, 14(2).

Larsson, H.C.E. & Sues, H.D. (2007) Cranial osteology and phylogenetic relationships of *Hamadasuchus rebouli* (Crocodyliformes: Mesoeucrocodylia) from the Cretaceous of Morocco. *Zoological Journal of the Linnean Society*, 149, 533–567.

Maddison, W.P. (2008) Mesquite: a modular system for evolutionary analysis. *Evolution*, 62, 1103–1118.

Marinho, T.S., Iori, F.V., de Souza Carvalho, I. & de Vasconcellos, F.M. (2013) *Gondwanasuchus scabrosus* gen. et sp. nov., a new terrestrial predatory crocodyliform (Mesoeucrocodylia: Baurusuchidae) from the Late Cretaceous Bauru Basin of Brazil. *Cretaceous Research*, 44, 104–111.

Martinelli, A.G. & Pais, D.F. (2008) A new baurusuchid crocodyliform (Archosauria) from the Late Cretaceous of Patagonia (Argentina). *Systematic Palaeontology*, 7, 371–381.

Menegazzo, M.C., Catuneanu, O. & Chang, H.K. (2016) The South American retroarc foreland system: The development of the Bauru Basin in the back-bulge province. *Marine and Petroleum Geology*, 73, 131–156.

Montefeltro, F.C. (2019) The osteoderms of baurusuchid crocodyliforms (Mesoeucrocodylia, Notosuchia). *Journal of Vertebrate Paleontology*, 39(2), e1594242.

Montefeltro, F.C., Andrade, D.V. & Larsson, H.C. (2016) The evolution of the meatal chamber in crocodyliforms. *Journal of Anatomy*, 228(5), 838–863.

Montefeltro, F.C., Larsson, H.C.E. & Langer, M.C. (2011) A new baurusuchid (Crocodyliformes, Mesoeucrocodylia) from the late Cretaceous of Brazil and phylogeny of Baurusuchidae. *PLoS One*, 6, e21916.

Montefeltro, F.C., Lautenschlager, S., Godoy, P.L., Ferreira, G.S. & Butler, R.J. (2020) A unique predator in a unique ecosystem: modelling the apex predator from the Late Cretaceous crocodyliform-dominated fauna in Brazil. *BioRxiv*, 843334.

Nascimento, P.M. (2014) *Revisão da família Baurusuchidae e seu posicionamento filogenético dentro do clado Mesoeucrocodylia*, (Doctoral dissertation. Universidade de São Paulo).

Nascimento, P.M. & Zaher, H. (2010) A new species of *Baurusuchus* (Crocodyliformes, Mesoeucrocodylia) from the Upper Cretaceous of Brazil, with the first complete postcranial skeleton described for the family Baurusuchidae. *Papéis avulsos de Zoologia*, 50(21), 323–361.

Oliveira, C.E.M., Santucci, R.M., Andrade, M.B., Fulfaro, V.J., José, A.F. & Benton, M.J. (2011) Crocodylomorph eggs and eggshells from the Adamantina Formation (Bauru Group). *Upper Cretaceous of Brazil. Paleontology*, 54(2), 309–321.

Paula e Silva, F., Kiang, C.H., & Caetano-Chang, M.R. (2003) Perfis de referência do Grupo Bauru (K) no estado de São Paulo. *Geociências*, 22(1), 127–139.

Pinheiro, A.E.P., Pereira, P.V.L.G.C., de Souza, R.G., Brum, A.S., Lopes, R.T., Machado, A.S. et al. (2018) Reassessment of the enigmatic crocodyliform "*Goniopholis*" *paulistanus* Roxo, 1936: Historical approach, systematic, and description by new materials. *PLoS One*, 13(8), e0199984.

Prasad, G.V.R. & Lapparent de Broin, F. (2002) Late Cretaceous crocodile remains from Naskal (India): comparisons and biogeographic affinities. *Annales de Paléontologie.*, 82, 19–71.

Price, L.I. (1945) A new reptile from the Cretaceous of Brazil. *Notas Preliminares e Estudos. Divisão de Geologia e Mineralogia*. Ministério da Agricultura. *Rio de Janeiro, Brasil*, 25, 1–8.

Riff, D. & Kellner, A.W.A. (2011) Baurusuchid crocodyliforms as theropod mimics: clues from the skull and appendicular morphology of Stratiotosuchus maxhechti (Upper Cretaceous of Brazil). *Zoological Journal of the Linnean Society*, 163.

Silva, F.d.P.e., Kiang, C.H. & Chang, M.R.C. (2005) Estratigrafia de subsuperfície do Grupo Bauru (K) no Estado de São Paulo. *Revista Brasileira de Geociências*, 35(1), 77–88.

Simpson, E.H. (1949) Measurement of diversity. *Nature*, 163(4148), 688.

Soares, P.C., Landim, P.M.B., Fulfaro, V.J. & Neto, A.F.S. (1980) Ensaio de caracterização estratigráfica do Cretáceo no Estado de São Paulo: Grupo Bauru. *Revista Brasileira de Geociências*, 10, 177–185.

Turner, A. & Calvo, J.O. (2005) A new sebecosuchian crocodyliform from the Late Cretaceous of Patagonia. *Journal of Vertebrate Paleontology*, 25, 87–98.

Vasconcellos, F.M. (2009) Análise morfofuncional e hábitos de vida de *Baurusuchus* (Crocodyliformes, Mesoeucrocodylia) na Bacia Bauru. Tese de Doutorado. Universidade Federal do Rio de Janeiro.

Walker, A.D. (1968) *Protosuchus*, *Proterochampsa*, and the origin of phytosaurs and crocodiles. *Geological Magazine*, 105, 1–14.

Wilson, J.A., Malkani, M.S. & Gingerich, P.D. (2001) New crocodyliform (Reptilia, Mesoeucrocodylia) from the Upper Cretaceous Pab Formation of Vitakri, Balochistan (Pakistan). *Contributions from the Museum of Paleontology of the University of Michigan.*, 30(12), 321–336.

Witmer, L.M. (1995) Homology of facial structures in extant archosaurs (birds and crocodilians), with special reference to paranasal pneumaticity and nasal conchae. *Journal of morphology*, 225(3), 269–327.

Woodward, A.S. (1896) On two mesozoic crocodilians, Notosuchus (genus novum) and *Cynodontosuchus* (gen. nov.) from the red sandstones of Territory of Neuquén (Argentina).

SUPPORTING INFORMATION

Additional supporting information may be found online in the Supporting Information section.

How to cite this article: Darlim G, Montefeltro FC, Langer MC. 3D skull modelling and description of a new baurusuchid (Crocodyliformes, Mesoeucrocodylia) from the Late Cretaceous (Bauru Basin) of Brazil. *J Anat*. 2021;00:1–41. https://doi.org/10.1111/joa.13442